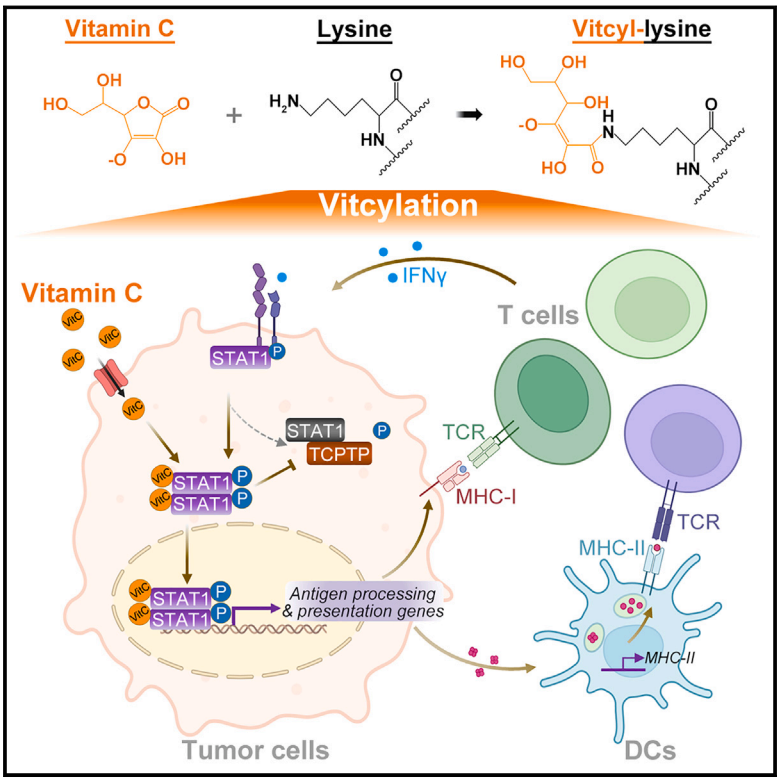
Cell

Lysine vitcylation is a vitamin C-derived protein modification that enhances STAT1-mediated immune response

Graphical abstract



Highlights

- Vitamin C modifies lysine in peptides/proteins, forming vitcyl-lysine (vitcylation)
- Vitcylation occurs *in vitro*/*in vivo*, dependent on dose, pH, and amino acid sequence
- STAT1 vitcylation increases its phosphorylation, enhancing IFN pathway activation
- STAT1 vitcylation enhances tumor antigen presentation and anti-tumor immunity

Authors

Xiadi He, Qiwei Wang, Xin Cheng, ..., Ke Zhang, Lewis C. Cantley, Jean J. Zhao

Correspondence

jean_zhao@dfci.harvard.edu

In brief

Vitamin C directly modifies lysine residues through vitcylation, regulating STAT1 signaling and enhancing anti-tumor immune responses by preventing STAT1 dephosphorylation.

He et al., 2025, Cell *188*, 1858–1877
April 3, 2025 © 2025 Elsevier Inc. All rights are reserved, including those for text and data mining, AI training, and similar technologies.
https://doi.org/10.1016/j.cell.2025.01.043

CellPress

Cell

Article

Lysine vitcylation is a vitamin C-derived protein modification that enhances STAT1-mediated immune response

Xiadi He,[1,2,3] Qiwei Wang,[1,2,4] Xin Cheng,[1,2] Weihua Wang,[1] Yutong Li,[1,2] Yabing Nan,[1,2] Jiang Wu,[5] Bingqiu Xiu,[1] Tao Jiang,[1] Johann S. Bergholz,[1,2,4] Hao Gu,[1,2] Fuhui Chen,[1,6] Guangjian Fan,[7] Lianhui Sun,[8] Shaozhen Xie,[1] Junjie Zou,[9] Sheng Lin,[9] Yun Wei,[1,10] James Lee,[1] John M. Asara,[11,12] Ke Zhang,[10] Lewis C. Cantley,[1,6] and Jean J. Zhao[1,2,4,13,14,*]

[1]Department of Cancer Biology, Dana-Farber Cancer Institute, Boston, MA 02215, USA
[2]Department of Biological Chemistry and Molecular Pharmacology, Harvard Medical School, Boston, MA 02115, USA
[3]Department of Endocrine and Metabolic Diseases, Shanghai Institute of Endocrine and Metabolic Diseases, National Clinical Research Center for Metabolic Diseases (Shanghai), Key Laboratory for Endocrine and Metabolic Diseases of the National Health Commission of the PR China, Lifecycle Health Management Center, Ruijin Hospital, Shanghai Jiao Tong University School of Medicine, Shanghai 200025, China
[4]Broad Institute of Harvard and MIT, Cambridge, MA 02142, USA
[5]College of Chemistry and Chemical Engineering, Lanzhou University, Lanzhou, Gansu 730000, China
[6]Department of Cell Biology, Harvard Medical School, Boston, MA 02115, USA
[7]Precision Research Center for Refractory Diseases, Institute for Clinical Research, Shanghai General Hospital, Shanghai Jiao Tong University School of Medicine, Shanghai 200080, China
[8]Department of Immunology, School of Cell and Gene Therapy, Songjiang Research Institute, Shanghai Jiao Tong University School of Medicine Affiliated Songjiang Hospital, Shanghai, China
[9]XtalPi Technology Co., Ltd., Shanghai 200131, China
[10]Department of Chemistry and Chemical Biology, Northeastern University, Boston, MA 02115, USA
[11]Division of Signal Transduction/Mass Spectrometry Core, Beth Israel Deaconess Medical Center, Boston, MA 02215, USA
[12]Department of Medicine, Harvard Medical School, Boston, MA 02115, USA
[13]Laboratory of Systems Pharmacology, Harvard Medical School, Boston, MA 02115, USA
[14]Lead contact
*Correspondence: jean_zhao@dfci.harvard.edu
https://doi.org/10.1016/j.cell.2025.01.043

SUMMARY

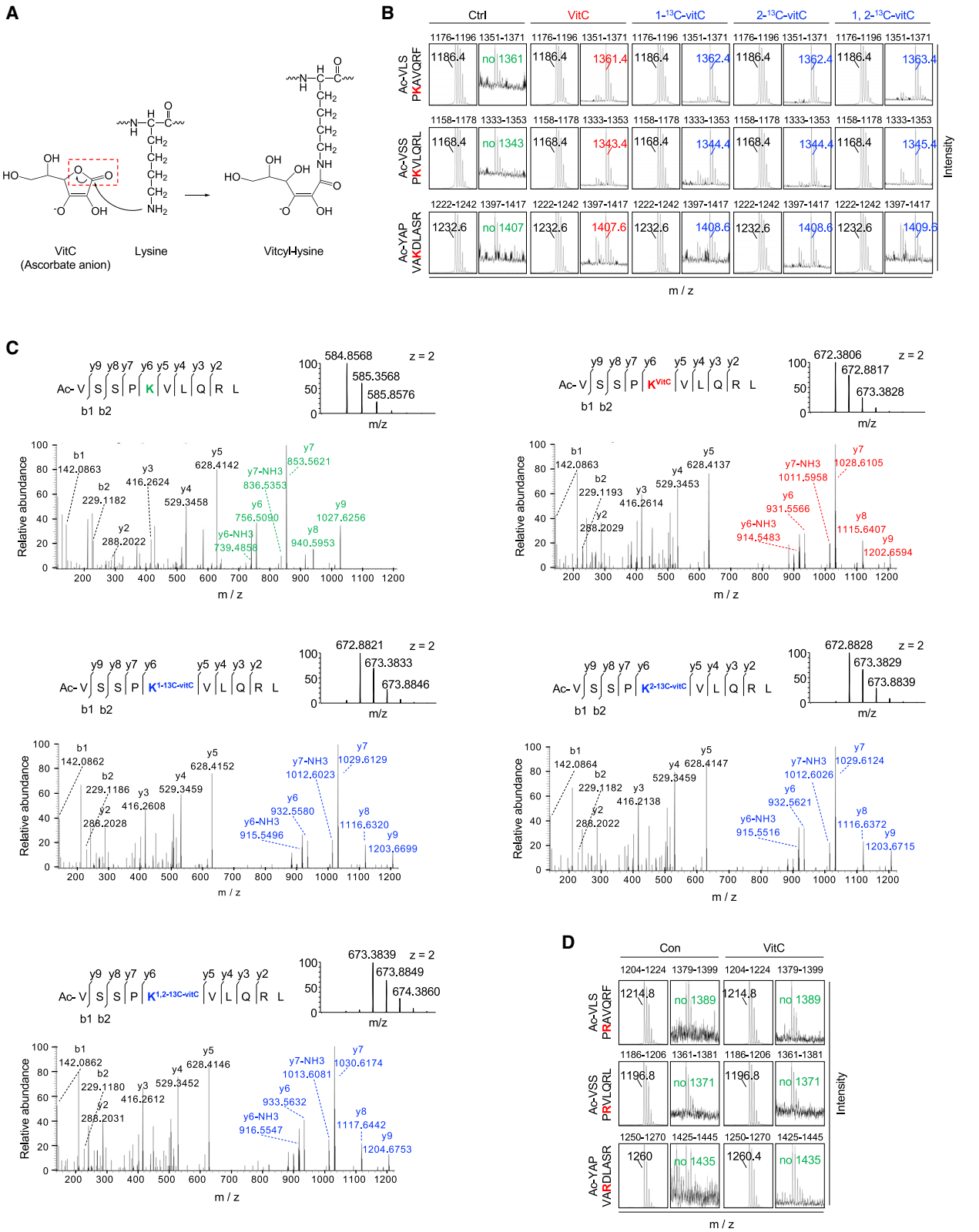
Vitamin C (vitC) is essential for health and shows promise in treating diseases like cancer, yet its mechanisms remain elusive. Here, we report that vitC directly modifies lysine residues to form "vitcyl-lysine"—a process termed vitcylation. Vitcylation occurs in a dose-, pH-, and sequence-dependent manner in both cell-free systems and living cells. Mechanistically, vitC vitcylates signal transducer and activator of transcription-1 (STAT1)- lysine-298 (K298), impairing its interaction with T cell protein-tyrosine phosphatase (TCPTP) and preventing STAT1-Y701 dephosphorylation. This leads to enhanced STAT1-mediated interferon (IFN) signaling in tumor cells, increased major histocompatibility complex (MHC)/human leukocyte antigen (HLA) class I expression, and activation of anti-tumor immunity *in vitro* and *in vivo*. The discovery of vitcylation as a distinctive post-translational modification provides significant insights into vitC's cellular function and therapeutic potential, opening avenues for understanding its biological effects and applications in disease treatment.

INTRODUCTION

Vitamin C (vitC), essential for humans who lack synthetic capability, has both basic nutritional roles and potential therapeutic applications.[1] While low doses prevent diseases like scurvy,[2] high-dose vitC's role in cancer treatment has long been debated.[3] Recent pharmacokinetic insights have renewed interest in its clinical applications,[4–8] though its anti-cancer mechanisms, including the generation of reactive oxygen species (ROS)[4–6,9–16] and ten-eleven translocation (TET) enzyme-mediated DNA demethylation,[17–21] are not fully understood.

Under physiological conditions, VitC exists primarily as the ascorbate anion (175 Da), with dehydroascorbic acid (DHA, 174 Da) as its oxidized form.[22–24] While DHA can undergo further oxidation at low pH to produce diketogulonate (DKG),[25] leading to protein modifications called ascorbylations in plants, food, and certain animal tissues,[26–29] these processes differ from physiological vitC modifications.

 © 2025 Elsevier Inc.
All rights are reserved, including those for text and data mining, AI training, and similar technologies.



(legend on next page)

Protein post-translational modifications (PTMs) are crucial for physiological regulation,[30–33] typically involving chemical alterations of specific amino acid side chains.[32] Common modifications include acetylation, methylation, phosphorylation, and glycosylation,[34–36] with recent mass spectrometry advances revealing several novel PTMs.[37–41] These modifications regulate protein function by affecting protein-protein interactions, enzymatic activity, protein stability, subcellular localization, and signaling pathways.

In this study, we show that ascorbate anion directly modifies lysine residues in peptides and proteins under physiological conditions, a process we term "vitcylation," distinct from DHA-induced ascorbylation. This modification occurs in a pH- and dose-dependent manner. We identify numerous vitcylated proteins and demonstrate that vitC vitcylates the signal transducer and activator of transcription-1 (STAT1) at lysine-298 (K298) in cancer cells, increasing its phosphorylation and nuclear translocation by impairing its interaction with T cell protein-tyrosine phosphatase (TCPTP).[42,43] This leads to activation of STAT1-mediated interferon (IFN) response pathways both *in vitro* and *in vivo*. Our findings provide molecular insights into vitC's role in protein modification and immune regulation, with important implications for therapeutic applications.

RESULTS

VitC directly modifies lysine to form vitcyl-lysine in cell-free systems in a pH- and dose-dependent manner

Previous studies have shown that anhydride intermediates and homocysteine thiolactone (HTL) can react with lysine in proteins to form specific modifications.[44] For example, succinic anhydride forms succinyl-lysine (succinylation) (Figure S1A),[44,45] while HTL forms homocysteinyl-lysine (Figure S1B).[46] Both these compounds share a common reactive lactone structure that enables lysine modification. We observed that vitC contains a similar reactive lactone structure (Figure 1A) and hypothesized it could modify the ε-amine group of lysine residues in peptides and proteins through its lactone structure to form a modified lysine, designated "vitcyl-lysine" (Figure 1A). To test this hypothesis, we incubated synthetic lysine-containing peptides with vitC at physiological pH (pH 7.4).[41] Matrix-assisted laser desorption/ionization time-of-flight/time-of-flight mass spectrometry (MALDI-TOF/TOF MS) analysis revealed a 175 Da mass shift (Figure 1B), confirming that ascorbate anion modifies lysine residues to form vitcyl-lysine (Figures 1A and S1C).

Previous studies showed that at low pH (~2.0), DHA oxidizes to DKG, modifying proteins in plants and food products with a mass shift of 58–148 Da, termed "ascorbylations" (Figure S1D).[26–29] To determine whether DHA can form the modification under physiological conditions, we incubated lysine-containing peptides with either ascorbate anion or DHA (2 mM, pH 7.4). Only ascorbate anion formed modifications (Figure S1E), leading us to term this modification vitcylation to distinguish it from DHA-induced ascorbylation.

To validate this finding, we used isotope-labeled vitC variants (1-^{13}C, 2-^{13}C, and 1, 2-^{13}C) (Figure S1F). MALDI-TOF/TOF MS analyses showed corresponding mass shifts: 176 Da for single-labeled (1-^{13}C or 2-^{13}C) and 177 Da for double-labeled (1, 2-^{13}C) (Figure 1B). High-performance liquid chromatography (HPLC)-MS and MS/MS analysis confirmed these specific mass shifts in vitcylated peptide fragments (Figures 1C, S1G, and S1H), verifying the specific incorporation of vitC into lysine residues.

To further validate this lysine-specific modification, we conducted several experiments. When we substituted lysine with arginine, alanine, or cysteine in our test peptides, vitcylation was abolished (Figures 1D, S2A, and S2B), confirming the modification's specificity for lysine residues. Using peptides with unprotected N termini and multiple lysine residues, we demonstrated that vitC can modify both the N terminus and multiple lysine residues within a peptide (Figures S2C and S2D). Importantly, no stable byproducts other than vitcylation were detected when using 1-^{13}C-vitC (Figure S2E). The modification occurred with similar efficiency in both amine-containing buffer (Tris) and non-amine-containing buffer (PBS) (Figure S2F), suggesting buffer composition does not significantly affect the process. Furthermore, the modification displayed sequence specificity, as not all lysine-containing peptides were modified (Figure S2G). Collectively, these results demonstrate that vitcylation is a selective, lysine-specific modification with partial sequence dependency.

To further characterize lysine vitcylation, we examined its dependency on vitC concentration and pH in our cell-free system. Using physiologically achievable vitC concentrations (0.1–10 mM),[47,48] we found that vitcylation increased with concentration, showing an EC_{50} of approximately 2 mM (Figure S2H). Stoichiometry and quantitative analysis confirmed substantial

Figure 1. VitC modifies lysine residues of peptides to form vitcyl-lysine in cell-free systems

(A) Proposed mechanism of lysine vitcylation formation by ascorbate anion. The reactive lactone bond on the ascorbate anion is circled.

(B) Representative results of vitC-induced vitcylation formation *in vitro*. Synthetic lysine-containing peptides (sequences of the peptides were listed on the left of the spectrum, "Ac-" means the N terminus of the peptide is protected by an acetyl group, hereafter for MALDI-TOF/TOF MS detection unless otherwise indicated) were incubated with either a vehicle, 2 mM vitC, 2 mM 1-^{13}C-vitC, 2 mM 2-^{13}C-vitC, or 2 mM 1,2-^{13}C-vitC at 37°C for 3 h. The formation of vitcylated peptides was detected by MALDI-TOF/TOF MS, with the m/z range of each spectrum displayed above the spectrum. The m/z values of unmodified peptides and modified peptides are listed.

(C) MS spectrum (upper) and MS/MS spectrum (lower) of the unmodified peptide, vitcylated peptide, 1-^{13}C-vitcylated peptide, 2-^{13}C-vitcylated peptide, and 1,2-^{13}C-vitcylated peptide (Ac-VSSPKVLQRL) detected by HPLC-MS/MS. Lysine-containing unmodified fragments, vitcylated fragments, 1-^{13}C-vitcylated fragments, 2-^{13}C-vitcylated fragments, and 1,2-^{13}C-vitcylated fragments are marked with green, red, and blue colors, respectively. The b ion refers to the N-terminal parts of the peptide, and the y ion refers to the C-terminal parts of the peptide (hereafter for HPLC-MS/MS analysis).

(D) Synthetic arginine-containing peptides were incubated with either a vehicle or 2 mM vitC at 37°C for 3 h. The formation of vitcylated peptides was detected by MALDI-TOF/TOF MS.

See also Figures S1 and S2.

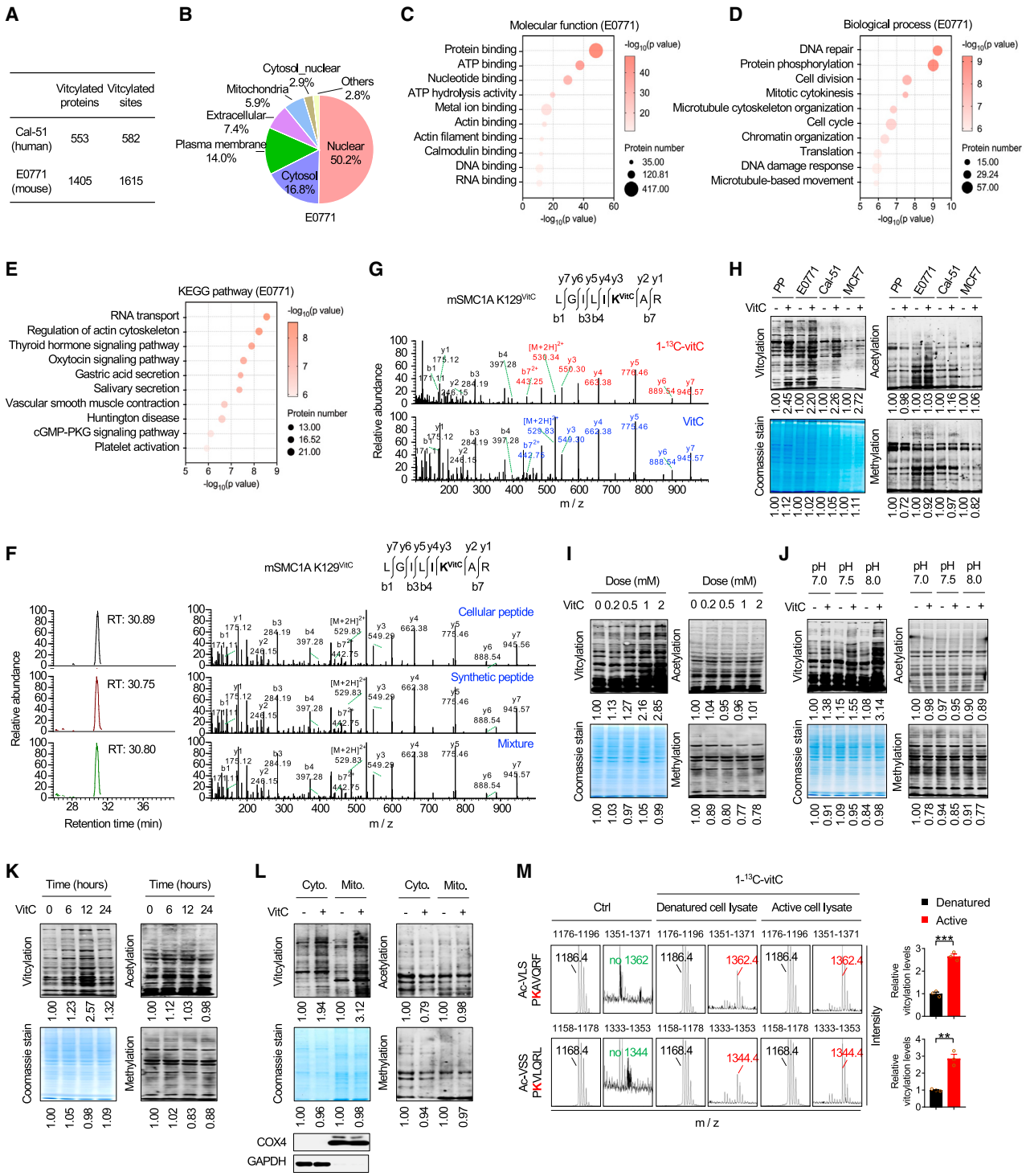


Figure 2. VitC induces lysine vitcylation on cellular proteins

(A) Summary of the numbers of vitcylated proteins and sites identified in Cal-51 (human) and E0771 (mouse) cells.

(B) Subcellular locations of lysine-vitcylated proteins identified in E0771 cells. The locations are classified into nuclear, cytosol, plasma membrane, extracellular, mitochondrial, cytosol_nuclear, and other compartments.

(C) Top ten Gene Ontology molecular function enrichment categories for vitcylated proteins identified in E0771 cells.

(D) Top ten Gene Ontology biological process enrichment categories for vitcylated proteins identified in E0771 cells.

(E) Top ten KEGG-based enrichment categories of lysine-vitcylated proteins identified in E0771 cells.

(legend continued on next page)

vitcylation formation at physiological concentrations (Figure S2I). We also assessed the pH dependency across a range of pH (4.0–11.5) covering physiological subcellular compartments (pH 6.5–8.2).[49–51] Using 2 mM vitC, we observed increased vitcylation from pH 7.0 to pH 9.5–10.0, followed by a decline at higher pH (Figure S2J). This pattern suggests that vitcylation may occur preferentially in certain cellular compartments or conditions.

Together, our data identify lysine vitcylation as a previously unknown modification by vitC in its ascorbate anion form. This modification occurs in our cell-free and enzyme-free systems in a manner dependent on vitC dose, pH, and peptide sequence.

VitC modifies lysine in cellular proteins to form lysine-vitcylated proteins

We next investigated the stoichiometry and specificity of vitcylation on purified proteins using HPLC-MS/MS. Significant vitcylation was detected on purified glyceraldehyde-3-phosphate dehydrogenase (GAPDH) and structural maintenance of chromosomes protein 1A (SMC1A) following vitC treatment (Figure S3A), demonstrating that this modification occurs on intact proteins. We further conducted vitcylation with a whole-cell protein mix, isolated and purified by acetone precipitation,[52] at two different pH conditions: pH 7.2 and pH 8.0. Our results indicated that vitC induced more abundant lysine vitcylation at pH 8.0 compared with pH 7.2 (Figure S3B; Table S1), suggesting that cellular location or physiological state may influence the extent of vitcylation.

To determine whether vitC modifies cellular proteins in intact cells, we measured intracellular vitC concentrations and detected vitcylated proteins after vitC treatment. Intracellular vitC levels increased significantly in a dose-dependent manner in both human (Cal-51) and murine (E0771 and PP) cancer cell lines (Figure S3C). PP is a recently developed syngeneic mouse breast tumor model driven by the concurrent loss of phosphatase and tensin homolog deleted on chromosome ten (PTEN) and p53.[53] Interestingly, even without vitC supplementation, cells cultured in standard medium with 10% fetal bovine serum (FBS) exhibited basal intracellular vitC levels of ~100 μM (Figure S3C), likely due to vitC present in the FBS.[54,55] Indeed, while basal medium contains no vitC, medium supplemented with 10% FBS contains approximately 10 μM vitC (Figure S3D). Supplementing medium with 10% FBS exhibits increased intracellular vitC levels from below 50 μM to approximately 100 μM or higher (Figure S3E), indicating effective vitC uptake from the culture medium.

We investigated protein vitcylation in human Cal-51 and mouse E0771 cells treated with 2 mM vitC. Mass spectrometry identified 553 and 1,405 vitcylated proteins in Cal-51 and E0771 cells, respectively, with 89 shared between both cell lines (Figures 2A and S3F; Tables S2, S3, and S4). Vitcylation was specific to lysine residues, with rare occurrences at the N terminus and no other nucleophilic amino acids (Tables S2 and S3), consistent with earlier cell-free experiments (Figures S2B and S2C). Higher vitC doses increased the number of vitcylated proteins and sites (Figure S3G). Bioinformatic analysis revealed that the vitcylated proteins are distributed across subcellular locations with potential roles in multiple cellular processes and signaling pathways (Figures 2B–2E and S3H–S3K). While enriched lysine vitcylation motifs were observed, consistent with sequence-specific vitcylation in synthetic peptides (Figure S2G), no strong consensus sequence for vitcylation was identified (Figure S3L).

We next determined whether vitC-induced lysine modifications in cellular proteins match those observed in synthetic peptides from our cell-free system (Figure 1). HPLC-MS/MS analysis showed that vitcylated peptides from vitC-treated cells co-eluted with and had similar MS/MS spectra to vitC-treated synthetic peptides in the cell-free system (Figures 2F, S3M, and S3N). Using isotopic 1-^{13}C-vitC followed by MS/MS analysis further confirmed lysine vitcylation in cellular proteins (Figures 2G, S3O, and S3P). These results demonstrate that vitC treatment induces lysine vitcylation in cellular proteins in a manner consistent with our cell-free studies.

To further validate cellular lysine vitcylation, we developed a specific polyclonal antibody against vitcyl-lysine, confirming its specificity through dot-blot and western blot (WB) analyses (Figures S3Q–S3S). WB analysis detected specific bands in vitC-treated cancer cell lysates, using methylation and acetylation as controls (Figures 2H and S3T). These bands are

(F) Extracted ion chromatograms (left) and MS/MS spectra (right) from HPLC-MS/MS analysis of vitcylated peptides (the K129 site of mouse SMC1A) derived from E0771 (cellular peptide), its *in vitro* generated counterpart (synthetic peptide), and their mixture.

(G) Extracted MS/MS spectra from HPLC-MS/MS analysis of 1-^{13}C-vitcylated peptides and vitcylated peptides (the K129 site of mouse SMC1A) derived from E0771 cells. Lysine-containing 1-^{13}C-vitcylated fragments and vitcylated fragments are marked by red and blue colors, respectively.

(H) Intracellular levels of lysine vitcylation, acetylation, and methylation were measured in PP, E0771, Cal-51, and MCF7 cells cultured in medium containing a vehicle or vitC for 12 h (2 mM vitC for PP and E0771, 0.5 mM vitC for Cal-51 and MCF7). Protein levels in each sample were normalized by Coomassie staining, hereafter for global vitcylation detection. The quantifications of WB and Coomassie staining were normalized to the untreated samples and are listed below.

(I) Intracellular levels of lysine vitcylation, acetylation, and methylation were measured in E0771 cells cultured in medium containing different concentrations of vitC for 12 h.

(J) Intracellular levels of lysine vitcylation, acetylation, and methylation were measured in E0771 cells cultured in medium containing a vehicle or 2 mM vitC for 12 h under different pH conditions.

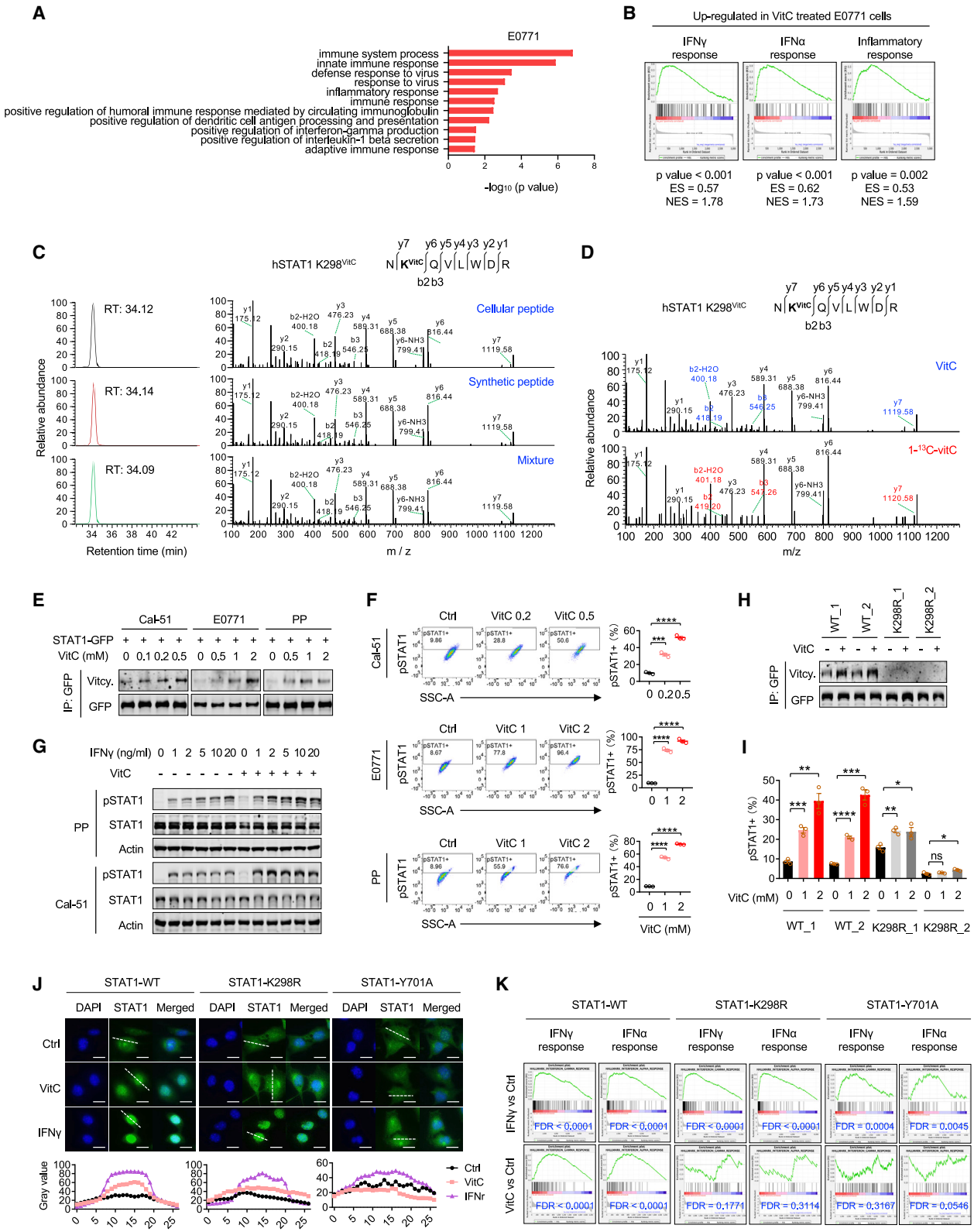
(K) Intracellular lysine vitcylation, acetylation, and methylation levels were measured in E0771 cells cultured in medium containing 2 mM vitC for the indicated times.

(L) Lysine vitcylation, acetylation, and methylation levels of cytosolic and mitochondrial proteins were measured from E0771 cells cultured in medium with a vehicle or 2 mM vitC for 12 h.

(M) Synthetic lysine-containing peptides were incubated with 2 mM of vitC in the presence of denatured cell lysate (99°C for 5 min to denature the cell lysate) or active cell lysate at 37°C for 3 h. The formation of vitcylated peptides was detected by MALDI-TOF/TOF MS. The relative vitcylation levels were quantified (right, $n = 3$).

Data are represented as mean ± SEM. $^{**}p < 0.01$, $^{***}p < 0.001$.

See also Figure S3 and Tables S1, S2, S3, and S4.



(legend on next page)

outcompeted by vitcylated peptides (Figure S3U), confirming lysine vitcylation in cells. Further WB analysis demonstrated that cellular lysine vitcylation levels respond to vitC in a dose-, time-, and pH-dependent manner (Figures 2I–2K). Cells cultured with 10% FBS showed higher intracellular vitC and vitcylation levels compared with serum-free conditions (Figure S3V). Due to the higher pH of the mitochondrial matrix (7.7–8.2) versus cytosol (7.0–7.4),[56,57] mitochondrial proteins showed more abundant vitcylation than cytosolic proteins (Figure 2L). These results demonstrate that vitC, as ascorbate anion, can modify lysine residues in proteins in both human and murine cells.

To investigate potential enzymatic regulation of vitcylation in cells, we compared vitcylation formation in active versus denatured cell lysates. Active lysates enhanced vitC-induced vitcylation, while denatured lysates did not (Figure 2M). This indicates that cellular enzymes may catalyze or promote vitcylation, potentially explaining the substrate selectivity observed in cells.

STAT1 vitcylation enhances STAT1 phosphorylation and activation

We next investigated the functional role of lysine vitcylation in cells. Expression analysis of 4,604 cancer- and immune-related genes in vitC-treated E0771 cells revealed upregulation of immune and inflammatory response genes (Figure 3A; Table S5). Gene set enrichment analysis (GSEA) confirmed that the top-ranked genes in vitC-treated cells were associated with IFN-γ response, IFN-α response, and inflammatory response pathways (Figures 3B, S4A, and S4B).

Since STAT1 activation drives IFN response programs,[58] and our initial analysis revealed STAT1 K298 vitcylation upon vitC treatment (Table S2), we focused on this modification. K298, a crucial regulatory site conserved in vertebrates (Figure S4C),[59–61] is surface-exposed and accessible for vitcylation (Figure S4D). We investigated STAT1 vitcylation in vitC-treated human Cal-51 and mouse E0771 breast cancer cells. HPLC-MS/MS analysis showed that vitcylated STAT1 K298 peptides from cells co-eluted with and matched MS/MS spectra of vitC-treated synthetic peptides (Figures 3C and S4E). Using isotopic 1-^{13}C-vitC confirmed K298 vitcylation in both human and mouse cells (Figures 3D and S4F), with quantification showing substantial modification at physiological vitC concentrations (Figure S4G).

We next explored whether STAT1 vitcylation affects cellular immunity and inflammatory responses. Since STAT1 tyrosine 701 phosphorylation (pSTAT1) is crucial for nuclear translocation and subsequent IFN responses,[62,63] we investigated the relationship between STAT1 vitcylation and phosphorylation. Using GFP-tagged STAT1 (STAT1-GFP) pull-down with GFP-antibody followed by WB analysis with anti-vitcylation antibody, we found that vitC treatment increased both STAT1 vitcylation and phosphorylation in a dose-dependent manner in Cal-51, E0771, and PP cells (Figures 3E, 3F, S4H, and S4I). Notably, vitC did not induce vitcylation of STAT2 and STAT3 (Figures S4J and S4K), indicating specificity among different STAT family members.

VitC treatment increased pSTAT1 levels across various tumor cell lines but showed no effect in STAT1-deficient AGS cell line (gastric adenocarcinoma cells) (Figure S4L),[64] suggesting vitcylation as a common mechanism for STAT1 activation in tumors. VitC increased both basal pSTAT1 levels and IFN-γ-induced pSTAT1 response, as shown by WB and flow cytometry (Figures 3G and S4M). Both STAT1 vitcylation and phosphorylation exhibited pH dependency (Figures S4N and S4O), consistent with findings in our cell-free system (Figure S2J).

Immunofluorescence studies confirmed that vitC treatment enhanced STAT1 nuclear translocation and increased pSTAT1 levels (Figures S4P–S4R). Further investigation revealed that vitcylation occurs on both phosphorylated and unphosphorylated forms of STAT1, as shown by analysis of STAT1-WT, STAT1-Y701A, and STAT1-Y701E (Figures S4S and S4T). We also found that vitC treatment promoted STAT1 ubiquitination and accelerated its degradation (Figures S4U and S4V), suggesting a dual role: while vitcylation enhances STAT1 phosphorylation and activation, it also promotes STAT1 degradation to prevent hyperactivation. This regulation indicates how vitC-induced STAT1 vitcylation coordinates phosphorylation, nuclear translocation, and protein turnover to achieve nuanced control of STAT1 activity and IFN response.

Figure 3. Vitcylation of STAT1 K298 regulates the phosphorylation and activation of STAT1

(A and B) Top-ranked upregulated Gene Ontology terms (A) and upregulated GSEA signatures (B) in E0771 cells treated with 1 mM vitC for 2 days ($n = 2$).

(C) Extracted ion chromatograms (left) and MS/MS spectra (right) from HPLC-MS/MS analysis of a vitcylated peptide (the K298 site of human STAT1) derived from Cal-51 cells (cellular peptide), its *in vitro* generated counterpart (synthetic peptide), and their mixture.

(D) Extracted MS/MS spectra from HPLC-MS/MS analysis of vitcylated peptide (upper) and 1-^{13}C-vitcylated peptide (lower) (the K298 site of human STAT1) derived from Cal-51 cells. Lysine-containing vitcylated fragments and 1-^{13}C-vitcylated fragments are marked by blue and red colors, respectively.

(E) STAT1 vitcylation levels were measured from STAT1-GFP-expressing cells (Cal-51, E0771, and PP cells) cultured in different concentrations of vitC for 12 h.

(F) pSTAT1 flow cytometric analysis of Cal-51, E0771, and PP cells cultured in different concentrations of vitC for 2 days (2 mM vitC for E0771 and PP, 0.5 mM vitC for Cal-51, $n = 3$). Data are represented as mean ± SEM. ***$p < 0.001$, ****$p < 0.0001$.

(G) WB analysis of pSTAT1 in PP and Cal-51 cells cultured in different concentrations of IFN-γ for 15 min with or without vitC treatment for 2 days (2 mM vitC for PP, 0.5 mM vitC for Cal-51).

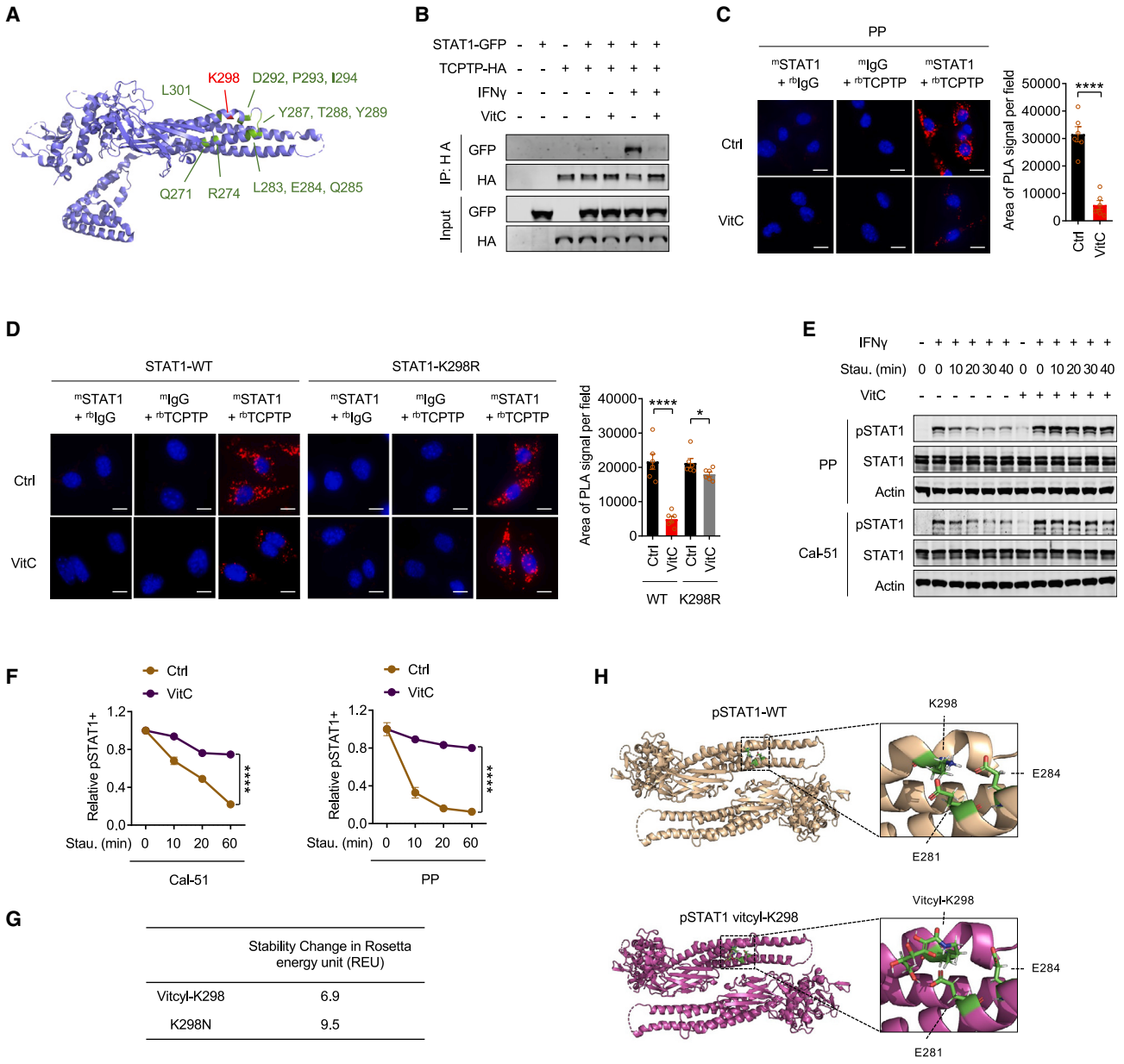
(H) Measurement of vitcylation levels of STAT1-WT and STAT1-K298R in PP-sgSTAT1_1 cells re-expressing STAT1-WT-GFP or STAT1-K298R-GFP, after being cultured in medium containing 2 mM vitC or control medium for 12 h.

(I) Flow cytometric analysis of pSTAT1 in PP-sgSTAT1_1 cell re-expressing STAT1-WT-GFP or STAT1-K298R-GFP, cultured in varying concentrations of vitC for 2 days ($n = 3$). Data are represented as mean ± SEM. *$p < 0.05$, **$p < 0.01$, ***$p < 0.001$, ****$p < 0.0001$.

(J) Nuclear translocation of STAT1 in PP-sgSTAT1_1 cell re-expressing STAT1-WT-GFP, STAT1-K298R-GFP, or STAT1-Y701A-GFP treated with 2 mM vitC (2 days) or 100 ng/mL IFN-γ (15 min) was assessed by immunofluorescence (scale bar, 30 μM). The quantifications of immunofluorescence intensity are listed below, hereafter for STAT1 nuclear translocation assay.

(K) GSEA signatures of IFN-γ response and IFN-α response in PP-sgSTAT1_1 cell re-expressing STAT1-WT-GFP, STAT1-K298R-GFP, or STAT1-Y701A-GFP treated with 2 mM vitC (2 days) or 100 ng/mL IFN-γ (24 h) ($n = 2$).

See also Figure S4 and Tables S2 and S5.



	Stability Change in Rosetta energy unit (REU)
Vitcyl-K298	6.9
K298N	9.5

Figure 4. Vitcylation of STAT1 K298 prevents its dephosphorylation by TCPTP

(A) Ribbon representation of human STAT1. The K298 site and several GoF mutation sites are marked by red and green colors, respectively. The side chain of K298 is shown.

(B) HeLa cells co-expressing STAT1-GFP and TCPTP-HA were treated with vehicle or 300 μM vitC for 24 h, followed by stimulation with 100 ng/mL IFN-γ for 15 min. The interaction between STAT1 and TCPTP was assayed by co-immunoprecipitation.

(C) STAT1-TCPTP PLA analysis (left) and quantification (right) of PP cells treated with a vehicle or 2 mM vitC for 2 days (scale bar, 30 μM). Data are represented as mean ± SEM. ****$p < 0.0001$.

(D) STAT1-TCPTP PLA analysis (left) and quantification (right) of PP-sgSTAT1_1 cell re-expressing STAT1-WT-GFP and STAT1-K298R-GFP treated with vehicle or 2 mM vitC for 24 h (scale bar, 15 μM). Data are represented as mean ± SEM. *$p < 0.05$, ****$p < 0.0001$.

(E) Cells were pretreated with vehicle or vitC (0.2 mM vitC for Cal-51, 1 mM vitC for PP) for 2 days, then stimulated with 100 ng/mL IFN-γ for 15 min followed by incubation with 1 μM staurosporine for the indicated times. The pSTAT1 levels were measured by WB immediately.

(F) Cells were pretreated with vehicle or vitC (0.2 mM vitC for Cal-51, 1 mM vitC for PP) for 2 days, then stimulated with 100 ng/mL IFN-γ for 15 min followed by incubation with 1 μM staurosporine for the indicated times. The relative pSTAT1+ populations were measured by flow cytometry immediately ($n = 3$). Data are represented as mean ± SEM. ****$p < 0.0001$.

(legend continued on next page)

To further study STAT1 vitcylation's role in phosphorylation and activation, we generated STAT1-null PP tumor cells using CRISPR-Cas9 (Figure S4W). We then reintroduced STAT1-WT, vitcylation-defective STAT1-K298R, or phosphorylation-defective STAT1-Y701A (Figure S4X). Only STAT1-WT, not STAT1-K298R, restored STAT1 vitcylation and enhanced phosphorylation upon vitC treatment in STAT1-null cells (Figures 3H, 3I, and S4Y). Both the STAT1-K298R and STAT1-Y701A mutations prevented vitC-induced STAT1 nuclear translocation (Figure 3J). RNA sequencing (RNA-seq) analysis further confirmed these mutations abolished vitC-triggered IFN response gene transcription, though STAT1-K298R mutation did not affect IFN-γ-induced responses (Figure 3K). These results demonstrate that STAT1 vitcylation activates STAT1 in tumor cells by modulating its phosphorylation, with K298 playing a crucial role in vitC-mediated STAT1 activation.

STAT1 vitcylation prevents STAT1 from dephosphorylation by its phosphatase TCPTP

We investigated the molecular mechanism linking STAT1 phosphorylation and vitcylation. Previous studies identified STAT1 gain-of-function (GOF) mutations in chronic mucocutaneous candidiasis (CMC), an autoimmune disorder.[65] This GOF mechanism involves impaired STAT1 dephosphorylation leading to Y701 hyperphosphorylation in response to IFNs.[65,66] Interestingly, one such mutation is K298N, which results in elevated pSTAT1 levels both in basal conditions and after IFN-γ stimulation.[59] Many STAT1 GOF mutations cluster near K298 in the protein structure (Figure 4A), suggesting a mechanistic link between K298 modification and STAT1 phosphorylation regulation.

Based on these observations, we hypothesized that STAT1-K298 vitcylation might prevent STAT1 dephosphorylation by blocking phosphatase interaction. We investigated STAT1's interaction with its phosphatase TCPTP through co-immunoprecipitation experiments, a well-documented association in previous studies.[42,43,67] We found that vitC treatment disrupted the STAT1-TCPTP interaction (Figure 4B), while not affecting STAT1's association with its kinase Janus kinase 1 (JAK1) (Figure S5A).[58] Proximity ligation assay (PLA) confirmed vitC's inhibitory effect on native STAT1-TCPTP interaction (Figures 4C and S5B), and this effect was impaired by the STAT1-K298R mutation (Figure 4D). In cells treated with vitC or a TCPTP inhibitor, STAT1 phosphorylation was sustained even after staurosporine treatment following IFN-γ stimulation (Figures 4E, 4F, and S5C). This highlights how vitC regulates STAT1 phosphorylation by disrupting STAT1-TCPTP interaction. These results demonstrate that STAT1 vitcylation enhances STAT1 phosphorylation by preventing TCPTP-mediated dephosphorylation, establishing a mechanistic link between vitcylation and STAT1 activation.

Previous studies showed that IFN-γ stimulation results in parallel pSTAT1 homodimers formation and recruitment to gamma IFN activation sites (GAS DNA elements), key events in the IFN signaling pathway.[68–70] Recent research revealed that pSTAT1 dimers must rapidly rearrange from parallel to antiparallel conformation to bind TCPTP.[71–73] Using Rosetta biomolecular modeling to analyze how STAT1-K298 modifications affect this conformational change, we found that both K298 vitcylation and K298N significantly destabilize the antiparallel dimer form of STAT1, with Rosetta energy unit (REU) changes of 6.9 and 9.5, respectively (Figure 4G). Further analysis of energy terms showed that both modifications disrupt salt bonds between K298 and E281/E284 in the antiparallel dimer conformation (Figures 4H, S5E, and S5F). Together, these data suggest that both STAT1-vitcyl-K298 and STAT1-K298N disrupt the structural transition of STAT1 between parallel dimers (required for DNA binding) and antiparallel dimer conformation (necessary for TCPTP-mediated dephosphorylation), favoring the parallel configuration and resulting in increased STAT1 phosphorylation. Intriguingly, while STAT1-K298N is a GOF genetic mutation and STAT1-K298-vitcylation is a chemical modification by vitC, they share a common molecular mechanism for enhancing immune response.

STAT1 vitcylation enhances MHC/HLA class I expression and immunogenicity of tumor cells

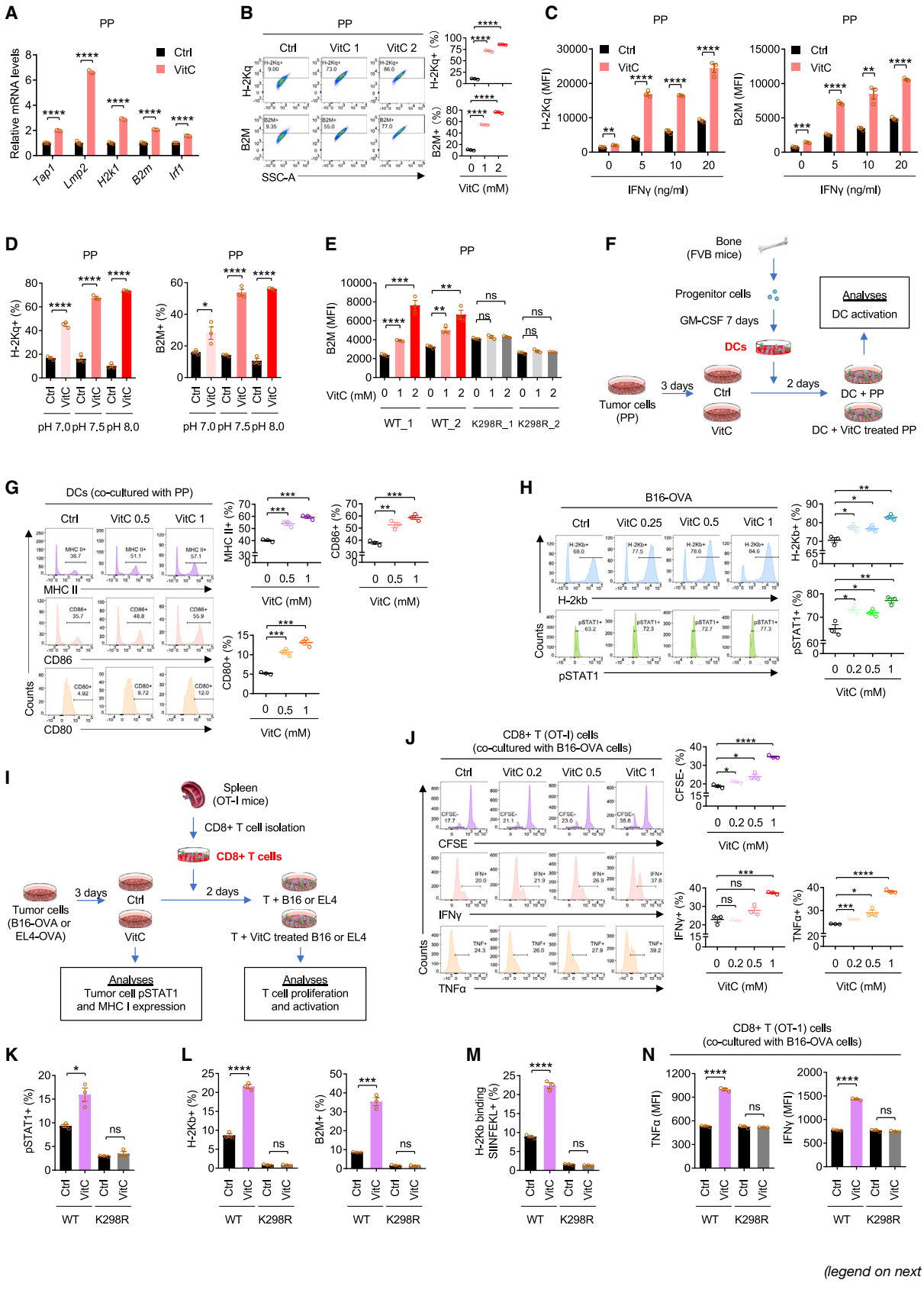
Since STAT1 phosphorylation and activation lead to IFN-mediated antigen processing and presentation in cells,[74] we analyzed related gene expression using real-time quantitative polymerase chain reaction (qPCR) and assessed major histocompatibility complex (MHC)/human leukocyte antigen (HLA) class I expression by flow cytometry. VitC treatment upregulated multiple antigen processing and presentation genes in both PP cells (*Tap1*, *Lmp2*, *H2k1*, *B2m*, and *Irf1*) and Cal-51 cells (*HLA-B*, *TAP1*, *TAP2*, *LMP2*, and *B2M*) (Figures 5A and S6A). Additionally, vitC enhanced MHC/HLA class I expression across various cancer cell lines, but not in the STAT1 deficient AGS cells (Figures 5B and S6B–S6D), and augmented IFN-γ-induced MHC/HLA class I expression (Figures 5C and S6E). Consistent with the pH-dependent pattern of vitcylation and pSTAT1 (Figures S2J, S4N, and S4O), MHC/HLA class I expression also showed pH-dependent pattern (Figures 5D and S6F). Moreover, STAT1 knockout (KO) eliminated vitC-induced MHC/HLA class I expression, which was rescued by STAT1-WT but not the STAT1-K298R mutant (Figures 5E and S6G). These results suggest that STAT1 vitcylation contributes to STAT1 activation and MHC/HLA class I upregulation, revealing vitcylation's role in modulating antigen processing and presentation pathways.

Previous studies showed that vitC functions through modulating ROS levels and acting as a cofactor for TET enzymes and hypoxia-inducible factor 1-alpha (HIF1α) prolyl hydroxylases (PHDs).[4,11,33,75–79] To assess whether these mechanisms contribute to increased MHC/HLA class I expression, we measured ROS levels alongside MHC/HLA class I expression

(G) Stability changes in Rosetta energy unit (REU) of STAT1 caused by K298 vitcylation and K298N mutation as determined by the Rosetta atom energy function model system.

(H) Structures of wild-type and K298 vitcylated pSTAT1 in the antiparallel dimer conformation from the last snapshot of MD simulation. Vitcyl-K298 loses the salt bridges of K298/E281 and K298/E284 in STAT1.

See also Figure S5.



(legend on next page)

at various vitC concentrations. While high-dose vitC (2 mM) increased ROS levels, lower doses (0.1–1 mM) reduced ROS levels (Figure S6H), consistent with vitC's dual antioxidative/pro-oxidative properties.[80–82] However, MHC/HLA class I expression increased linearly with vitC concentration (Figure S6H), suggesting that ROS modulation is not the primary mechanism for this effect. To determine the potential role of TET or PHD enzymes, we used specific inhibitors Bobcat 339 for TET and IOX2 for PHD.[83,84] While these inhibitors effectively reduced TET activity and increased HIF1α levels, respectively (Figures S6I and S6J), they did not affect vitC-induced increase in pSTAT1 and MHC/HLA class I expression (Figure S6K). These results suggest that the vitC's effects on STAT1 phosphorylation and MHC/HLA class I expression occur independently of ROS, TET, or PHD pathways, supporting a more direct mechanism through STAT1 vitcylation.

We next investigated vitC's impact on tumor-immune cell interactions through co-cultured experiments (Figure 5F). When vitC-pretreated PP cells were co-cultured with dendritic cells (DCs) derived from naive syngeneic Friend Virus B (FVB) mice, we observed DC activation through increased MHC class II (MHC II) and co-stimulatory molecules CD86 and CD80 (Figures 5G and S6L).[85,86] To further examine functional consequences of vitC-induced MHC/HLA class I expression, we employed ovalbumin (OVA)-expressing mouse tumor cell lines, B16-OVA and EL4-OVA.[74] VitC treatment increased pSTAT1 and MHC I expression in these cells (Figures 5H and S6M). Co-culture of vitC-pretreated B16-OVA or EL4-OVA cells with MHC I-restricted OVA-specific $CD8^+$ T cells harvested from OT-I mice (Figure 5I) showed increased $CD8^+$ T cell proliferation and anti-tumor cytokine production, including IFN-γ and tumor necrosis factor-α (TNF-α) (Figures 5J and S6N–S6P).[74] Importantly, STAT1-K298R mutation in B16-OVA cells eliminated vitC-induced effects: STAT1 phosphorylation (Figures 5K and S6Q), MHC I expression (Figure 5L), OVA peptide presentation (Figure 5M), and OT-I $CD8^+$ T cell activation in the co-culture system (Figure 5N). This suggests that vitC triggers tumor cell immunogenicity through STAT1 vitcylation.

To validate that STAT1 vitcylation induces tumor cell immunogenicity independently of TET2 and HIF1α, we generated TET2 and HIF1α KO B16-OVA cells (Figure S6R). Neither TET2-KO nor HIF1α-KO significantly affected vitC-induced changes in pSTAT1 levels (Figure S6S), OVA peptide presentation (Figure S6T), and MHC I expression (Figure S6U). TET2-KO also did not impact MHC I-related gene transcription (Figure S6V). Furthermore, in co-culture experiments with OT-I-derived $CD8^+$ T cells, neither TET2-KO nor HIF1α-KO significantly affected vitC-induced T cell activation (Figure S6W). These results suggest that vitC regulates STAT1 activity and tumor cell immunogenicity independent of TET2 and HIF1α pathways. Together, these results demonstrate that STAT1 vitcylation enhances tumor cell immunogenicity and immune cell activation through a pathway distinct from vitC's known mechanisms.

STAT1 vitcylation triggers anti-tumor immunity *in vivo*

We next investigated vitC's roles on tumors and tumor-immune microenvironment *in vivo* using mice bearing mouse E0771 tumor transplants treated with vitC via intraperitoneal injection (4 g/kg/day). VitC treatment suppressed tumor growth and prolonged survival in immunocompetent syngeneic mice (Figures 6A–6C), but not in immunocompromised mice (Figures 6D and 6E). VitC-induced vitcylation in both tumor cells and immune cells within the tumor microenvironment (Figures 6F

Figure 5. Vitcylation of STAT1 K298 enhances the expression of MHC/HLA class I and promotes immunogenicity in tumor cells

(A) Quantitative PCR analysis of antigen processing and presentation gene expression in PP cells ($n = 3$) treated with either vehicle or 2 mM vitC for 2 days. Data are represented as mean ± SEM. $^{****}p < 0.0001$.

(B) Representative flow cytometry plots (left) and quantifications (right) of MHC I expression on PP cells cultured in varying concentrations of vitC for 2 days ($n = 3$). Data are represented as mean ± SEM. $^{****}p < 0.0001$.

(C) Flow cytometric analysis of MHC I expression on PP cells cultured in varying concentrations of IFN-γ (100 ng/mL, 24 h) with or without 2 mM vitC for 2 days ($n = 3$). Data are represented as mean ± SEM. $^{*}p < 0.05$, $^{***}p < 0.001$, $^{****}p < 0.0001$.

(D) Flow cytometric analysis of MHC I expression on PP cells cultured in different pH mediums with or without 2 mM vitC for 2 days ($n = 3$). Data are represented as mean ± SEM. $^{*}p < 0.05$, $^{****}p < 0.0001$.

(E) Flow cytometric analysis of MHC I expression on PP-sgSTAT1_1 cell overexpressing with STAT1-WT-GFP (2 single clones) or STAT1-K298R-GFP (2 single clones) cultured in varying concentrations of vitC for 2 days ($n = 3$). Data are represented as mean ± SEM. $^{**}p < 0.01$, $^{***}p < 0.001$, $^{****}p < 0.0001$.

(F) Workflow for co-culturing of vitC-treated PP cells with bone marrow-derived DCs.

(G) Flow cytometry analysis of DCs co-cultured with vitC-pretreated PP cells. DCs ($CD45^+$ $CD11c^+$) were plotted, and quantifications of MHC II^+, $CD86^+$, and $CD80^+$ were used to identify DC activity ($n = 3$). Data are represented as mean ± SEM. $^{**}p < 0.01$, $^{***}p < 0.001$.

(H) Flow cytometric analysis of H-2Kb and pSTAT1 expression on B16-OVA cells treated with varying doses of vitC for 3 days ($n = 3$). Data are represented as mean ± SEM. $^{*}p < 0.05$, $^{**}p < 0.01$.

(I) Workflow for co-culturing of vitC-treated B16-OVA or EL4-OVA cells with OT-I mice spleen-derived $CD8^+$ T cells.

(J) Flow cytometric analysis of OT-I $CD8^+$ T cells co-cultured with B16-OVA cells pretreated with 2 mM vitC. T cells ($CD45^+$ $CD3^+$ $CD8^+$) proliferation and activity were quantified as $CFSE^-$ and IFN-γ^+, TNF-α^+ cells, respectively ($n = 3$). Data are represented as mean ± SEM. $^{*}p < 0.05$, $^{***}p < 0.001$, $^{****}p < 0.0001$.

(K) Flow cytometric analysis of pSTAT1 in B16-OVA-sgSTAT1 cells re-expressing STAT1-WT-GFP or STAT1-K298R-GFP treated with vitC for 3 days ($n = 3$). Data are represented as mean ± SEM. $^{*}p < 0.05$.

(L) Flow cytometric analysis of MHC I expression on B16-OVA-sgSTAT1 cells re-expressing STAT1-WT-GFP or STAT1-K298R-GFP treated with vitC for 3 days ($n = 3$). Data are represented as mean ± SEM. $^{***}p < 0.001$, $^{****}p < 0.0001$.

(M) Flow cytometric analysis of H-2Kb binding SIINFEKL peptide on B16-OVA-sgSTAT1 cells re-expressing STAT1-WT-GFP or STAT1-K298R-GFP treated with vitC for 3 days ($n = 3$). Data are represented as mean ± SEM. $^{****}p < 0.0001$.

(N) Flow cytometric analysis of OT-I $CD8^+$ T cells co-cultured with B16-OVA-sgSTAT1 cells re-expressing STAT1-WT-GFP or STAT1-K298R-GFP pretreated with 2 mM vitC. T cells ($CD45^+$ $CD3^+$ $CD8^+$) activity was quantified ($n = 3$). Data are represented as mean ± SEM. $^{****}p < 0.0001$.

See also Figure S6.

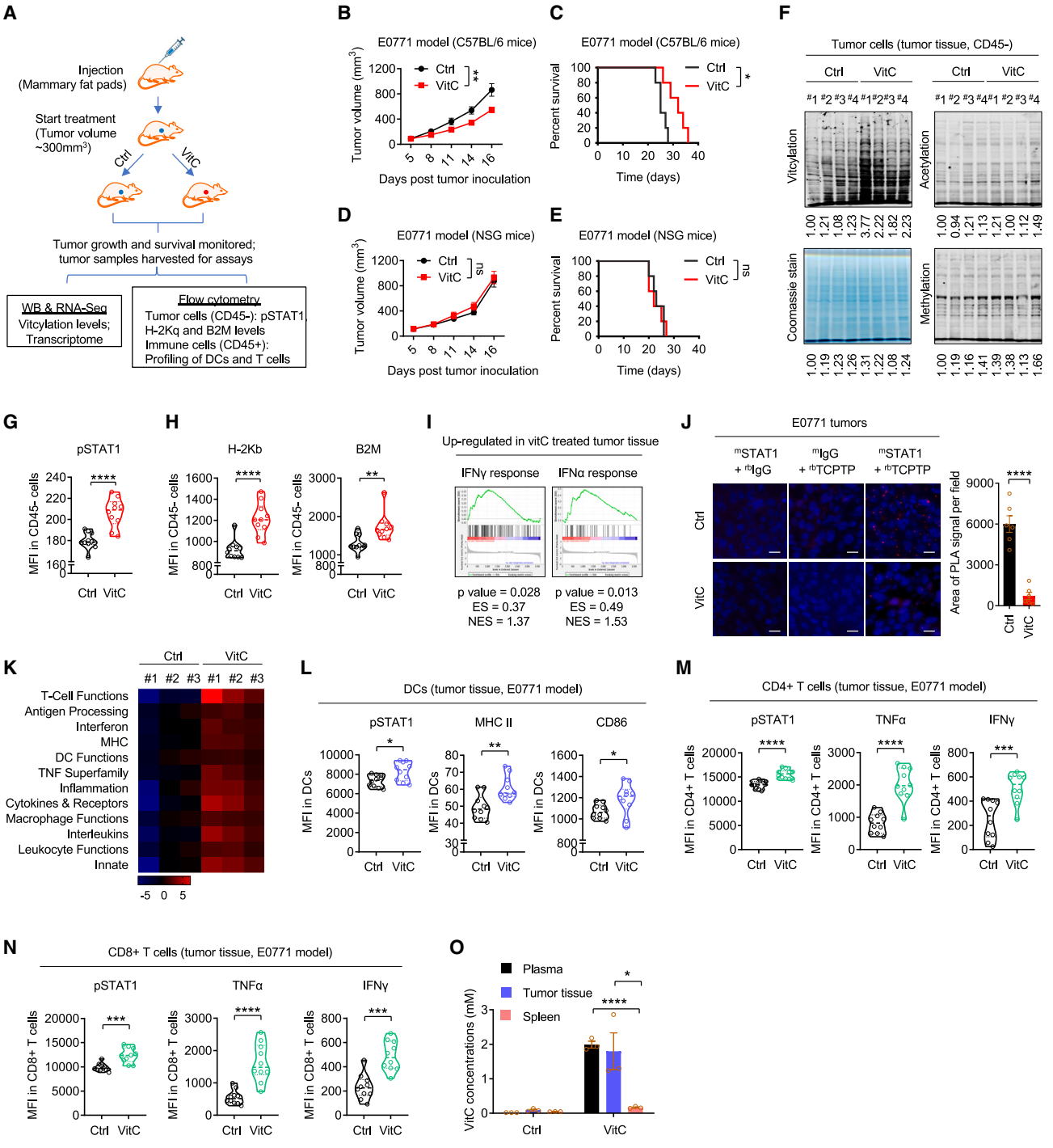


Figure 6. VitC induces vitcylation in tumor cells *in vivo* with increased STAT1-mediated immune responses

(A) Workflow for monitoring tumor growth, as well as analyzing vitcylation levels and immune cell infiltration in tumors *in vivo*. Tumor cells were injected into the mammary fat pads of syngeneic female mice. Tumor-bearing mice were administered vitC (i.p. 4 g/kg/day) when tumor volume reached approximately 300 mm^3. Following treatment, tumor growth and survival were monitored, and tumor tissues were harvested for analysis.

(B and C) Tumor growth (B) and survival (C) of E0771 allografts in C57BL/6 mice treated with vitC were analyzed (vehicle, $n = 5$; vitC treated, $n = 5$).

(D and E) Tumor growth (D) and survival (E) of E0771 allografts in NSG mice treated with vitC was analyzed, and results were compared between the vehicle group and the vitC-treated group (vehicle, $n = 5$; vitC treated, $n = 5$).

(F) Lysine vitcylation, acetylation, and methylation levels of tumor cells ($CD45^-$) in E0771 tumors were measured by WB ($n = 4$ for each group). Protein levels were normalized by Coomassie staining.

(legend continued on next page)

and S7A), with minimal effects on splenic immune cells (Figure S7B).

Consistent with *in vitro* findings, vitC treatment increased pSTAT1 (Figure 6G), MHC I expression (Figure 6H), and IFN responses (Figure 6I; Table S6), while impairing STAT1-TCPTP interaction in tumor cells (Figure 6J). NanoString analysis revealed enhanced antigen processing gene expression in immune cells (Figure 6K). VitC treatment significantly activated tumor-infiltrating DCs and T cells (Figures 6L–6N, S7C, and S7D) but had minimal effects on immune cells in the spleen and lymph nodes (Figures S7E–S7L). Notably, high-dose vitC administration accumulated significantly in tumor tissues and plasma but remained relatively low in the spleen (Figure 6O), consistent with previous reports.[87–90] This suggests selective tumor uptake of vitC enhances anti-tumor immunity without systemic immune activation. Similar results were observed in PP tumor-bearing syngeneic mice treated with vitC (Figures S7M–S7S).

To validate the importance of STAT1 vitcylation and phosphorylation in vitC-triggered anti-tumor immunity, we performed *in vivo* experiments utilizing tumor cells harboring the STAT1-K298R or STAT1-Y701A mutations. Both mutations abolished vitC-induced tumor growth suppression (Figure S7T) and impaired pSTAT1 and MHC I expression (Figures 7A and 7B). They also prevented the production of STAT1-targeted immunosuppressive molecules indoleamine 2,3-dioxygenase 1 (IDO1) and programmed death-ligand 1 (PD-L1) in tumor cells (Figure S7U) and blocked immune cell activation in the tumor microenvironment (Figures 7C, S7V, and S7W). These findings suggest that vitC's anti-tumor effects require both STAT1 vitcylation at K298 and phosphorylation at Y701.

To investigate whether vitC regulates STAT1 independently of TET2 or HIF1α in tumor suppression, we conducted *in vivo* experiments using TET2-KO and HIF1α-KO B16-OVA tumor cells (Figure 7D). Notably, neither TET2-KO nor HIF1α-KO negated vitC's effects on tumor suppression (Figures 7E and 7F), pSTAT1 levels (Figure S7X), OVA peptide presentation (Figure S7Y), or immune cell activation in the tumor microenvironment (Figure S7Z). By contrast, STAT1-K298R mutation abolished all these vitC-induced effects (Figures 7G–7K). These results suggest that STAT1 vitcylation mediates anti-tumor effects through a pathway independent of TET2 or HIF1α.

Given vitC's anti-tumor effects, we explored its potential to enhance immune checkpoint therapy. We treated E0771 tumor-bearing mice with vitC and anti-Programmed cell death protein 1 (PD1), alone or in combination. The combination treatment more effectively suppressed tumor growth than either agent alone (Figures 7L and S7AA), suggesting that high-dose vitC can enhance immunotherapy responses.

In summary, our studies reveal that vitC-induced STAT1 vitcylation enhances STAT1 phosphorylation, leading to increased antigen processing and presentation in tumor cells. This, in turn, activates various immune cells, including DCs and T cells, in the tumor microenvironment, triggering STAT1-mediated anti-tumor immunity. These findings provide a mechanistic explanation for vitC's role in enhancing anti-tumor-immune responses and suggest promising therapeutic strategies combining vitC with immunotherapy.

DISCUSSION

The evolutionary loss of vitC synthesis in humans through L-gulonolactone oxidase gene (encoding the enzyme responsible for converting glucose to vitC) raises intriguing questions about high-dose vitC supplementation's necessity and safety. However, this change does not necessarily imply that high vitC intake is harmful. The mutation amid complex evolutionary pressures and environmental factors, and humans may have retained the ability to benefit from varying dietary vitC levels. Evolution often produces adequate rather than perfect solutions for survival. While losing vitC synthesis ability may have been advantageous in the ancestral environment, this does not preclude benefits from higher intake in our modern context, given the drastically different environmental and dietary conditions we face today. Therefore, while evolutionary history provides valuable context, it alone cannot determine the harm or benefit of high vitC intake. The effects of high-dose vitC supplementation should be evaluated based on current scientific evidence, considering modern human physiology and health challenges.

This study reveals that vitC directly modifies lysine residues in peptides and proteins through vitcylation, a process occurring across a broader pH range, peaking around pH 9–10. The pH and dose dependence suggest that high-dose vitC may offer distinct therapeutic effects compared with lower doses.

The discovery of lysine vitcylation opens new possibilities for biomarker development in various conditions. Analysis of specific vitcylated proteins and their modification patterns could reveal unique signatures associated with certain diseases or physiological states. These signatures could serve as diagnostic tools or biomarkers for monitoring treatment responses,

(G and H) Flow cytometry analysis of pSTAT1 (G) and MHC I expression (H) on E0771 tumor cells ($CD45^-$) from vehicle- or vitC-treated mice (vehicle, $n = 10$; vitC treated, $n = 10$). Data are represented as mean ± SEM. $^{**}p < 0.01$, $^{****}p < 0.0001$.

(I) Top-ranked upregulated GSEA signatures in the tumor tissue of vitC-treated E0771 tumor-bearing mice at 7 days ($n = 2$).

(J) STAT1-TCPTP PLA analysis (left) and quantification (right) were performed on formalin-fixed paraffin-embedding (FFPE) preparations of E0771 tumor tissues (scale bar, 20 μM).

(K) Gene signatures associated with immune cells ($CD45^+$) in E0771 tumors that were enriched following vitC treatment were analyzed by NanoString.

(L) Flow cytometry analysis of the pSTAT1 level, MHC II, and CD86 expression in DCs in E0771 tumor tissue from vehicle- or vitC-treated mice (vehicle, $n = 9$; vitC treated, $n = 9$). Data are represented as mean ± SEM. $^{*}p < 0.05$, $^{**}p < 0.01$.

(M and N) Flow cytometry analysis of pSTAT1 level, TNF-α, and IFN-γ expression in $CD4^+$ T cells (M) and $CD8^+$ T cells (N) in E0771 tumor tissue from vehicle- or vitC-treated mice (vehicle, $n = 9$; vitC treated, $n = 9$). Data are represented as mean ± SEM. $^{***}p < 0.001$, $^{****}p < 0.0001$.

(O) VitC concentrations were analyzed in the plasma, tumor tissue, and spleen of vehicle- or vitC-treated E0771 tumor-bearing C57BL/6 mice (vehicle, $n = 3$; vitC treated, $n = 3$). Data are represented as mean ± SEM. $^{*}p < 0.05$, $^{****}p < 0.0001$.

See also Figure S7 and Table S6.

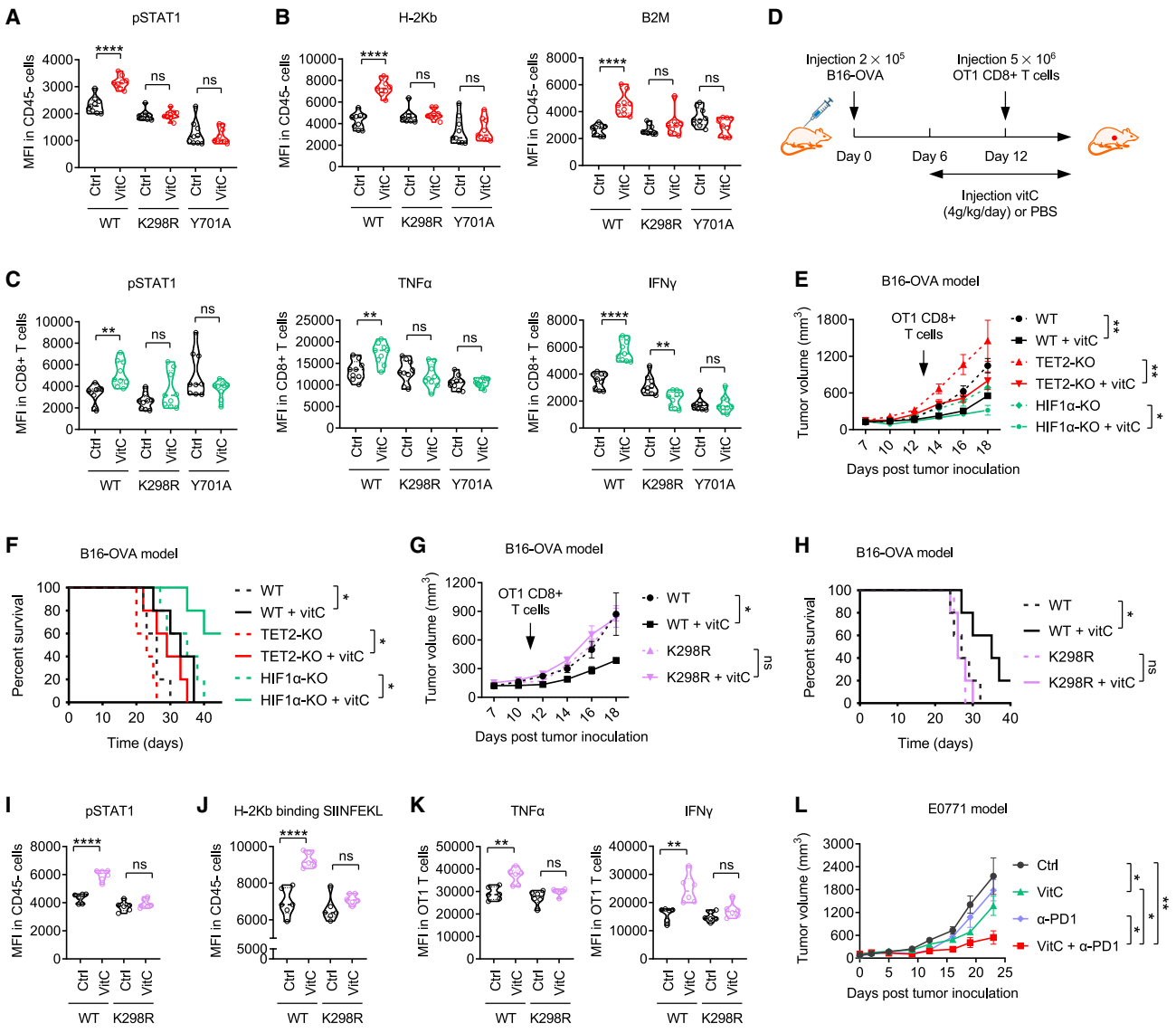


Figure 7. VitC modulates the immune milieu via STAT1 vitcylation

(A and B) Flow cytometry analysis of pSTAT1 (A) and MHC I expression (B) on the xenografts of PP-sgSTAT1_1 tumor cells re-expressing STAT1-WT-GFP, STAT1-K298R-GFP, or STAT1-Y701A-GFP treated with vehicle or vitC (vehicle, $n = 9$; vitC treated, $n = 9$). Data are represented as mean ± SEM. $^{****}p < 0.0001$.

(C) Flow cytometry analysis of pSTAT1 level, TNF-α, and IFN-γ expression in $CD8^+$ T cells on the xenografts of PP-sgSTAT1_1 tumor cells re-expressing STAT1-WT-GFP, STAT1-K298R-GFP, or STAT1-Y701A-GFP treated with vehicle or vitC (vehicle, $n = 9$; vitC treated, $n = 9$). Data are represented as mean ± SEM. $^{**}p < 0.01$, $^{****}p < 0.0001$.

(D) Workflow for analyzing tumor growth, pSTAT1, OVA peptide presentation, and immune cell infiltration in the xenografts of B16-OVA, B16-OVA (TET2-KO), and B16-OVA (HIF1α-KO) tumor cells treated with vehicle or vitC *in vivo*.

(E and F) Tumor growth (E) and survival (F) of the xenografts of B16-OVA, B16-OVA (TET2-KO), and B16-OVA (HIF1α-KO) tumor cells treated with vehicle or vitC (vehicle, $n = 5$; vitC treated, $n = 5$).

(G) Tumor growth of the xenografts of B16-OVA (STAT1-WT) and B16-OVA (STAT1-K298R) tumor cells treated with vehicle or vitC (vehicle, $n = 5$; vitC treated, $n = 5$). Data are represented as mean ± SEM. $^{*}p < 0.05$.

(H) Survival of the xenografts of B16-OVA (STAT1-WT) and B16-OVA (STAT1-K298R) tumor cells treated with vehicle or vitC (vehicle, $n = 5$; vitC treated, $n = 5$). Data are represented as mean ± SEM. $^{*}p < 0.05$.

(I and J) Flow cytometry analysis of pSTAT1 (I) and OVA peptide presentation (J) on the xenografts of B16-OVA (STAT1-WT) and B16-OVA (STAT1-K298R) tumor cells treated with vehicle or vitC (vehicle, $n = 6$; vitC treated, $n = 6$). Data are represented as mean ± SEM. $^{****}p < 0.0001$.

(legend continued on next page)

particularly valuable in cancer, where determining appropriate vitC dosage and monitoring treatment effects remain challenging.

Our understanding of STAT1 regulation has been enhanced by findings on K298 vitcylation. This modification destabilizes pSTAT1's anti-parallel conformation, which is crucial for TCPTP binding and dephosphorylation. Consequently, this leads to elevated pSTAT1 levels and enhanced IFN-mediated immune responses. Interestingly, the disease-causing STAT1-K298N mutation in autoimmune conditions shares a similar molecular mechanism with STAT1-vitcyl-K298. However, their biological effects differ significantly: while K298N mutation causes chronic immune activation contributing to autoimmune disease, K298-vitcylation temporarily augments immune response in a manner that can be beneficial for combating pathological conditions, such as cancer and viral infections.

Our study addressed concerns about high-dose vitC's systemic toxicity and physiological relevance. We observed that vitC accumulates preferentially in tumor tissues and plasma while maintaining relatively low in the spleen, suggesting a favorable pharmacokinetic profile for cancer treatment. These findings support the renewed interest in high-dose vitC as an anticancer agent. Clinical trials have demonstrated its safety and tolerability, showing promise both as a standalone treatment and in combination therapy.[6,91,92] Moreover, vitC has shown benefit in mitigating chemotherapy side effects and improving quality of life for cancer patients, including those in palliative care.[93,94]

The identification of vitcylation as a distinctive PTM provides significant insights into vitC's role in protein regulation and cellular function. This discovery expands our understanding of how protein modifications contribute to health and disease, while highlighting vitC's importance as a regulatory molecule in the complex interplay between nutrients, cellular processes, and overall physiology. Further research will be crucial to fully elucidate the extent of vitcylation and its relevance in biological processes. This may lead to the discovery of new biomarkers and therapeutic targets, thereby deepening our understanding of vitC's health benefits. These insights could fundamentally change our approach to nutritional biochemistry and medical treatment, offering new perspectives on the intersection of nutrition and health.

Limitations of the study

While we identify lysine vitcylation as a vitC-responsive modification, several aspects require further investigation. At the molecular and cellular level, we need to explore the pathological significance of diverse vitcylated proteins, understand the role of enhanced mitochondrial protein vitcylation and determine potential enzymatic regulation and substrate specificity mechanisms.

In terms of tumor and immune effects, single-cell sequencing analysis is needed to fully characterize vitC's impact on different cell populations. Additional studies should examine vitC's influence on tumor cell behavior (growth, proliferation, invasion, and metastasis) and antigen presentation in non-tumor cells, as well as the balance between local and systemic immune responses. Understanding these areas will be crucial for realizing the therapeutic potential of vitC-based therapeutic strategies in cancer and other diseases. Particularly important is determining how vitC's targeting specificity influences its differential effects on tumor growth versus immune activation.

RESOURCE AVAILABILITY

Lead contact

Further information and requests for resources and reagents should be directed to and will be fulfilled by the lead contact, Jean J. Zhao (jean_zhao@dfci.harvard.edu).

Materials availability

Plasmids generated in this study are available from the lead contact upon request.

Data and code availability

This paper does not report original code. Any additional information required to reanalyze the data reported in this paper is available from the lead contact upon request.

ACKNOWLEDGMENTS

This work was supported in part by grants from the Department of Defense Breast Cancer Research Program Breakthrough award HT9425-23-1-0026 (Q.W.), the Breast Cancer Research Foundation BCRF-24-179 (J.J.Z.), and the National Institutes of Health (NIH) P50 CA168504 (J.J.Z.) and CA210057 (J.J.Z.). The graphical abstract was created with BioRender.com.

AUTHOR CONTRIBUTIONS

X.H. and J.J.Z. conceived of and designed the study. X.H. performed most of the experiments. Q.W., X.C., T.J., Y.L., Y.N., and W.W. assisted with *in vivo* treatments. Y.W. and J.W. assisted with structure analysis. S.X. conducted transcriptomic assays. J.M.A., G.F., L.S., and J.L. performed mass spectrometric analysis. Q.W. and H.G. assisted with flow cytometry. J.Z. and S.L. performed the thermostability change calculation. J.S.B., B.X., F.C., and Q.W. provided critical materials. Y.W., J.W., Q.W., J.S.B., K.Z., and L.C.C. contributed to scientific discussions. J.J.Z. directed the research and oversaw the experiments. X.H. and J.J.Z. wrote the manuscript with assistance from other authors.

DECLARATION OF INTERESTS

Q.W. is a scientific consultant for Crimson Biopharm Inc. J.S.B. is a scientific consultant for Geode Therapeutics Inc. L.C.C. is a co-founder and scientific advisory board member of Agios Pharmaceuticals, Faeth Therapeutics, Petra Pharma Corporation, Larkspur Therapeutics, and Volastra Pharmaceuticals and a scientific advisory board member for Scorpion Therapeutics. J.J.Z. is

(K) Flow cytometry analysis of TNF-α and IFN-γ expression in OT1 CD8$^+$ T cells on the xenografts of B16-OVA-sgSTAT1 tumor cells re-expressing STAT1-WT-GFP or STAT1-K298R-GFP treated with vehicle or vitC (vehicle, $n = 6$; vitC treated, $n = 6$). Data are represented as mean ± SEM. $^{**}p < 0.01$.

(L) Tumor growth of E0771 allografts in C57BL/6 mice treated with vitC as a single agent or in combination with anti-PD1 antibody ($n = 4$). Data are represented as mean ± SEM. $^{*}p < 0.05$, $^{**}p < 0.01$.

See also Figure S7.

co-founder and director of Crimson Biopharm Inc. and Geode Therapeutics Inc.

STAR★METHODS

Detailed methods are provided in the online version of this paper and include the following:

- KEY RESOURCES TABLE
- EXPERIMENTAL MODEL AND STUDY PARTICIPANT DETAILS
  - Cell lines
  - Animals
- METHOD DETAILS
  - *In vitro* vitcylation reaction
  - Liquid chromatography-tandem mass spectrometry analysis
  - Quantifications of targeted vitcylation peptides
  - Transcriptome methodology
  - Bioinformatic analysis
  - Flow cytometry
  - Western blots
  - Dot-blot assays
  - Thermostability change calculation
  - Cellular levels of vitC, ROS, and TET activity assay
  - Preparation of pan-specific anti-vitcyllysine polyclonal antibody
  - Proximity ligation assay (PLA)
  - Measurement of *in vivo* vitC concentrations by HPLC-MS
  - Real-time qPCR
  - Generation of mouse DCs
  - Co-culture experiments
  - Generation of STAT1, TET2 and HIF1α deficient cells
  - Co-immunoprecipitation (Co-IP) and immunoprecipitation (IP)
  - Immunofluorescence
- QUANTIFICATION AND STATISTICAL ANALYSIS

SUPPLEMENTAL INFORMATION

Supplemental information can be found online at https://doi.org/10.1016/j.cell.2025.01.043.

Received: June 23, 2023
Revised: January 4, 2025
Accepted: January 30, 2025
Published: February 28, 2025

REFERENCES

1. Nishikimi, M., and Yagi, K. (1991). Molecular basis for the deficiency in humans of gulonolactone oxidase, a key enzyme for ascorbic acid biosynthesis. Am. J. Clin. Nutr. *54*, 1203S–1208S. https://doi.org/10.1093/ajcn/54.6.1203s.
2. Meisel, K., Daggubati, S., and Josephson, S.A. (2015). Scurvy in the 21st century?: vitamin C deficiency presenting to the neurologist. Neurol. Clin. Pract. *5*, 491–493. https://doi.org/10.1212/CPJ.0000000000000158.
3. Ngo, B., Van Riper, J.M., Cantley, L.C., and Yun, J. (2019). Targeting cancer vulnerabilities with high-dose vitamin C. Nat. Rev. Cancer *19*, 271–282. https://doi.org/10.1038/s41568-019-0135-7.
4. Chen, Q., Espey, M.G., Krishna, M.C., Mitchell, J.B., Corpe, C.P., Buettner, G.R., Shacter, E., and Levine, M. (2005). Pharmacologic ascorbic acid concentrations selectively kill cancer cells: action as a pro-drug to deliver hydrogen peroxide to tissues. Proc. Natl. Acad. Sci. USA *102*, 13604–13609. https://doi.org/10.1073/pnas.0506390102.
5. Chen, Q., Espey, M.G., Sun, A.Y., Lee, J.H., Krishna, M.C., Shacter, E., Choyke, P.L., Pooput, C., Kirk, K.L., Buettner, G.R., et al. (2007). Ascorbate in pharmacologic concentrations selectively generates ascorbate radical and hydrogen peroxide in extracellular fluid in vivo. Proc. Natl. Acad. Sci. USA *104*, 8749–8754. https://doi.org/10.1073/pnas.0702854104.
6. Chen, Q., Espey, M.G., Sun, A.Y., Pooput, C., Kirk, K.L., Krishna, M.C., Khosh, D.B., Drisko, J., and Levine, M. (2008). Pharmacologic doses of ascorbate act as a prooxidant and decrease growth of aggressive tumor xenografts in mice. Proc. Natl. Acad. Sci. USA *105*, 11105–11109. https://doi.org/10.1073/pnas.0804226105.
7. Böttger, F., Vallés-Martí, A., Cahn, L., and Jimenez, C.R. (2021). High-dose intravenous vitamin C, a promising multi-targeting agent in the treatment of cancer. J. Exp. Clin. Cancer Res. *40*, 343. https://doi.org/10.1186/s13046-021-02134-y.
8. Magrì, A., Germano, G., Lorenzato, A., Lamba, S., Chilà, R., Montone, M., Amodio, V., Ceruti, T., Sassi, F., Arena, S., et al. (2020). High-dose vitamin C enhances cancer immunotherapy. Sci. Transl. Med. *12*, eaay8707. https://doi.org/10.1126/scitranslmed.aay8707.
9. Verrax, J., and Calderon, P.B. (2009). Pharmacologic concentrations of ascorbate are achieved by parenteral administration and exhibit antitumoral effects. Free Radic. Biol. Med. *47*, 32–40. https://doi.org/10.1016/j.freeradbiomed.2009.02.016.
10. Espey, M.G., Chen, P., Chalmers, B., Drisko, J., Sun, A.Y., Levine, M., and Chen, Q. (2011). Pharmacologic ascorbate synergizes with gemcitabine in preclinical models of pancreatic cancer. Free Radic. Biol. Med. *50*, 1610–1619. https://doi.org/10.1016/j.freeradbiomed.2011.03.007.
11. Ma, Y., Chapman, J., Levine, M., Polireddy, K., Drisko, J., and Chen, Q. (2014). High-dose parenteral ascorbate enhanced chemosensitivity of ovarian cancer and reduced toxicity of chemotherapy. Sci. Transl. Med. *6*, 222ra18. https://doi.org/10.1126/scitranslmed.3007154.
12. Serrano, O.K., Parrow, N.L., Violet, P.C., Yang, J., Zornjak, J., Basseville, A., and Levine, M. (2015). Antitumor effect of pharmacologic ascorbate in the B16 murine melanoma model. Free Radic. Biol. Med. *87*, 193–203. https://doi.org/10.1016/j.freeradbiomed.2015.06.032.
13. Xia, J., Xu, H., Zhang, X., Allamargot, C., Coleman, K.L., Nessler, R., Frech, I., Tricot, G., and Zhan, F. (2017). Multiple myeloma tumor cells are selectively killed by pharmacologically-dosed ascorbic acid. EBioMedicine *18*, 41–49. https://doi.org/10.1016/j.ebiom.2017.02.011.
14. Yun, J., Mullarky, E., Lu, C., Bosch, K.N., Kavalier, A., Rivera, K., Roper, J., Chio, I.I.C., Giannopoulou, E.G., Rago, C., et al. (2015). Vitamin C selectively kills KRAS and BRAF mutant colorectal cancer cells by targeting GAPDH. Science *350*, 1391–1396. https://doi.org/10.1126/science.aaa5004.
15. Di Tano, M., Raucci, F., Vernieri, C., Caffa, I., Buono, R., Fanti, M., Brandhorst, S., Curigliano, G., Nencioni, A., de Braud, F., et al. (2020). Synergistic effect of fasting-mimicking diet and vitamin C against KRAS mutated cancers. Nat. Commun. *11*, 2332. https://doi.org/10.1038/s41467-020-16243-3.
16. Aguilera, O., Muñoz-Sagastibelza, M., Torrejón, B., Borrero-Palacios, A., Del Puerto-Nevado, L., Martínez-Useros, J., Rodriguez-Remirez, M., Zazo, S., García, E., Fraga, M., et al. (2016). Vitamin C uncouples the Warburg metabolic switch in KRAS mutant colon cancer. Oncotarget *7*, 47954–47965. https://doi.org/10.18632/oncotarget.10087.
17. Agathocleous, M., Meacham, C.E., Burgess, R.J., Piskounova, E., Zhao, Z., Crane, G.M., Cowin, B.L., Bruner, E., Murphy, M.M., Chen, W., et al. (2017). Ascorbate regulates haematopoietic stem cell function and leukaemogenesis. Nature *549*, 476–481. https://doi.org/10.1038/nature23876.
18. Cimmino, L., Dolgalev, I., Wang, Y., Yoshimi, A., Martin, G.H., Wang, J., Ng, V., Xia, B., Witkowski, M.T., Mitchell-Flack, M., et al. (2017). Restoration of TET2 function blocks aberrant self-renewal and leukemia progression. Cell *170*, 1079–1095.e20. https://doi.org/10.1016/j.cell.2017.07.032.
19. Liu, M., Ohtani, H., Zhou, W., Ørskov, A.D., Charlet, J., Zhang, Y.W., Shen, H., Baylin, S.B., Liang, G., Grønbæk, K., et al. (2016). Vitamin C increases viral mimicry induced by 5-aza-2'-deoxycytidine. Proc. Natl. Acad. Sci. USA *113*, 10238–10244. https://doi.org/10.1073/pnas.1612262113.

20. Shenoy, N., Bhagat, T., Nieves, E., Stenson, M., Lawson, J., Choudhary, G.S., Habermann, T., Nowakowski, G., Singh, R., Wu, X., et al. (2017). Upregulation of TET activity with ascorbic acid induces epigenetic modulation of lymphoma cells. Blood Cancer J. *7*, e587. https://doi.org/10.1038/bcj.2017.65.

21. Gustafson, C.B., Yang, C., Dickson, K.M., Shao, H., Van Booven, D., Harbour, J.W., Liu, Z.J., and Wang, G. (2015). Epigenetic reprogramming of melanoma cells by vitamin C treatment. Clin. Epigenet. *7*, 51. https://doi.org/10.1186/s13148-015-0087-z.

22. Figueroa-Méndez, R., and Rivas-Arancibia, S. (2015). Vitamin C in health and disease: its role in the metabolism of cells and redox state in the brain. Front. Physiol. *6*, 397. https://doi.org/10.3389/fphys.2015.00397.

23. Du, J., Cullen, J.J., and Buettner, G.R. (2012). Ascorbic acid: chemistry, biology and the treatment of cancer. Biochim. Biophys. Acta *1826*, 443–457. https://doi.org/10.1016/j.bbcan.2012.06.003.

24. Padayatty, S.J., and Levine, M. (2016). Vitamin C: the known and the unknown and Goldilocks. Oral Dis. *22*, 463–493. https://doi.org/10.1111/odi.12446.

25. Smirnoff, N. (2018). Ascorbic acid metabolism and functions: A comparison of plants and mammals. Free Radic. Biol. Med. *122*, 116–129. https://doi.org/10.1016/j.freeradbiomed.2018.03.033.

26. Hasenkopf, K., Rönner, B., Hiller, H., and Pischetsrieder, M. (2002). Analysis of glycated and ascorbylated proteins by gas chromatography-mass spectrometry. J. Agric. Food Chem. *50*, 5697–5703. https://doi.org/10.1021/jf020411u.

27. Linetsky, M., Shipova, E., Cheng, R., and Ortwerth, B.J. (2008). Glycation by ascorbic acid oxidation products leads to the aggregation of lens proteins. Biochim. Biophys. Acta *1782*, 22–34. https://doi.org/10.1016/j.bbadis.2007.10.003.

28. Ahammer, L., Unterhauser, J., Eidelpes, R., Meisenbichler, C., Nothegger, B., Covaciu, C.E., Cova, V., Kamenik, A.S., Liedl, K.R., Breuker, K., et al. (2022). Ascorbylation of a reactive cysteine in the major apple allergen mal d 1. Foods *11*, 2953. https://doi.org/10.3390/foods11192953.

29. Fan, X., and Monnier, V.M. (2008). Inhibition of crystallin ascorbylation by nucleophilic compounds in the hSVCT2 mouse model of lenticular aging. Invest. Ophthalmol. Vis. Sci. *49*, 4945–4952. https://doi.org/10.1167/iovs.08-1813.

30. Walsh, C.T., Garneau-Tsodikova, S., and Gatto, G.J., Jr. (2005). Protein posttranslational modifications: the chemistry of proteome diversifications. Angew. Chem. Int. Ed. Engl. *44*, 7342–7372. https://doi.org/10.1002/anie.200501023.

31. Witze, E.S., Old, W.M., Resing, K.A., and Ahn, N.G. (2007). Mapping protein post-translational modifications with mass spectrometry. Nat. Methods *4*, 798–806. https://doi.org/10.1038/nmeth1100.

32. Keenan, E.K., Zachman, D.K., and Hirschey, M.D. (2021). Discovering the landscape of protein modifications. Mol. Cell *81*, 1868–1878. https://doi.org/10.1016/j.molcel.2021.03.015.

33. Shenoy, N., Creagan, E., Witzig, T., and Levine, M. (2018). Ascorbic acid in cancer treatment: let the phoenix fly. Cancer Cell *34*, 700–706. https://doi.org/10.1016/j.ccell.2018.07.014.

34. Shi, L., and Tu, B.P. (2015). Acetyl-CoA and the regulation of metabolism: mechanisms and consequences. Curr. Opin. Cell Biol. *33*, 125–131. https://doi.org/10.1016/j.ceb.2015.02.003.

35. Detich, N., Hamm, S., Just, G., Knox, J.D., and Szyf, M. (2003). The methyl donor S-adenosylmethionine inhibits active demethylation of DNA: a candidate novel mechanism for the pharmacological effects of S-adenosylmethionine. J. Biol. Chem. *278*, 20812–20820. https://doi.org/10.1074/jbc.M211813200.

36. Nagata, R., Fujihashi, M., Sato, T., Atomi, H., and Miki, K. (2018). Identification of a pyrophosphate-dependent kinase and its donor selectivity determinants. Nat. Commun. *9*, 1765. https://doi.org/10.1038/s41467-018-04201-z.

37. Zhai, Y., Chen, L., Zhao, Q., Zheng, Z.H., Chen, Z.N., Bian, H., Yang, X., Lu, H.Y., Lin, P., Chen, X., et al. (2023). Cysteine carboxyethylation generates neoantigens to induce HLA-restricted autoimmunity. Science *379*, eabg2482. https://doi.org/10.1126/science.abg2482.

38. Lepack, A.E., Werner, C.T., Stewart, A.F., Fulton, S.L., Zhong, P., Farrelly, L.A., Smith, A.C.W., Ramakrishnan, A., Lyu, Y., Bastle, R.M., et al. (2020). Dopaminylation of histone H3 in ventral tegmental area regulates cocaine seeking. Science *368*, 197–201. https://doi.org/10.1126/science.aaw8806.

39. Zhang, D., Tang, Z., Huang, H., Zhou, G., Cui, C., Weng, Y., Liu, W., Kim, S., Lee, S., Perez-Neut, M., et al. (2019). Metabolic regulation of gene expression by histone lactylation. Nature *574*, 575–580. https://doi.org/10.1038/s41586-019-1678-1.

40. Mills, E.L., Ryan, D.G., Prag, H.A., Dikovskaya, D., Menon, D., Zaslona, Z., Jedrychowski, M.P., Costa, A.S.H., Higgins, M., Hams, E., et al. (2018). Itaconate is an anti-inflammatory metabolite that activates Nrf2 via alkylation of KEAP1. Nature *556*, 113–117. https://doi.org/10.1038/nature25986.

41. He, X.D., Gong, W., Zhang, J.N., Nie, J., Yao, C.F., Guo, F.S., Lin, Y., Wu, X.H., Li, F., Li, J., et al. (2018). Sensing and transmitting intracellular amino acid signals through reversible lysine aminoacylations. Cell Metab. *27*, 151–166.e6. https://doi.org/10.1016/j.cmet.2017.10.015.

42. Mo, W., Zhang, L., Yang, G., Zhai, J., Hu, Z., Chen, Y., Chen, X., Hui, L., Huang, R., and Hu, G. (2008). Nuclear beta-arrestin1 functions as a scaffold for the dephosphorylation of STAT1 and moderates the antiviral activity of IFN-gamma. Mol. Cell *31*, 695–707. https://doi.org/10.1016/j.molcel.2008.06.017.

43. ten Hoeve, J., de Jesus Ibarra-Sanchez, M., Fu, Y., Zhu, W., Tremblay, M., David, M., and Shuai, K. (2002). Identification of a nuclear Stat1 protein tyrosine phosphatase. Mol. Cell. Biol. *22*, 5662–5668. https://doi.org/10.1128/MCB.22.16.5662-5668.2002.

44. Wagner, G.R., Bhatt, D.P., O'Connell, T.M., Thompson, J.W., Dubois, L.G., Backos, D.S., Yang, H., Mitchell, G.A., Ilkayeva, O.R., Stevens, R.D., et al. (2017). A class of reactive acyl-CoA species reveals the non-enzymatic origins of protein acylation. Cell Metab. *25*, 823–837.e8. https://doi.org/10.1016/j.cmet.2017.03.006.

45. Zhang, Z., Tan, M., Xie, Z., Dai, L., Chen, Y., and Zhao, Y. (2011). Identification of lysine succinylation as a new post-translational modification. Nat. Chem. Biol. *7*, 58–63. https://doi.org/10.1038/nchembio.495.

46. Perła-Kaján, J., Twardowski, T., and Jakubowski, H. (2007). Mechanisms of homocysteine toxicity in humans. Amino Acids *32*, 561–572. https://doi.org/10.1007/s00726-006-0432-9.

47. Stephenson, C.M., Levin, R.D., Spector, T., and Lis, C.G. (2013). Phase I clinical trial to evaluate the safety, tolerability, and pharmacokinetics of high-dose intravenous ascorbic acid in patients with advanced cancer. Cancer Chemother. Pharmacol. *72*, 139–146. https://doi.org/10.1007/s00280-013-2179-9.

48. Hoffer, L.J., Levine, M., Assouline, S., Melnychuk, D., Padayatty, S.J., Rosadiuk, K., Rousseau, C., Robitaille, L., and Miller, W.H., Jr. (2008). Phase I clinical trial of i.v. ascorbic acid in advanced malignancy. Ann. Oncol. *19*, 1969–1974. https://doi.org/10.1093/annonc/mdn377.

49. Prescott, D.M., Charles, H.C., Poulson, J.M., Page, R.L., Thrall, D.E., Vujaskovic, Z., and Dewhirst, M.W. (2000). The relationship between intracellular and extracellular pH in spontaneous canine tumors. Clin. Cancer Res. *6*, 2501–2505.

50. Hou, Y., Kitaguchi, T., Kriszt, R., Tseng, Y.H., Raghunath, M., and Suzuki, M. (2017). Ca(2+)-associated triphasic pH changes in mitochondria during brown adipocyte activation. Mol. Metab. *6*, 797–808. https://doi.org/10.1016/j.molmet.2017.05.013.

51. Casey, J.R., Grinstein, S., and Orlowski, J. (2010). Sensors and regulators of intracellular pH. Nat. Rev. Mol. Cell Biol. *11*, 50–61. https://doi.org/10.1038/nrm2820.

52. Simpson, D.M., and Beynon, R.J. (2010). Acetone precipitation of proteins and the modification of peptides. J. Proteome Res. *9*, 444–450. https://doi.org/10.1021/pr900806x.

53. Bergholz, J.S., Wang, Q., Wang, Q., Ramseier, M., Prakadan, S., Wang, W., Fang, R., Kabraji, S., Zhou, Q., Gray, G.K., et al. (2023). PI3Kbeta controls immune evasion in PTEN-deficient breast tumours. Nature *617*, 139–146. https://doi.org/10.1038/s41586-023-05940-w.

54. Subbiahanadar Chelladurai, K., Selvan Christyraj, J.D., Rajagopalan, K., Yesudhason, B.V., Venkatachalam, S., Mohan, M., Chellathurai Vasantha, N., and Selvan Christyraj, J.R.S. (2021). Alternative to FBS in animal cell culture - an overview and future perspective. Heliyon *7*, e07686. https://doi.org/10.1016/j.heliyon.2021.e07686.

55. Lee, D.Y., Lee, S.Y., Yun, S.H., Jeong, J.W., Kim, J.H., Kim, H.W., Choi, J.S., Kim, G.D., Joo, S.T., Choi, I., et al. (2022). Review of the current research on fetal bovine serum and the development of cultured meat. Food Sci. Anim. Resour. *42*, 775–799. https://doi.org/10.5851/kosfa.2022.e46.

56. Poburko, D., Santo-Domingo, J., and Demaurex, N. (2011). Dynamic regulation of the mitochondrial proton gradient during cytosolic calcium elevations. J. Biol. Chem. *286*, 11672–11684. https://doi.org/10.1074/jbc.M110.159962.

57. Bright, G.R., Fisher, G.W., Rogowska, J., and Taylor, D.L. (1987). Fluorescence ratio imaging microscopy: temporal and spatial measurements of cytoplasmic pH. J. Cell Biol. *104*, 1019–1033. https://doi.org/10.1083/jcb.104.4.1019.

58. Platanias, L.C. (2005). Mechanisms of type-I- and type-II-interferon-mediated signalling. Nat. Rev. Immunol. *5*, 375–386. https://doi.org/10.1038/nri1604.

59. Martinez-Martinez, L., Martinez-Saavedra, M.T., Fuentes-Prior, P., Barnadas, M., Rubiales, M.V., Noda, J., Badell, I., Rodríguez-Gallego, C., and de la Calle-Martin, O. (2015). A novel gain-of-function STAT1 mutation resulting in basal phosphorylation of STAT1 and increased distal IFN-gamma-mediated responses in chronic mucocutaneous candidiasis. Mol. Immunol. *68*, 597–605. https://doi.org/10.1016/j.molimm.2015.09.014.

60. Liu, S., Jiang, M., Wang, W., Liu, W., Song, X., Ma, Z., Zhang, S., Liu, L., Liu, Y., and Cao, X. (2018). Nuclear RNF2 inhibits interferon function by promoting K33-linked STAT1 disassociation from DNA. Nat. Immunol. *19*, 41–52. https://doi.org/10.1038/s41590-017-0003-0.

61. Chang, W., Luo, Q., Wu, X., Nan, Y., Zhao, P., Zhang, L., Luo, A., Jiao, W., Zhu, Q., Fu, Y., et al. (2022). OTUB2 exerts tumor-suppressive roles via STAT1-mediated CALML3 activation and increased phosphatidylserine synthesis. Cell Rep. *41*, 111561. https://doi.org/10.1016/j.celrep.2022.111561.

62. Darnell, J.E., Jr., Kerr, I.M., and Stark, G.R. (1994). Jak-STAT pathways and transcriptional activation in response to IFNs and other extracellular signaling proteins. Science *264*, 1415–1421. https://doi.org/10.1126/science.8197455.

63. Villarino, A.V., Kanno, Y., and O'Shea, J.J. (2017). Mechanisms and consequences of Jak-STAT signaling in the immune system. Nat. Immunol. *18*, 374–384. https://doi.org/10.1038/ni.3691.

64. Abril, E., Real, L.M., Serrano, A., Jimenez, P., García, A., Canton, J., Trigo, I., Garrido, F., and Ruiz-Cabello, F. (1998). Unresponsiveness to interferon associated with STAT1 protein deficiency in a gastric adenocarcinoma cell line. Cancer Immunol. Immunother. *47*, 113–120. https://doi.org/10.1007/s002620050511.

65. Okada, S., Asano, T., Moriya, K., Boisson-Dupuis, S., Kobayashi, M., Casanova, J.L., and Puel, A. (2020). Human STAT1 gain-of-function heterozygous mutations: chronic mucocutaneous candidiasis and Type I interferonopathy. J. Clin. Immunol. *40*, 1065–1081. https://doi.org/10.1007/s10875-020-00847-x.

66. Yamazaki, Y., Yamada, M., Kawai, T., Morio, T., Onodera, M., Ueki, M., Watanabe, N., Takada, H., Takezaki, S., Chida, N., et al. (2014). Two novel gain-of-function mutations of STAT1 responsible for chronic mucocutaneous candidiasis disease: impaired production of IL-17A and IL-22, and the presence of anti-IL-17F autoantibody. J. Immunol. *193*, 4880–4887. https://doi.org/10.4049/jimmunol.1401467.

67. Guo-Wei, H., Chun-Quan, L., Lian-Di, L., Ji-Wei, J., Lin, L., Ji-Yu, D., Jin-Cheng, G., En-Min, L., and Li-Yan, X. (2019). LncRNA625 inhibits STAT1-mediated transactivation potential in esophageal cancer cells. Int. J. Biochem. Cell Biol. *117*, 105626. https://doi.org/10.1016/j.biocel.2019.105626.

68. Shuai, K., Horvath, C.M., Huang, L.H., Qureshi, S.A., Cowburn, D., and Darnell, J.E., Jr. (1994). Interferon activation of the transcription factor Stat91 involves dimerization through SH2-phosphotyrosyl peptide interactions. Cell *76*, 821–828. https://doi.org/10.1016/0092-8674(94)90357-3.

69. Schindler, C., Shuai, K., Prezioso, V.R., and Darnell, J.E., Jr. (1992). Interferon-dependent tyrosine phosphorylation of a latent cytoplasmic transcription factor. Science *257*, 809–813. https://doi.org/10.1126/science.1496401.

70. Horvath, C.M., Wen, Z., and Darnell, J.E., Jr. (1995). A STAT protein domain that determines DNA sequence recognition suggests a novel DNA-binding domain. Genes Dev. *9*, 984–994. https://doi.org/10.1101/gad.9.8.984.

71. Mertens, C., Zhong, M., Krishnaraj, R., Zou, W., Chen, X., and Darnell, J.E., Jr. (2006). Dephosphorylation of phosphotyrosine on STAT1 dimers requires extensive spatial reorientation of the monomers facilitated by the N-terminal domain. Genes Dev. *20*, 3372–3381. https://doi.org/10.1101/gad.1485406.

72. Staab, J., Herrmann-Lingen, C., and Meyer, T. (2013). A rapid conformational rearrangement of STAT1 dimers is required for termination rather than for amplification of interferon-gamma signaling. JAK-STAT *2*, e23576. https://doi.org/10.4161/jkst.23576.

73. Zhong, M., Henriksen, M.A., Takeuchi, K., Schaefer, O., Liu, B., ten Hoeve, J., Ren, Z., Mao, X., Chen, X., Shuai, K., et al. (2005). Implications of an antiparallel dimeric structure of nonphosphorylated STAT1 for the activation-inactivation cycle. Proc. Natl. Acad. Sci. USA *102*, 3966–3971. https://doi.org/10.1073/pnas.0501063102.

74. Goel, S., DeCristo, M.J., Watt, A.C., BrinJones, H., Sceneay, J., Li, B.B., Khan, N., Ubellacker, J.M., Xie, S., Metzger-Filho, O., et al. (2017). CDK4/6 inhibition triggers anti-tumour immunity. Nature *548*, 471–475. https://doi.org/10.1038/nature23465.

75. Tronci, L., Serreli, G., Piras, C., Frau, D.V., Dettori, T., Deiana, M., Murgia, F., Santoru, M.L., Spada, M., Leoni, V.P., et al. (2021). Vitamin C cytotoxicity and its effects in redox homeostasis and energetic metabolism in papillary thyroid carcinoma cell lines. Antioxidants (Basel) *10*, 809. https://doi.org/10.3390/antiox10050809.

76. Hwang, N.R., Yim, S.H., Kim, Y.M., Jeong, J., Song, E.J., Lee, Y., Lee, J.H., Choi, S., and Lee, K.J. (2009). Oxidative modifications of glyceraldehyde-3-phosphate dehydrogenase play a key role in its multiple cellular functions. Biochem. J. *423*, 253–264. https://doi.org/10.1042/BJ20090854.

77. Blaschke, K., Ebata, K.T., Karimi, M.M., Zepeda-Martínez, J.A., Goyal, P., Mahapatra, S., Tam, A., Laird, D.J., Hirst, M., Rao, A., et al. (2013). Vitamin C induces Tet-dependent DNA demethylation and a blastocyst-like state in ES cells. Nature *500*, 222–226. https://doi.org/10.1038/nature12362.

78. Miles, S.L., Fischer, A.P., Joshi, S.J., and Niles, R.M. (2015). Ascorbic acid and ascorbate-2-phosphate decrease HIF activity and malignant properties of human melanoma cells. BMC Cancer *15*, 867. https://doi.org/10.1186/s12885-015-1878-5.

79. Brabson, J.P., Leesang, T., Mohammad, S., and Cimmino, L. (2021). Epigenetic regulation of genomic stability by vitamin C. Front. Genet. *12*, 675780. https://doi.org/10.3389/fgene.2021.675780.

80. Kaźmierczak-Barańska, J., Boguszewska, K., Adamus-Grabicka, A., and Karwowski, B.T. (2020). Two faces of vitamin C-antioxidative and pro-oxidative agent. Nutrients *12*, 1501. https://doi.org/10.3390/nu12051501.

81. Fukumura, H., Sato, M., Kezuka, K., Sato, I., Feng, X., Okumura, S., Fujita, T., Yokoyama, U., Eguchi, H., Ishikawa, Y., et al. (2012). Effect of ascorbic acid on reactive oxygen species production in chemotherapy and hyperthermia in prostate cancer cells. J. Physiol. Sci. *62*, 251–257. https://doi.org/10.1007/s12576-012-0204-0.

82. Heiser, P., Sommer, O., Schmidt, A.J., Clement, H.W., Hoinkes, A., Hopt, U.T., Schulz, E., Krieg, J.C., and Dobschütz, E. (2010). Effects of antipsychotics and vitamin C on the formation of reactive oxygen species. J. Psychopharmacol. *24*, 1499–1504. https://doi.org/10.1177/0269881109102538.

83. Chua, G.N.L., Wassarman, K.L., Sun, H., Alp, J.A., Jarczyk, E.I., Kuzio, N.J., Bennett, M.J., Malachowsky, B.G., Kruse, M., and Kennedy, A.J. (2019). Cytosine-based TET enzyme inhibitors. ACS Med. Chem. Lett. *10*, 180–185. https://doi.org/10.1021/acsmedchemlett.8b00474.

84. Murray, J.K., Balan, C., Allgeier, A.M., Kasparian, A., Viswanadhan, V., Wilde, C., Allen, J.R., Yoder, S.C., Biddlecome, G., Hungate, R.W., et al. (2010). Dipeptidyl-quinolone derivatives inhibit hypoxia inducible factor-1alpha prolyl hydroxylases-1, -2, and -3 with altered selectivity. J. Comb. Chem. *12*, 676–686. https://doi.org/10.1021/cc100073a.

85. Worbs, T., Hammerschmidt, S.I., and Förster, R. (2017). Dendritic cell migration in health and disease. Nat. Rev. Immunol. *17*, 30–48. https://doi.org/10.1038/nri.2016.116.

86. Eisenbarth, S.C. (2019). Dendritic cell subsets in T cell programming: location dictates function. Nat. Rev. Immunol. *19*, 89–103. https://doi.org/10.1038/s41577-018-0088-1.

87. Honegger, C.G., Torhorst, J., Langemann, H., Kabiersch, A., and Krenger, W. (1988). Quantitative determination of water-soluble scavengers in neoplastic and non-neoplastic human breast tissue. Int. J. Cancer *41*, 690–694. https://doi.org/10.1002/ijc.2910410509.

88. Langemann, H., Torhorst, J., Kabiersch, A., Krenger, W., and Honegger, C.G. (1989). Quantitative determination of water- and lipid-soluble antioxidants in neoplastic and non-neoplastic human breast tissue. Int. J. Cancer *43*, 1169–1173. https://doi.org/10.1002/ijc.2910430634.

89. Ohno, S., Ohno, Y., Suzuki, N., Soma, G.I., and Inoue, M. (2009). High-dose vitamin C (ascorbic acid) therapy in the treatment of patients with advanced cancer. Anticancer Res. *29*, 809–815.

90. Agus, D.B., Vera, J.C., and Golde, D.W. (1999). Stromal cell oxidation: a mechanism by which tumors obtain vitamin C. Cancer Res. *59*, 4555–4558.

91. Schoenfeld, J.D., Sibenaller, Z.A., Mapuskar, K.A., Wagner, B.A., Cramer-Morales, K.L., Furqan, M., Sandhu, S., Carlisle, T.L., Smith, M.C., Abu Hejleh, T., et al. (2017). O2•- and H2O2-Mediated Disruption of Fe Metabolism Causes the Differential Susceptibility of NSCLC and GBM Cancer Cells to Pharmacological Ascorbate. Cancer Cell *32*, 268. https://doi.org/10.1016/j.ccell.2017.07.008.

92. Polireddy, K., Dong, R., Reed, G., Yu, J., Chen, P., Williamson, S., Violet, P.C., Pessetto, Z., Godwin, A.K., Fan, F., et al. (2017). High Dose parenteral ascorbate Inhibited Pancreatic Cancer Growth and Metastasis: mechanisms and a Phase I/IIa study. Sci. Rep. *7*, 17188. https://doi.org/10.1038/s41598-017-17568-8.

93. Yeom, C.H., Jung, G.C., and Song, K.J. (2007). Changes of terminal cancer patients' health-related quality of life after high dose vitamin C administration. J. Korean Med. Sci. *22*, 7–11. https://doi.org/10.3346/jkms.2007.22.1.7.

94. Vollbracht, C., Schneider, B., Leendert, V., Weiss, G., Auerbach, L., and Beuth, J. (2011). Intravenous vitamin C administration improves quality of life in breast cancer patients during chemo-/radiotherapy and aftercare: results of a retrospective, multicentre, epidemiological cohort study in Germany. In Vivo *25*, 983–990.

95. Berrueta, L., Bergholz, J., Munoz, D., Muskaj, I., Badger, G.J., Shukla, A., Kim, H.J., Zhao, J.J., and Langevin, H.M. (2018). Stretching reduces tumor growth in a mouse breast cancer model. Sci. Rep. *8*, 7864. https://doi.org/10.1038/s41598-018-26198-7.

96. Reardon, D.A., Gokhale, P.C., Klein, S.R., Ligon, K.L., Rodig, S.J., Ramkissoon, S.H., Jones, K.L., Conway, A.S., Liao, X., Zhou, J., et al. (2016). Glioblastoma eradication following immune checkpoint blockade in an orthotopic, immunocompetent model. Cancer Immunol. Res. *4*, 124–135. https://doi.org/10.1158/2326-6066.CIR-15-0151.

97. Schulze, W.X., and Usadel, B. (2010). Quantitation in mass-spectrometry-based proteomics. Annu. Rev. Plant Biol. *61*, 491–516. https://doi.org/10.1146/annurev-arplant-042809-112132.

98. Subramanian, A., Tamayo, P., Mootha, V.K., Mukherjee, S., Ebert, B.L., Gillette, M.A., Paulovich, A., Pomeroy, S.L., Golub, T.R., Lander, E.S., et al. (2005). Gene set enrichment analysis: a knowledge-based approach for interpreting genome-wide expression profiles. Proc. Natl. Acad. Sci. USA *102*, 15545–15550. https://doi.org/10.1073/pnas.0506580102.

99. Horton, P., Park, K.J., Obayashi, T., Fujita, N., Harada, H., Adams-Collier, C.J., and Nakai, K. (2007). WoLF PSORT: protein localization predictor. Nucleic Acids Res. *35*, W585–W587. https://doi.org/10.1093/nar/gkm259.

100. Huang da, W., Sherman, B.T., and Lempicki, R.A. (2009). Systematic and integrative analysis of large gene lists using David bioinformatics resources. Nat. Protoc. *4*, 44–57. https://doi.org/10.1038/nprot.2008.211.

101. Bu, D., Luo, H., Huo, P., Wang, Z., Zhang, S., He, Z., Wu, Y., Zhao, L., Liu, J., Guo, J., et al. (2021). KOBAS-i: intelligent prioritization and exploratory visualization of biological functions for gene enrichment analysis. Nucleic Acids Res. *49*, W317–W325. https://doi.org/10.1093/nar/gkab447.

102. Crooks, G.E., Hon, G., Chandonia, J.M., and Brenner, S.E. (2004). WebLogo: a sequence logo generator. Genome Res. *14*, 1188–1190. https://doi.org/10.1101/gr.849004.

103. Conway, P., Tyka, M.D., DiMaio, F., Konerding, D.E., and Baker, D. (2014). Relaxation of backbone bond geometry improves protein energy landscape modeling. Protein Sci. *23*, 47–55. https://doi.org/10.1002/pro.2389.

104. Khatib, F., Cooper, S., Tyka, M.D., Xu, K., Makedon, I., Popovic, Z., Baker, D., and Players, F. (2011). Algorithm discovery by protein folding game players. Proc. Natl. Acad. Sci. USA *108*, 18949–18953. https://doi.org/10.1073/pnas.1115898108.

105. Tyka, M.D., Keedy, D.A., André, I., Dimaio, F., Song, Y., Richardson, D.C., Richardson, J.S., and Baker, D. (2011). Alternate states of proteins revealed by detailed energy landscape mapping. J. Mol. Biol. *405*, 607–618. https://doi.org/10.1016/j.jmb.2010.11.008.

106. Renfrew, P.D., Choi, E.J., Bonneau, R., and Kuhlman, B. (2012). Incorporation of noncanonical amino acids into Rosetta and use in computational protein-peptide interface design. PLoS One *7*, e32637. https://doi.org/10.1371/journal.pone.0032637.

107. Drew, K., Renfrew, P.D., Craven, T.W., Butterfoss, G.L., Chou, F.C., Lyskov, S., Bullock, B.N., Watkins, A., Labonte, J.W., Pacella, M., et al. (2013). Adding diverse noncanonical backbones to rosetta: enabling peptidomimetic design. PLoS One *8*, e67051. https://doi.org/10.1371/journal.pone.0067051.

108. Maier, J.A., Martinez, C., Kasavajhala, K., Wickstrom, L., Hauser, K.E., and Simmerling, C. (2015). ff14SB: improving the accuracy of protein side chain and backbone parameters from ff99SB. J. Chem. Theor. Comput. *11*, 3696–3713. https://doi.org/10.1021/acs.jctc.5b00255.

109. Wang, J., Wolf, R.M., Caldwell, J.W., Kollman, P.A., and Case, D.A. (2004). Development and testing of a general amber force field. J. Comput. Chem. *25*, 1157–1174. https://doi.org/10.1002/jcc.20035.

110. Woods, R.J., and Chappelle, R. (2000). Restrained electrostatic potential atomic partial charges for condensed-phase simulations of carbohydrates. THEOCHEM *527*, 149–156. https://doi.org/10.1016/S0166-1280(00)00487-5.

111. Alford, R.F., Leaver-Fay, A., Jeliazkov, J.R., O'Meara, M.J., DiMaio, F.P., Park, H., Shapovalov, M.V., Renfrew, P.D., Mulligan, V.K., Kappel, K., et al. (2017). The Rosetta all-atom energy function for macromolecular

modeling and design. J. Chem. Theor. Comput. *13*, 3031–3048. https://doi.org/10.1021/acs.jctc.7b00125.

112. Park, H., Bradley, P., Greisen, P., Jr., Liu, Y., Mulligan, V.K., Kim, D.E., Baker, D., and DiMaio, F. (2016). Simultaneous optimization of biomolecular energy functions on features from small molecules and macromolecules. J. Chem. Theor. Comput. *12*, 6201–6212. https://doi.org/10.1021/acs.jctc.6b00819.

113. Hansler, A., Chen, Q., Gray, J.D., Ross, M.E., Finnell, R.H., and Gross, S.S. (2014). Untargeted metabolite profiling of murine embryos to reveal metabolic perturbations associated with neural tube closure defects. Birth Defects Res. A Clin. Mol. Teratol. *100*, 623–632. https://doi.org/10.1002/bdra.23272.

114. Goel, S., Wang, Q., Watt, A.C., Tolaney, S.M., Dillon, D.A., Li, W., Ramm, S., Palmer, A.C., Yuzugullu, H., Varadan, V., et al. (2016). Overcoming therapeutic resistance in HER2-positive breast cancers with CDK4/6 inhibitors. Cancer Cell *29*, 255–269. https://doi.org/10.1016/j.ccell.2016.02.006.

115. Guo, X., Zhou, Y., Wu, T., Zhu, X., Lai, W., and Wu, L. (2016). Generation of mouse and human dendritic cells in vitro. J. Immunol. Methods *432*, 24–29. https://doi.org/10.1016/j.jim.2016.02.011.

116. Ran, F.A., Hsu, P.D., Wright, J., Agarwala, V., Scott, D.A., and Zhang, F. (2013). Genome engineering using the CRISPR-Cas9 system. Nat. Protoc. *8*, 2281–2308. https://doi.org/10.1038/nprot.2013.143.

STAR★METHODS

KEY RESOURCES TABLE

REAGENT or RESOURCE	SOURCE	IDENTIFIER
Antibodies		
pSTAT1 (Y701)	Cell Signaling	Cat #9167S; RRID: AB_561284
STAT1	Cell Signaling	Cat #14994S; RRID: AB_2737027
GAPDH	Cell Signaling	Cat #5174S; RRID: AB_10622025
ACTIN	Cell Signaling	Cat #4967S; RRID: AB_330288
GFP	Cell Signaling	Cat #2955S; RRID: AB_1196614
HA	Cell Signaling	Cat #2367S; RRID: AB_10691311
COX4	Cell Signaling	Cat #4850S; RRID: AB_2085424
Lysine acetylation	Cell Signaling	Cat #9441S; RRID: AB_331805
Lysine methylation	Cell Signaling	Cat #14679S; RRID: AB_2798567
PE-human pSTAT1(Y701)	Biolegend	Cat #666403; RRID: AB_2734525
APC-human HLA-A, B, C	Biolegend	Cat #311410; RRID: AB_314879
PE/Cy7-human B2M	Biolegend	Cat #395716; RRID: AB_2801065
PE-mouse pSTAT1(Y701)	Cell Signaling	Cat #8062S; RRID: AB_10859888
AF647-mouse H-2Kq	Biolegend	Cat #115106; RRID: AB_893562
AF647-mouse H-2Kb	Biolegend	Cat #114612; RRID: AB_492931
PE/Cy7-mouse B2M	Biolegend	Cat #154508; RRID: AB_2728213
PerCP/Cy5.5-mouse CD45	Biolegend	Cat #103132; RRID: AB_893340
PE/Dazzle594-mouse CD3	Biolegend	Cat #100348; RRID: AB_2564029
APC/Cy7-mouse CD4	Biolegend	Cat #100414; RRID: AB_312699
AF700-mouse CD8	Biolegend	Cat #300920; RRID: AB_528885
PE-mouse IFNγ	Biolegend	Cat #505808; RRID: AB_315402
APC-mouse TNFα	Biolegend	Cat #506307; RRID: AB_315428
PE/Cy7-mouse CD11c	Biolegend	Cat #117318; RRID: AB_493568
BV785-mouse CD86	Biolegend	Cat #105043; RRID: AB_2566722
BV421-mouse CD80	Biolegend	Cat #104725; RRID: AB_10900989
APC/Cy7-mouse MHC II	Biolegend	Cat #107628; RRID: AB_2069377
PerCP/Cy5.5-mouse CD103	Biolegend	Cat #121416; RRID: AB_2128621
PE/Cy7-H-2Kb binding SIINFEKL	Biolegend	Cat #141608; RRID: AB_11218593
APC/Cy7-mouse I-A/I-E (MHC II)	Biolegend	Cat #107628; RRID: AB_2069377
AF700-mouse CD206	Biolegend	Cat #141734; RRID: AB_2629637
PerCP/Cy5.5-mouse CD11b	Biolegend	Cat #101228; RRID: AB_893232
Vitcylation	This Study	N/A
Chemicals, peptides, and recombinant proteins		
RPMI 1640 medium	Life Technologies	Cat #11875119
DMEM	Life Technologies	Cat #11965118
DMEM F12	Life Technologies	Cat #10565042
FBS	Gibco	Cat #A5256801
PenStrep	Life Technologies	Cat #15070063
HEPES	Life Technologies	Cat #15630080
G418	Invitrogen	Cat #ant-gn-5
Hydrocortisone	Sigma-Aldrich	Cat #H0888
Insulin	Life Technologies	Cat #12585014
Cholera toxin	EMD Millipore	Cat #227036

(*Continued on next page*)

Continued

REAGENT or RESOURCE	SOURCE	IDENTIFIER
EGF	Sigma-Aldrich	Cat #E9644
Y-27632	Selleck	Cat #S1049
PBS	Life Technologies	Cat #20012050
VitC	Sigma-Aldrich	Cat #A4034
1-^{13}C-vitC	Omicron	Cat #ASC-001
2-^{13}C-vitC	Omicron	Cat #ASC-002
1,2-^{13}C-vitC	Omicron	Cat #ASC-011
DHA	Sigma-Aldrich	Cat #261556
Staurosporine	TargetMol	Cat #T6680
IOX2	TargetMol	Cat #T1823
Bobcat 399	TargetMol	Cat #T5198
Osunprotafib	TargetMol	Cat #T61699
Acetonitrile	Sigma-Aldrich	Cat #E-060
Leukocyte Activation Cocktail	BD Biosciences	Cat #550583
GM-CSF	Stem Cell Technologies	Cat #78017
CFSE	Biolegend	Cat #423801
2-Mercaptoethanol	Life Technologies	Cat #21985023
CD3/CD28 Dynabeads	Life Technologies	Cat #11456D
IL-7	Biolegend	Cat #577802
IL-15	Biolegend	Cat #566302
IL-2	Biolegend	Cat #575402
Human IFNγ	Biolegend	Cat #570204
Murine IFNγ	Peprotech	Cat #315-05
lipofectamine 3000	Invitrogen	Cat # L3000015
NP-40	Roche Diagnostics	Cat #11332473001
GFP-Trap magnetic agarose	Chromotek	Cat #gtma-20
DAPI	Sigma-Aldrich	Cat #D9542
Ac-VLSPKAVQRF	GL Biochem	N/A
Ac-VSSPKVLQRL	GL Biochem	N/A
Ac-YAPVAKDLASR	GL Biochem	N/A
FTEGAFKDWGYQLAR	GL Biochem	N/A
Ac-RDLIFKEREED	GL Biochem	N/A
Ac-IISKQDDL	GL Biochem	N/A
Ac-LLDGKNVNAG	GL Biochem	N/A
Ac-LDNKINEVLALA	GL Biochem	N/A
Ac-EAAWKVTDEC	GL Biochem	N/A
Ac-NNQHKLTLS	GL Biochem	N/A
Ac-VIDIKVVAGA	GL Biochem	N/A
LGILIKAR	Genscript	N/A
VKVGVNGFGR	Genscript	N/A
ANKQFIRNTQIR	Genscript	N/A
NKQVLWDR	Genscript	N/A
NKQVLSDR	Genscript	N/A
Critical commercial assays		
Cellular Vita-C assay kit	Cayman	Cat #700420
ROS/superoxide detection assay kit	Abcam	Cat #ab139476
Epigenase 5mC-hydroxylase TET activity/ inhibition assay kit	Epigentek	Cat #P-3086-48

(*Continued on next page*)

Continued

REAGENT or RESOURCE	SOURCE	IDENTIFIER
Duolink In Situ Red Starter Kit Mouse/ Rabbit	Sigma-Aldrich	Cat #DUO92101
$CD8a^+$ T-cell isolation kit	StemCell Technologies	Cat #19853
Experimental models: Cell lines		
Cal-51	Creative Bioarray	Cat #CSC-C0382
MCF7	ATCC	Cat #HTB-22
E0771	ATCC	Cat #CRL-3461
PP	This Study	N/A
HeLa	ATCC	Cat #CRM-CCL-2
B16	ATCC	Cat #CRL-6475
EMT6	ATCC	Cat #CRL-2755
HCT116	ATCC	Cat #CRL-247
MC38	Sigma-Aldrich	Cat #SCC172
CT26	ATCC	Cat #CRL-2638
HEK293T	ATCC	Cat #CRL-3216
B16-OVA	This Study	N/A
EL4-OVA	This Study	N/A
Experimental models: Organisms/strains		
Mouse: C57BL/6J	Jackson Laboratory	Cat #000664
Mouse: FVB	Jackson Laboratory	Cat #001800
Mouse: NOD-SCID IL-2receptor gamma null (NSG)	Jackson Laboratory	Cat #005557
Oligonucleotides		
Sg mouse *Stat1*_1-F	IDT	CACCGGAACCCCCCGTGCGCGTGG
Sg mouse *Stat1*_1-R	IDT	AAACCCACGCGCACGGGGGGTTCC
Sg mouse *Stat1*_2-F	IDT	CACCGGTCGCAAACGAGACATCAT
Sg mouse *Stat1*_2-R	IDT	AAACATGATGTCTCGTTTGCGACC
Human-*HLA-B*-qPCR-F	IDT	CAGTTCGTGAGGTTCGACAG
Human-*HLA-B*-qPCR-R	IDT	CAGCCGTACATGCTCTGGA
Human-*TAP1*-qPCR-F	IDT	CTGGGGAAGTCACCCTACC
Human-*TAP1*-qPCR-R	IDT	CAGAGGCTCCCGAGTTTGTG
Human-*TAP2*-qPCR-F	IDT	TGGACGCGGCTTTACTGTG
Human-*TAP2*-qPCR-R	IDT	GCAGCCCTCTTAGCTTTAGCA
Human-*LMP2*-qPCR-F	IDT	GCACCAACCGGGGACTTAC
Human-*LMP2*-qPCR-R	IDT	CACTCGGGAATCAGAACCCAT
Human-*B2M*-qPCR-F	IDT	GAGGCTATCCAGCGTACTCCA
Human-*B2M*-qPCR-R	IDT	CGGCAGGCATACTCATCTTTT
Human-*ACTIN*-qPCR-F	IDT	CACCAACTGGGACGACAT
Human-*ACTIN*-qPCR-R	IDT	ACAGCCTGGATAGCAACG
Mouse-*Tap1*-qPCR-F	IDT	GGACTTGCCTTGTTCCGAGAG
Mouse-*Tap1*-qPCR-R	IDT	GCTGCCACATAACTGATAGCGA
Mouse-*Lmp2*-qPCR-F	IDT	ATGTGGTACTCAATTCACAAGCA
Mouse-*Lmp2*-qPCR-R	IDT	AAGCAAGGATGGTTCCTGGAG
Mouse-*B2m*-qPCR-F	IDT	TTCTGGTGCTTGTCTCACTGA
Mouse-*B2m*-qPCR-R	IDT	CAGTATGTTCGGCTTCCCATTC
Mouse-*Irf1*-qPCR-F	IDT	GTTGTGCCATGAACTCCCTG
Mouse-*Irf1*-qPCR-R	IDT	GTGTCCGGGCTAACATCTCC
Mouse-*H2k1*-qPCR-F	IDT	CAGGTGGAGCCCGAGTATTG
Mouse-*H2k1*-qPCR-R	IDT	CGTACATCCGTTGGAACGTG

(*Continued on next page*)

Continued

REAGENT or RESOURCE	SOURCE	IDENTIFIER
Mouse-*Actin*-qPCR-F	IDT	CGCCACCAGTTCGCCATGGA
Mouse-*Actin*-qPCR-R	IDT	TACAGCCCGGGGAGCATCGT
Recombinant DNA		
pcDNA3.1-STAT1-GFP	This Study	N/A
pBABE-STAT1-GFP	This Study	N/A
pBABE-STAT1-K298R-GFP	This Study	N/A
pcDNA3.1-PTPN2-HA	This Study	N/A
pcDNA3.1-JAK1-HA	This Study	N/A
pX458-sgSTAT1(mouse)_1-Cas9	This Study	N/A
pX458-sgSTAT1(mouse)_2-Cas9	This Study	N/A
pX458-sgTET2(mouse)_1-Cas9	This Study	N/A
pX458-sgTET2 (mouse)_2-Cas9	This Study	N/A
pX458-sgHIF1α(mouse)_1-Cas9	This Study	N/A
pX458-sgHIF1α(mouse)_2-Cas9	This Study	N/A
Software and algorithms		
Graphpad Prism 9	Graphpad Software	https://www.graphpad.com/scientific-software/prism/
PyMOL	Schrodinger	http://www.pymol.org/
Data Explorer 4.5	Applied Biosystems	https://data-explorer-tm-software.software.informer.com/4.5/
Mascot 2.6.1	Matrix Science	https://www.matrixscience.com/mascot_support_v2_6.html
WoLF PSORT	NAKAI Lab	https://wolfpsort.hgc.jp
DAVID 6.8	DAVID Bioinformatic Team	https://david.ncifcrf.gov/home.jsp
KOBAS	Peking University	http://kobas.cbi.pku.edu.cn/genelist/
WebLogo	University of California, Berkeley	http://weblogo.berkeley.edu/logo.cgi
FlowJo	BD Biosciences	https://www.flowjo.com/solutions/flowjo/downloads
ImageStudioLite	LI-COR	https://www.licor.com/bio/image-studio-lite/

EXPERIMENTAL MODEL AND STUDY PARTICIPANT DETAILS

Cell lines

Cells were cultured under standard conditions in a humidified incubator with 5% CO_2 at 37°C. Cal-51, MCF7, E0771, PC-9, HCT116, and HeLa cells were obtained from the American Type Culture Collection (ATCC), verified to be negative for mycoplasma, and authenticated by short tandem repeat analysis using the Promega GenePrint 10 System. Cal-51, MCF7, PC-9, HCT116, and HeLa cells were cultured in RPMI 1640 (Gibco) supplemented with 10% FBS (Life Technologies) and PenStrep (Hyclone). E0771 cells were cultured in RPMI 1640 supplemented with 10% FBS, PenStrep, and 10 mM HEPES (Life Technologies, 15630080). B16-OVA and EL4-OVA cells were cultured in DMEM (Gibco) supplemented with 10% FBS and 250 μg/ml G418 (Invitrogen). PP cells were derived from mouse mammary tumors and cultured in DMEM/F12 media supplemented with 10% FBS, 25 ng/ml hydrocortisone, 5 μg/ml insulin, 8.5 ng/ml cholera toxin, 0.125 ng/ml epidermal growth factor (EGF), 5 μM Y-27632 Rock1 inhibitor, and PenStrep, as previously described.[95]

Animals

All mouse experiments were conducted in compliance with federal laws and institutional guidelines, as approved by the Institutional Animal Care and Use Committees of Dana-Farber Cancer Institute and Harvard Medical School. The relevant animal protocols limited the maximum tumor diameter to 25 mm, which was not exceeded in any experiment. CO_2 inhalation was used to euthanize the mice. Female wild-type FVB and C57BL/6 mice, aged six-to-eight weeks, were obtained from the Jackson Laboratory. For tumor formation assays, 5×10^5 PP cells or 10^5 E0771 cells were injected into the thorracic fat pad in 50% matrigel. VitC (Sigma-Aldrich, A4034) was prepared daily by resuspending the powder in PBS (Hyclone). Anti-mouse PD1 antibody (clone 332.8H3, kindly provided

by Dr. Gordon Freeman at DFCI) was injected by intraperitoneal administration at a dose of 10 mg/kg every 3 days.[96] Intraperitoneal administration of vitC was conducted at a dose of 4 g/kg, qd. Mice in the control group were treated with PBS.

METHOD DETAILS

In vitro vitcylation reaction

In vitro vitcylation reactions were conducted using a 30 μl reaction mixture containing 50 mM Tris-HCl (pH 7.5), 2 mM sodium ascorbate (vitC), and 0.05 mg/ml synthetic substrate peptide. The reaction was allowed to proceed for 3 hours at 37°C. The peptide was then desalted by passing it through a C18 ZipTip (Millipore) and subjected to analysis using a MALDI-TOF/TOF mass spectrometer (SCIEX-5800).

Liquid chromatography-tandem mass spectrometry analysis

The proteome of breast cancer cells was digested with sequencing grade modified trypsin (Promega) overnight at the protease/protein ratio at 1:50. The resulting peptide mixture was desalted by C18, dried by vacuum centrifugation, and stored at -80 °C prior to analysis. Peptides were resuspended in 5% acetonitrile with 0.1% formic acid and analyzed by nanoLC/MS/MS using a NanoAcquity UPLC system (Waters Corporation, Milford, USA) interfaced to an Orbitrap Lumos mass spectrometer. Peptides were trapped on a self-packed precolumn (4 cm 7 μm Symmetry C18), separated on an analytical column (50 cm 5 μm Monitor C18) using an HPLC gradient (5-35% B in 90 minutes, A=0.1% formic acid, B=acetonitrile with 0.1% formic acid), and introduced to the mass spectrometer by electrospray ionization. The mass spectrometer was operated in data-dependent mode and subjected the top 10 most abundant ions in each MS scan (120k resolution, m/z 300-2000, 800% AGC target) to MS/MS (7500 resolution, 35% NCE, m/z 100-2000). Dynamic exclusion was enabled with a 30-second duration. Raw MS files were converted to mgf and analyzed by Mascot version 2.6.1 using a forward/reverse database of human proteins (NCBI RefSeq). Search parameters included precursor and product ion tolerances of 10 ppm and 25 mmu, variable oxidation of methionine, vitcylation of lysine (+175.0237 Da), and fixed carbamidomethylation of cysteine residues.

Quantifications of targeted vitcylation peptides

A published method was employed.[97] Briefly, a ratio of vitcylated peptide signal (the total ion counts (TIC) of vitcylated form) to the total peptide signal (TIC of vitcylated form + TIC of the non-vitcylated form) was calculated according to the following equation: $TIC^{vita.}/(TIC^{vita.}+TIC^{non\text{-}vita.})$=Ratio of vitcylation.

Transcriptome methodology

An Ion AmpliSeq Custom Panel containing 4,604 cancer- and immune-associated genes (designed by Thermo Fisher using Ion AmpliSeq designer) was utilized for our studies, as previously described.[74] For each sample, 10 ng total RNA was used to prepare the cDNA library. Libraries were multiplexed and amplified using an Ion OneTouch 2 System and sequenced on an Ion Torrent Proton system (Thermo Fisher). Count data was generated using Thermo Fisher's Torrent suite and ampliSeqRNA analysis plugin. For Gene Ontology enrichment and Kyoto Encyclopedia of Genes and Genomes (KEGG) pathway analysis, genes with a mean fold change (vitC treated vs control) greater than 2 or lesser than 0.5 were utilized. Gene Ontology enrichment and KEGG pathway analysis were carried out using Cytoscape Software and STRING plugin. For GSEA analysis, genes were first ranked according to $\log_2$(fold change) and then analyzed using the GSEAPreanked tool with MsigDB v7.1 Hallmarks gene sets and the 'classic' method.[98]

Bioinformatic analysis

The subcellular localization of vitcylated proteins was predicted using WoLF PSORT, a subcellular localization prediction program (https://wolfpsort.hgc.jp).[99] Gene Ontology enrichment analysis for the vitcylated proteins was carried out using DAVID bioinformatics resources 6.8 (https://david.ncifcrf.gov/home.jsp).[100] KEGG pathway analysis was performed using KOBAS (http://kobas.cbi.pku.edu.cn/genelist/).[101] For vitcylation motif analysis, the 10 amino acid residues (-10 to +10) on either side of the vitcylation site were selected and a consensus logo was generated using the WebLogo webserver (http://weblogo.berkeley.edu/logo.cgi).[102]

Flow cytometry

For tumor cell lines, one million cells were stained with the appropriate antibodies diluted in PBS (Hyclone) plus 2% FBS (Life Technologies) for 30 min on ice. For tumor samples, tumors were mechanically disrupted by chopping and chemically digested in dissociation buffer (2 mg/ml collagenase type IV (Worthington Biochemical), 0.02 mg/ml DNase (Sigma Aldrich) in DMEM (Life Technologies) containing 5% FBS (Life Technologies), PenStrep (Hyclone) with agitation at 37°C for 45 min. After lysing of red blood cells (BD Biosciences), single-cell suspensions were incubated with appropriate antibodies for 30 min on ice.

For human antibodies, antibodies were purchased from BioLegend unless otherwise indicated: pSTAT1(Y701) (clone A17012A), HLA (clone W6/32), B2M (clone A17082A). Mouse antibodies: pSTAT1(Y701) (Cell Signaling Technology, 8062S), H-2Kq (clone KH114), H-2Kb (clone 28-8-6), B2M (clone A16041A), CD45 (clone 30-F11), CD3 (clone 145-2C11), CD4 (clone RM4-5), CD8 (clone HIT8a), IFNγ (clone XMG12), TNFα (clone MP6-XT22), CD11c (clone N418), CD86 (clone GL-1), CD80 (clone 16-10A1), MHC II (clone M5/114.15.2), CD103 (clone 2E7), H-2Kb binding SIINFEKL (clone 25-D1.16), I-A/I-E (MHC II, clone M5/114.15.2), CD206 (clone C068C2), CD11b (clone M1/70). Anti-mouse/rat FoxP3 staining set (eBioscience) was used for intracellular staining

according to the manufacturer's instructions. For IFNγ and TNFα analysis, cells were stimulated *in vitro* with the Leukocyte Activation Cocktail with protein transport inhibitor Brefeldin A (BD Biosciences, 550583).

Western blots

Western blotting was performed as previously described,[74] using the following antibodies: anti-vitcylation antibody (generated by Abclonal Technology) and Cell Signaling Technology antibodies to pSTAT1 (9167S), STAT1 (14994S), GAPDH (5174S), ACTIN (4967S), GFP (2955S), HA (2367S), lysine acetylation (9441S), lysine methylation (14679S) and COX4 (4850S).

Dot-blot assays

Peptides were spotted on nitrocellulose membranes. After the membrane dried, the membrane was blocked with 5% skimmed milk in TBST for 1 hour, followed by the incubation with the anti-vitcylation antibody overnight at 4°C and the secondary antibody overnight at 4°C. After washing three times with TBST, the membrane was scanned by Odyssey Dlx Imaging System (LI-COR).

Thermostability change calculation

The antiparallel dimer structure from PDB 1YVL (Asymmetric Unit) is initially considered with 3.00Å X-ray resolution. The whole calculation includes several steps as below:

1. The input structure preparation

The wild type K298, the mutation K298N and the vitcyl-K298 (in two chains) were relaxed with Cartesian coordination type and constraints.[103–105] The option/flag was set as follows.

```
-nstruct 200
-ex1
-ex2
-relax:constrain_relax_to_start_coords
-ramp_constraints true
-use_input_sc
-flip_HNQ
-no_optH false
-relax:cartesian
-beta_nov16_cart
-corrections::beta_nov16
-crystal_refine
-in:auto_setup_metals
-extra_res PTM.params
```

The structures with the lowest scores were used in the next step.

2. The preparation of params and rotlib files

To make the vitcyl-K298 recognized by Rosetta, the params and rotlib files were generated by related modules using Lysine as reference.[106,107]

3. MD sampling

The side chain of vitcyl-K298 has more than 10 chi angles, which is beyond the recommended limitation of Rosetta. To better find the low energy conformations of vitcyl-K298, we adopted molecular dynamics (MD) simulations to perform the sampling. Ff14SB was used to parameterize the protein.[108] The vitcyl-K298 was parameterized using GAFF and its partial charge was parameterized using RESP.[109,110]

10ns MD simulations were performed using Amber20 and 100 frames of snapshots were extracted from the last 5ns scoring using Rosetta. A 100kcal/mol positional restraints were given on residues 9 Å away from α-carbon of K298 to minimize the noise arose from the thermal fluctuation during the MD simulations.

4. Scoring and ddG calculation

The score_jd2 module was used with the following options.[111,112]

```
-beta_nov16_cart
-corrections::beta_nov16
-fa_max_dis 9.0
-extra_res VLY.params
```

Average scores for K298, N298 and vitcyl-K298 were calculated on the 100 frames of snapshots. Values of ddG were calculated from the difference as:

$$ddG = \text{Score avg}(\text{Mut}/\text{Mod}) - \text{Score ave}(\text{WT})$$

Cellular levels of vitC, ROS, and TET activity assay

Cellular vitC assay kit (Cayman, 700420), ROS/superoxide detection assay kit (abcam, ab139476), and epigenase 5mC-hydroxylase TET activity/inhibition assay kit (Epigentek, P-3086-48) were used for cellular vitC level assay, ROS level assay, and TET activity assay according to the manufacturer's instructions, respectively.

Preparation of pan-specific anti-vitcyllysine polyclonal antibody

The pan-vitcyllysine antibody was generated using a synthetic vitcylated lysine-containing peptide mix, conjugated to keyhole limpet hemocyanin (KLH) as an antigen. The sequence of the peptide mix is CXXXXXK*XXXX, where X represents any of the 20 standard amino acids, excluding cysteine; A cysteine residue was added to the peptide's N terminus to facilitate conjugation with KLH. This conjugation reaction was carried out in 0.2% glutaraldehyde solution. The resulting vitcylated KLH was subjected to immunize rabbits. The population of the pan-specific antibodies recognizing vitcylated lysine was then purified using the vitcylated lysine-containing peptide mix. The specificity of the antibodies was evaluated using dot blots.

Proximity ligation assay (PLA)

PLA was performed using the Duolink In Situ Red Starter Kit Mouse/Rabbit (Sigma, DUO92101) according to the manufacturer's instructions. All reagents used for the procedure are from this kit, except the antibody for STAT1 (Santa Cruz, SC-464) and TCPTP (abcam, ab227916).

Measurement of *in vivo* vitC concentrations by HPLC-MS

VitC concentrations *in vivo* were measured by HPLC-MS as previously described.[14] Briefly, excised tumors and spleens were placed in 2 mL Eppendorf tubes with 1 mL of 3 mM monobrombimane (MBB) in CH3OH:H2O (80:20) at 4°C and incubated for 3 h. After this, tissues were disrupted using stainless steel beads in a TissueLyser (Qiagen) and incubated for another 30 minutes at -20°C. Extracts were centrifuged for 10 minutes at 13,000 rpm to pellet insoluble material, and supernatants were transferred to clean tubes. This extraction was repeated twice more, and all three supernatants were dried in a speed-vac (Savant) and stored at -80°C until analysis. Plasma samples were incubated with 2.5 mM MBB in CH3OH:H2O (80:20) at room temperature for 30 min, then diluted with CH3CN:H2O (70:30) containing 0.025% formic acid. The samples were vortexed, centrifuged for 20 minutes at 20,000g, and the supernatants transferred to autosampler vials for LC/MS analysis. For absolute vitC concentrations, MBB-treated plasma was diluted with 70% CH_3CN containing 0.025% formic acid, and 1 μL was injected for LC/MS.

Q-TOF LC/MS analysis was conducted as referenced,[113] detecting ascorbic acid in negative mode ($[M-H]^-$ at m/z 175.0248) and positive mode ($[M+H]^+$ at m/z 177.0394) with retention times of 1.92 minutes and 0.99 minutes for ANP and RP columns, respectively. A vitC calibration curve was established for plasma, tumor lysate, and spleen lysate in the 0-600 μM range. Accuracy and precision were evaluated using spiked vitC standards in these samples. Intracellular vitC concentrations in tumor and spleen samples were calculated as nM/mg protein and converted to mM, assuming 1 g of protein equals 1 mL in volume.

Real-time qPCR

Real-time qPCR was performed as previously described.[114] Primer sequences used for real-time qPCR were as follows. *Tap1* (mouse) forward: 5'- GGACTTGCCTTGTTCCGAGAG-3'; reverse: 5'-GCTGCCACATAACTGATAGCGA-3'. *Lmp2* (mouse) forward: 5'-ATGTGG TACTCAATTCACAAGCA-3'; reverse: 5'-AAGCAAGGATGGTTCCTGGAG-3'. *B2m* (mouse) forward: 5'-TTCTGGTGCTTGTCTC ACTGA-3'; reverse: 5'-CAGTATGTTCGGCTTCCCATTC-3'. *Irf1* (mouse) forward: 5'- GTTGTGCCATGAACTCCCTG-3'; reverse: 5'-GTGTCCGGGCTAACATCTCC-3'. *H2k1* (mouse) forward: 5'- CAGGTGGAGCCCGAGTATTG-3'; reverse: 5'- CGTACATCCG TTGGAACGTG-3'. *Actin* (mouse) forward: 5'- CGCCACCAGTTCGCCATGGA-3'; reverse: 5'- TACAGCCCGGGGAGCATCGT-3'. *HLA-B* (human) forward: 5'- CAGTTCGTGAGGTTCGACAG-3'; reverse: 5'-CAGCCGTACATGCTCTGGA-3'. *TAP1* (human) forward: 5'-CTGGGGAAGTCACCCTACC-3'; reverse: 5'- CAGAGGCTCCCGAGTTTGTG-3'. *TAP2* (human) forward: 5'- TGGACGCGGCTTTA CTGTG-3'; reverse: 5'- GCAGCCCTCTTAGCTTTAGCA-3'. *LMP2* (human) forward: 5'- GCACCAACCGGGGACTTAC-3'; reverse: 5'-CACTCGGGAATCAGAACCCAT-3'. *B2M* (human) forward: 5'- GAGGCTATCCAGCGTACTCCA-3'; reverse: 5'- CGGCAGGCATACTC ATCTTTT-3'. *ACTIN* (human) forward: 5'-CACCAACTGGGACGACAT-3'; reverse: 5'-ACAGCCTGGATAGCAACG-3'. Relative copy number was determined by calculating the fold change difference in the gene of interest relative to *Actin* (mouse) or *ACTIN* (human). Real-time qPCR was performed on an Applied Biosystems 7300 machine.

Generation of mouse DCs

Mouse DCs were obtained from the bone marrow of FVB/NJ mice by modifying the previously described protocol.[115] For DC generation, bone marrow cells were cultured in RPMI 1640 supplemented with 20 ng/ml GM-CSF (Stem Cell Technologies, 78017), 10% FBS, and 100 μg/ml PenStrep. Fresh RPMI 1640 with 20 ng/ml GM-CSF, 10% FBS, and 100 μg/ml PenStrep was added after 3 days, and non-adherent cells (DCs) were harvested and co-cultured with PP cells after another 2 days.

Co-culture experiments

For *in vitro* co-culture of tumor cells with $CD8^+$ T cells, B16-OVA and EL4-OVA cells were pretreated with vitC or PBS for 3 days. $CD8^+$ T cells were isolated from spleens of OT-I mice using a $CD8a^+$ T-cell isolation kit (StemCell Technologies) with an autoMACS Pro

Separator. Isolated $CD8^+$ T cells were suspended in RPMI 1640 medium (Gibco) with 5% FBS, labeled with 5 μM carboxyfluorescein succinimidyl ester (CFSE) (Biolegend) for 10 min in the dark at room temperature, and washed twice in 10× volume of T cell media (RPMI 1640 with 10% FBS and 55 μM 2-mercaptoethanol (Gibco)). One hundred thousand $CD8^+$ T cells were co-cultured with vitC- or control-pretreated tumor cells at a ratio of 1:8 tumor cells: T cells in RPMI 1640 supplemented with CD3/CD28 Dynabeads (1:1 ratio of cells: beads, ThermoFisher) 2.5 ng/ml IL-7 (Biolegend), 50 ng/ml IL-15 (Biolegend), and 2 ng/ml IL-2 (Biolegend) for 2 days at 37°C in the dark. At the experimental endpoint, $CD8^+$ T cell proliferation and activation were analyzed by flow cytometry.

For *in vitro* co-culture of tumor cells with DCs, PP cells were pretreated with vitC or PBS for 3 days. One hundred thousand mouse bone marrow-derived DCs were co-cultured with vitC- or control-pretreated PP cells at a ratio of 1:4 tumor cells: DCs in RPMI 1640 supplemented with 20 ng/ml GM-CSF, 10% FBS and lipofectamine 3000 (2 μl/ml, Invitrogen) for 2 days at 37°C. At the experimental endpoint, DCs activation was analyzed by flow cytometry.

Generation of STAT1, TET2 and HIF1α deficient cells

CRISPR-Cas9 genome editing systems were used to generate STAT1-deficient cells.[116] Oligos sequences for guide RNAs were as follows. *Stat1* (mouse) #1 forward: 5'- CACCGGAACCCCCCGTGCGCGTGG-3'; #1 reverse: 5'- AAACCCACGCGCACGGGGG GTTCC-3'. *Stat1* (mouse) #2 forward: 5'- CACCGGTCGCAAACGAGACATCAT-3'; #2 reverse: 5'- AAACATGATGTCTCGTTTGC GACC-3'. *Tet2* (mouse) #1 forward: 5'- CACCGCTACACGGCAGCAGCTTCG-3'; #1 reverse: 5'- AAACCGAAGCTGCTGCCGT GTAGC-3'. *Tet2* (mouse) #2 forward: 5'- CACCGAGTGCTTCATGCAAATTCG-3'; #2 reverse: 5'- AAACCGAATTTGCATGAAGC ACTC-3'. *Hif1α* (mouse) #1 forward: 5'- CACCGGGCGACACCATCATCTCTC-3'; #1 reverse: 5'- AAACGAGAGATGATGGTGTCG CCC-3'. *Hif1α* (mouse) #2 forward: 5'- CACCGCAACCTCTTGATTCAGTGC-3'; #2 reverse: 5'- AAACGCACTGAATCAAGAGG TTGC-3'. Annealed guide oligos were cloned into the CRISPR-Cas9 expression vector PX458. The constructed plasmids were transfected into cells. The next day, single GFP^+ cells were sorted into 96-well plates by flow cytometry. Two weeks later, colonies emerged and single colonies were expanded into 6 well plates. STAT1, TET2, HIF1α knockout cells, and control cells were selected by western blot.

Co-immunoprecipitation (Co-IP) and immunoprecipitation (IP)

Cells were lysed using lysis buffer (50 mM Tris-HCl (pH 7.4), 150 mM NaCl and 0.1% NP-40 (for Co-IP) or 0.5% NP-40 (for IP)) at 4°C for 30 minutes. Cell lysates were then centrifuged at 12,000 rcf for 15 min and the supernatants were collected and incubated with GFP-Trap magnetic agarose (Chromotek, gtma-20) overnight at 4°C. After washing the beads with lysis buffer three times, they were resuspended in 1× western blotting loading buffer and denatured at 95°C for 10 minutes.

Immunofluorescence

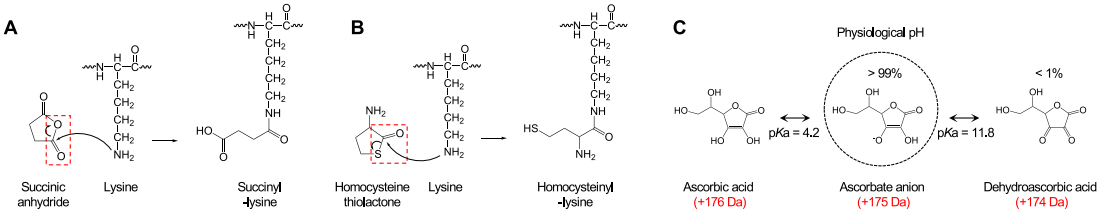
For endogenous STAT1 immunofluorescence, cultured cells were fixed with 4% formaldehyde in PBS for 15 min at room temperature. The fixative was aspirated, and the cells were rinsed three times in PBS for 5 min each. The cells were then covered with ice-cold 100% methanol and incubated for 10 min at -20°C. After incubation, the cells were rinsed in PBS for 5 min. The specimen was blocked in blocking buffer (5% normal serum from the same species as the secondary antibody and 0.3% Triton X-100 in PBS) for 60 min. The blocking solution was aspirated, and diluted STAT1 antibody (Cell Signaling Technology, 14994) was applied and incubated overnight at 4°C. The cells were rinsed three times in PBS for 5 min each, followed by incubation with a fluorochrome-conjugated secondary antibody (ThermoFisher, A-11008) diluted in antibody dilution buffer (1% BSA and 0.3% Triton X-100 in PBS) for 2 hours at room temperature in the dark. The cells were then rinsed in PBS and incubated in PBS with DAPI (Cell Signaling Technology, 8961). Specimens were examined immediately using the appropriate excitation wavelength. For overexpressed STAT1-GFP immunofluorescence, cultured cells were fixed with 4% formaldehyde in PBS for 15 min at room temperature. The fixative was aspirated, and the cells were rinsed three times in PBS for 5 min each. The cells were then incubated in PBS with DAPI (Cell Signaling Technology, 8961). Specimens were examined immediately using the appropriate excitation wavelength.

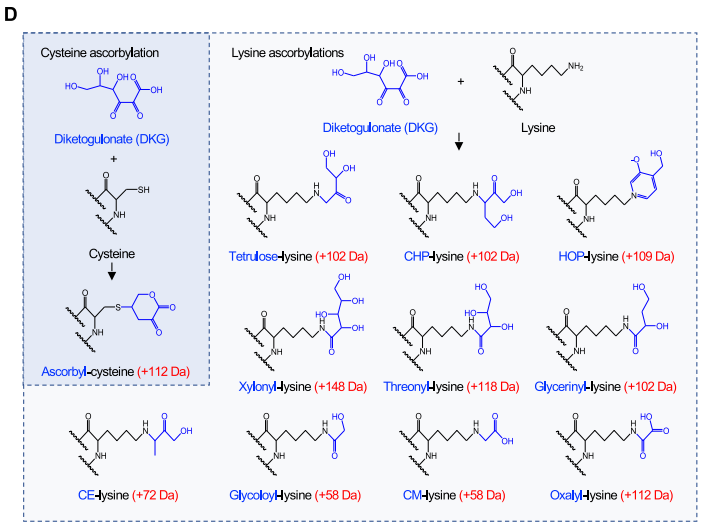
QUANTIFICATION AND STATISTICAL ANALYSIS

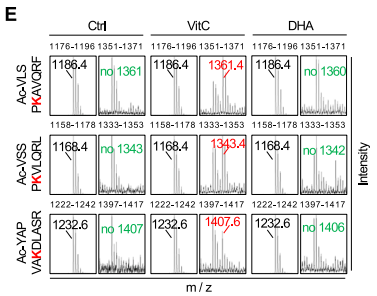
Statistical analysis was performed with Prism 9 (Graphpad Software Inc.). Two-way ANOVA with Tukey's multiple comparisons test was used for tumor growth analysis. For other analysis, unpaired two-tailed Student's test (for normally distributed data) and Mann-Whitney nonparametric test (for skewed data that deviated from normality) were used to compare two conditions. One-way ANOVA with Tukey's multiple comparisons test (for normally distributed data) and Kruskal-Wallis nonparametric test (for skewed data) were used to compare three or more means. Quantitative data are expressed as means ± SEM. Differences with $p < 0.05$ were considered statistically significant; ns, not significant; *$p < 0.05$; **$p < 0.01$; ***$p < 0.001$; ****$p < 0.0001$.

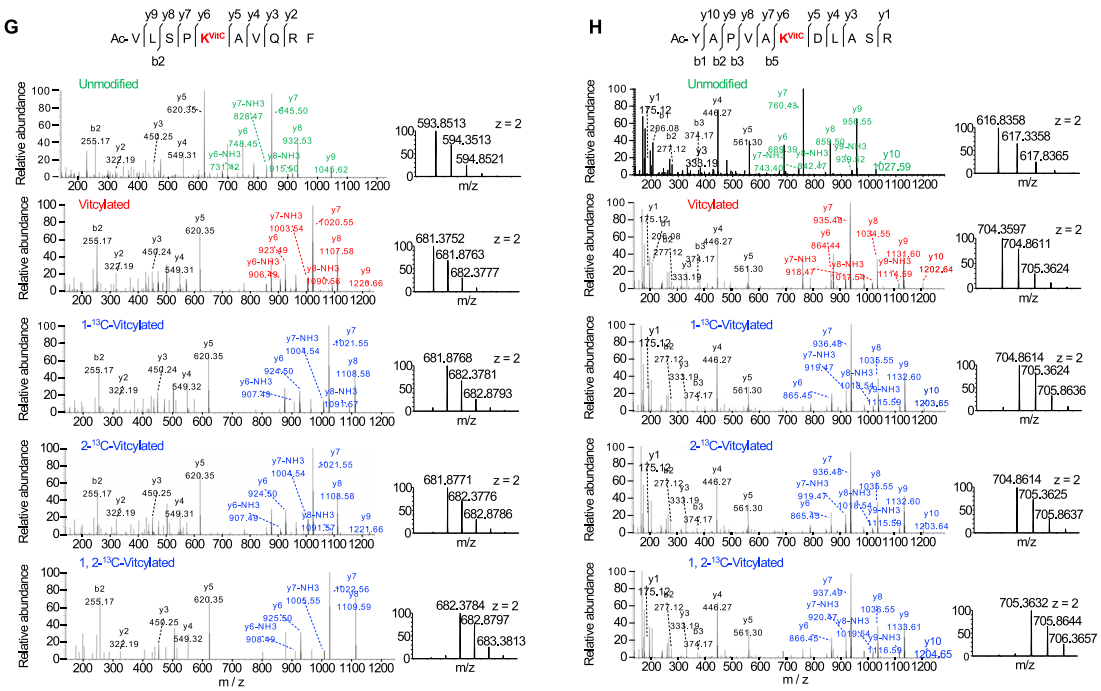
CellPress

Supplemental figures









(legend on next page)

Figure S1. Formation of vitC-derived vitcylation *in vitro*, related to Figure 1

(A and B) Molecular mechanisms of lysine succinylation (A) and homocysteinylation formation (B) are presented, with the reactive lactone bonds circled for clarity.

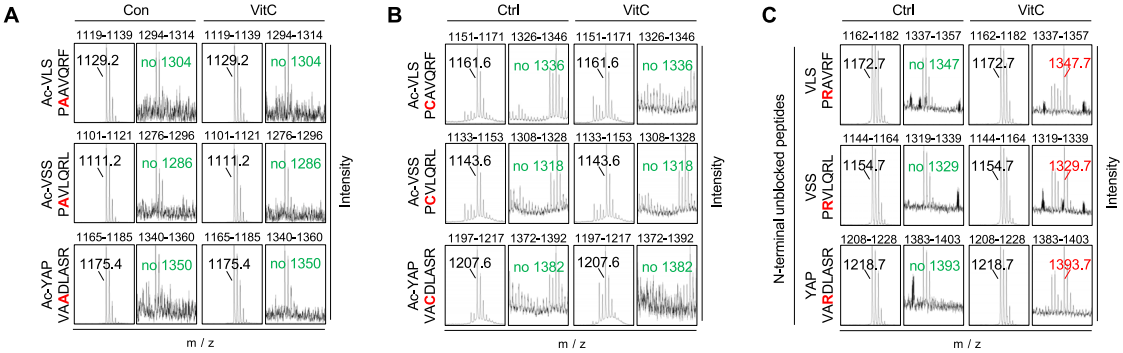
(C) The structures, molecular weights, and pKa values of ascorbic acid, ascorbate anion, and dehydroascorbic acid are shown.

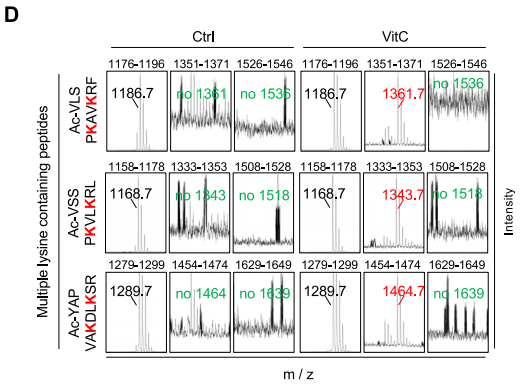
(D) The structures of cysteine ascorbylation and lysine ascorbylations are illustrated to differentiate them from lysine vitcylation.

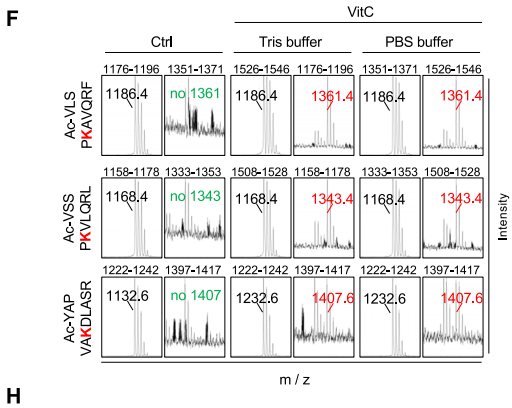
(E) Synthetic lysine-containing peptides were incubated with vehicle, 2 mM vitC, or 2 mM DHA at 37°C for 3 h, and the formation of vitcylated peptides was detected by MALDI-TOF/TOF MS.

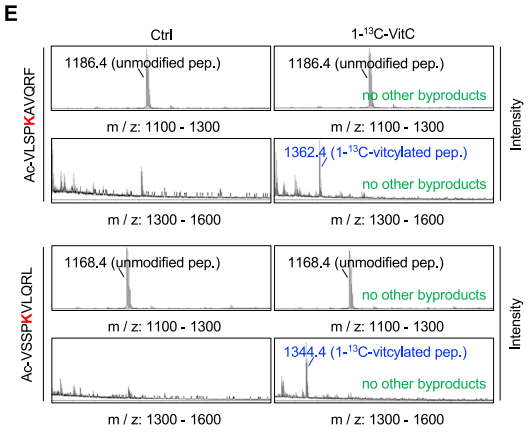
(F) The structures of vitC, 1-^{13}C-vitC, 2-^{13}C-vitC, and 1, 2-^{13}C-vitC used in this study are displayed.

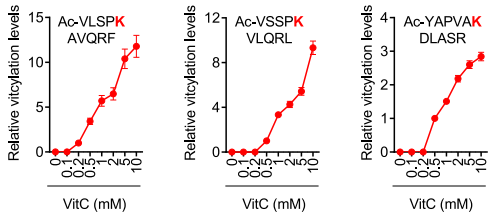
(G and H) MS/MS spectrum (left) and MS spectrum (right) of the unmodified peptide, vitcylated peptide, 1-^{13}C-vitcylated peptide, 2-^{13}C-vitcylated peptide, and 1, 2-^{13}C-vitcylated peptide (Ac-VLSPKAVQRF (G) and Ac-YAPVAKDLASR (H)) detected by HPLC-MS/MS. Lysine-containing unmodified fragments, vitcylated fragments, 1-^{13}C-vitcylated fragments, 2-^{13}C-vitcylated fragments, and 1, 2-^{13}C-vitcylated fragments are marked with green, red, and blue colors, respectively.

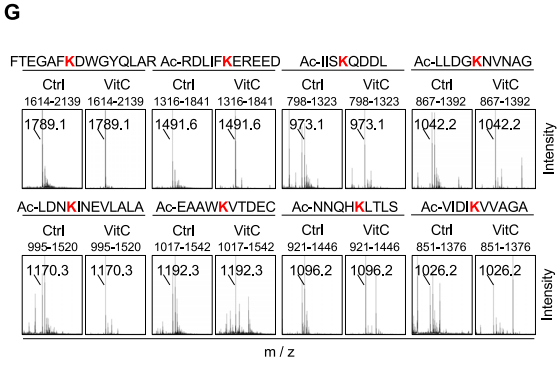






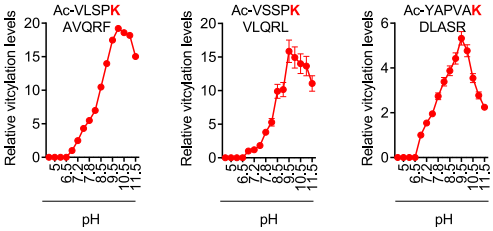






I

Peptides	Vitcylation (%, mean ± SEM)			
	VitC 0 mM	VitC 0.5 mM	VitC 1 mM	VitC 2 mM
Ac-YAPV AKDLASR	N.D.	10.3 ± 3.2	35.5 ± 6.1	42.9 ± 7.3
Ac-VSSP KVLQRL	N.D.	15.1 ± 2.6	40.3 ± 5.7	61.3 ± 9.8
Ac-VLSP KAVQRF	N.D.	18.4 ± 4.5	43.8 ± 7.9	67.0 ± 8.2



(legend on next page)

Figure S2. VitC specifically induces lysine vitcylation *in vitro*, related to Figure 1

(A and B) Synthetic alanine-containing peptides (A) and cysteine-containing peptides (B) were incubated with either a vehicle or 2 mM vitC at 37°C for 3 h. The formation of vitcylated peptides was detected by MALDI-TOF/TOF MS.

(C and D) Synthetic N-terminal unblocked peptides (C) and multiple lysine-containing peptides (D) were incubated with either a vehicle or 2 mM vitC at 37°C for 3 h. The formation of vitcylated peptides was detected by MALDI-TOF/TOF MS.

(E) Synthetic lysine-containing peptides were incubated with vehicle or 2 mM 1-^{13}C-vitC at 37°C for 3 h, and the formation of vitcylated peptides, along with any other byproducts, was detected by MALDI-TOF/TOF MS.

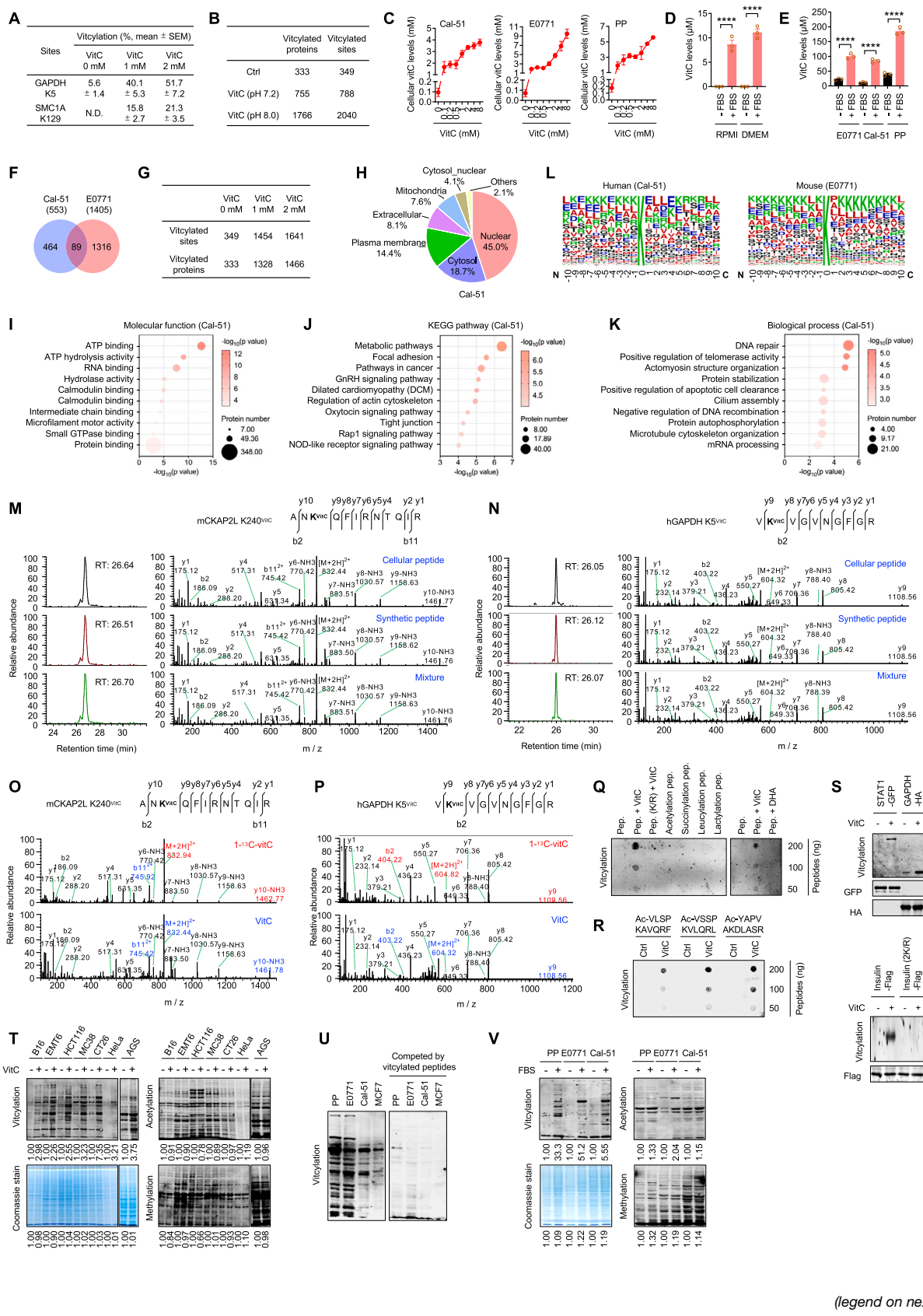
(F) Synthetic lysine-containing peptides were incubated with a vehicle or 2 mM vitC in tris buffer or PBS buffer at 37°C for 3 h. The formation of vitcylated peptides was detected by MALDI-TOF/TOF MS.

(G) Synthetic lysine-containing peptides (peptide sequences were listed above the spectrum) were incubated with a vehicle or 2 mM vitC at 37°C for 3 h. The formation of vitcylated peptides was detected by MALDI-TOF/TOF MS.

(H) Synthetic lysine-containing peptides were incubated with varying concentrations of vitC at 37°C for 3 h. The formation of vitcylated peptides was detected by MALDI-TOF/TOF MS. The relative vitcylation levels were quantified (n = 3). Data are represented as mean ± SEM.

(I) Synthetic lysine-containing peptides were incubated with varying concentrations of vitC at 37°C for 3 h. Corresponding lysine-to-arginine substitution peptides were used as controls. The formation of vitcylated peptides was detected by MALDI-TOF/TOF MS, and accurate vitcylation levels were quantified (n = 3). Data are represented as mean ± SEM. (N.D., not detectable.)

(J) Synthetic lysine-containing peptides were incubated with 2 mM vitC in tris-HCl buffer at different pH levels at 37°C for 3 h. The formation of vitcylated peptides was detected by MALDI-TOF/TOF MS, and the relative vitcylation levels were quantified (n = 3). Data are represented as mean ± SEM.



(legend on next page)

Figure S3. Lysine vitcylation exists in cells, related to Figure 2

(A) Levels of vitcylation of mouse GAPDH K5 and mouse SMC1A K129 were determined by HPLC-MS/MS analysis ($n = 3$). Data are represented as mean ± SEM.

(B) Summary of the numbers of vitcylated proteins and sites identified in E0771 proteomic samples and E0771 proteomic samples incubated with vitC (1 mM for 12 h) in Tris-HCl buffer at the indicated pH *in vitro*. E0771 proteomic samples were extracted by acetone.

(C) Intracellular vitC levels were measured in Cal-51, E0771, and PP cells cultured in varying concentrations of vitC for 12 h ($n = 3$). Data are represented as mean ± SEM.

(D) VitC levels were measured in RPMI 1640 medium and DMEM/F12 medium with or without 10% FBS ($n = 3$). Data are represented as mean ± SEM. ****$p < 0.0001$.

(E) Intracellular vitC levels were measured in Cal-51, E0771, and PP cells cultured in medium with or without 10% FBS ($n = 3$). Data are represented as mean ± SEM, ****$p < 0.0001$.

(F) Venn diagram of shared vitcylated proteins identified in Cal-51 cells (human) and E0771 cells (mouse).

(G) Numbers of vitcylated proteins and sites identified in E0771 cells treated with varying concentrations of vitC are summarized.

(H) Subcellular locations of lysine-vitcylated proteins identified in Cal-51 cells. The locations are classified as nuclear, cytosol, plasma membrane, extracellular, mitochondrial, cytosol_nuclear, and other compartments.

(I) Top ten Gene Ontology molecular function enrichment categories of vitcylated proteins identified in Cal-51 cells.

(J) Top ten KEGG-based enrichment categories of lysine-vitcylated proteins identified in Cal-51 cells.

(K) Top ten Gene Ontology biological process enrichment categories of vitcylated proteins identified in Cal-51 cells.

(L) Sequence probability logos of significantly enriched vitcylated site motifs for ±10 amino acids around the lysine vitcylation sites identified in Cal-51 cells (human) and E0771 cells (mouse). The size of each letter represents the frequency of the amino acid residue at that position.

(M and N) Extracted ion chromatograms (left) and MS/MS spectra (right) from HPLC-MS/MS analysis of vitcylated peptides (M, mouse CKAP2L and K240; N, human GAPDH and K5) derived from E0771 and Cal-51 cells (cellular peptide), respectively, their *in vitro* generated counterparts (synthetic peptide), and their mixture.

(O and P) Extracted MS/MS spectra from HPLC-MS/MS analysis of 1-^{13}C-vitcylated peptides and vitcylated peptides (O, mouse CKAP2L and K240; P, human GAPDH and K5) derived from E0771 and Cal-51 cells. The lysine-containing 1-^{13}C-vitcylated fragments and vitcylated fragments are marked by red and blue colors, respectively.

(Q) The pan anti-vitcylation antibody was tested for its reactivity with vitcylated peptide (pep. + vitC, peptide pre-incubated with 2 mM vitC at 37°C for 3 h) and cross-reactivity with unmodified peptides (pep. and pep. (K/R) + vitC), DHA-derived modification peptide (pep. + DHA, peptide pre-incubated with 2 mM DHA at 37°C for 3 h), as well as synthetic acetylated, succinylated, leucylated, and lactylated peptides (peptide sequence: Ac-VLSPKAVQRF).

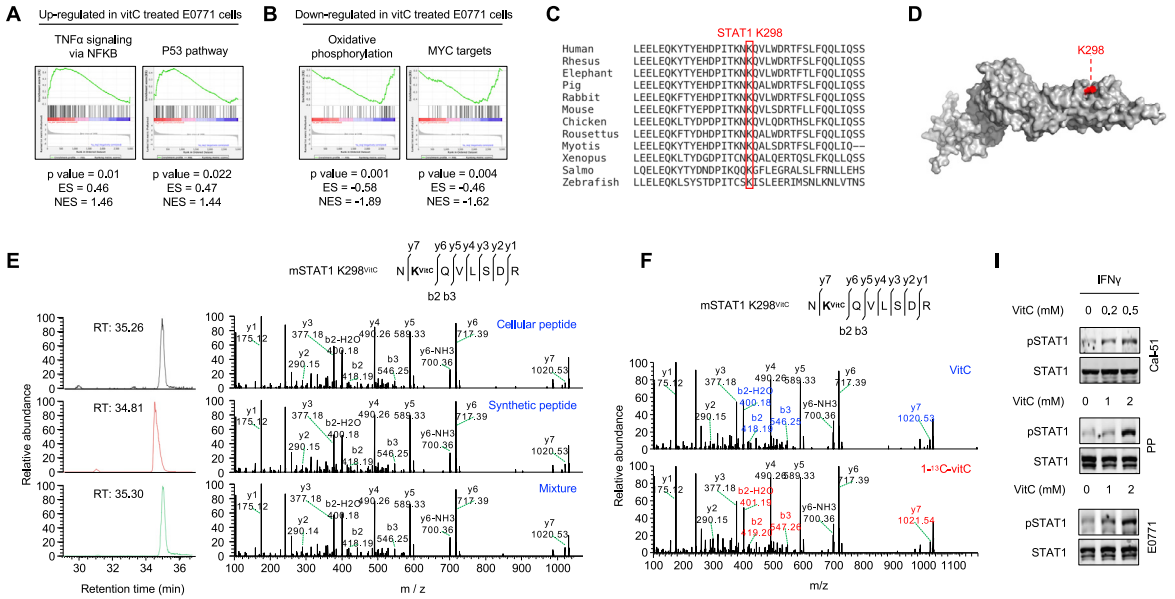
(R) The pan anti-vitcylation antibody was tested for its reactivity with vitcylated peptides (pep. + vitC, peptide pre-incubated with 2 mM vitC at 37°C for 3 h) and cross-reactivity with unmodified peptides (pep. + ctrl).

(S) HEK293T cells expressing STAT1-GFP, GAPDH-HA, insulin-FLAG, and a variant of insulin-FLAG with two lysine residues substituted by arginine (insulin-FLAG 2K/R) were used. The proteins STAT1-GFP, GAPDH-HA, insulin-FLAG, and insulin-FLAG (2K/R) were purified with GFP, HA, and FLAG beads, respectively. The reactivity of the pan anti-vitcylation antibody was tested with the purified STAT1-GFP, GAPDH-HA, insulin-FLAG, and insulin-FLAG (2K/R) proteins, which were treated with either a vehicle or 2 mM vitC at 37°C for 3 h *in vitro*.

(T) Intracellular lysine vitcylation, acetylation, and methylation levels were measured from indicated cells cultured in medium containing a vehicle or 2 mM vitC for 12 h.

(U) Vitcylation signals of indicated cells were competed off by vitcylated peptide (Ac-VLSPKAVQRF peptide pre-incubated with 2 mM vitC at 37°C for 3 h).

(V) Intracellular lysine vitcylation, acetylation, and methylation levels were measured in PP, E0771, and Cal-51 cells cultured in medium with or without 10% FBS for 12 h.



(legend on next page)

Figure S4. Vitcylation of STAT1 K298 activates STAT1, related to Figure 3

(A and B) Upregulated (A) and downregulated (B) GSEA signatures were observed in E0771 cells treated with 2 mM vitC for 2 days (n = 3).

(C) Sequence analysis of the STAT1 K298 site across multiple vertebrate species was conducted.

(D) The structure of human STAT1 (PDB: 8d3f, amino acids: 132–713) is displayed as a surface model, with the K298 site highlighted in red.

(E) Extracted ion chromatograms (left) and MS/MS spectra (right) from HPLC-MS/MS analysis of a vitcylated peptide (mouse STAT1, K298) derived from E0771 (cellular peptide), its *in vitro* generated counterparts (synthetic peptide), and their mixture.

(F) Extracted MS/MS spectra from HPLC-MS/MS analysis of vitcylated peptides (upper) and 1-^{13}C-vitcylated peptides (lower) (mouse STAT1, K298) derived from E0771 cells. The lysine-containing vitcylated fragments and 1-^{13}C-vitcylated fragments are marked by blue and red colors, respectively.

(G) Levels of 1-^{13}C-vitcylation of human STAT1 K298 were determined by HPLC-MS/MS analysis (n = 3). Data are represented as mean ± SEM. (N.D., not detectable.)

(H) Flow cytometric analysis of pSTAT1 in indicated cells cultured with 2 mM (PP and E0771 cells) or 0.5 mM (Cal-51 cells) vitC for 2 days or 100 ng/mL IFN-γ for 15 min. Blank and isotype antibody staining was added as a control.

(I) WB analysis of pSTAT1 in Cal-51, PP, and E0771 cells cultured in indicated concentrations of vitC for 2 days. Cells were treated with 10 ng/mL IFN-γ for 1 h before harvesting.

(J) Sequence analysis was performed for the K298 site in STAT1, STAT2, and STAT3.

(K) Vitcylation levels of human STAT1, STAT2, and STAT3 as well as mouse STAT1, STAT2, and STAT3 expressed in Cal-51 and PP cells, respectively, were measured. The cells were cultured in medium with or without vitC for 12 h (0.5 mM vitC for Cal-51, 2 mM vitC for PP).

(L) Flow cytometric analysis of pSTAT1 in indicated cells cultured with or without 2 mM vitC for 2 days (n = 3). Data are represented as mean ± SEM. ***$p < 0.001$, ****$p < 0.0001$.

(M) Flow cytometric analysis of pSTAT1 in Cal-51 and PP cells cultured in varying concentrations of IFN-γ for 15 min with or without vitC treatment for 2 days (2 mM vitC for PP, 0.5 mM vitC for Cal-51) (n = 3). Data are represented as mean ± SEM. ***$p < 0.001$, ****$p < 0.0001$.

(N) STAT1 vitcylation levels were measured from STAT1-GFP-expressing cells (Cal-51 and PP cells) cultured in varying pH mediums with or without vitC for 12 h (2 mM vitC for PP, 0.5 mM vitC for Cal-51).

(O) Flow cytometric analysis of pSTAT1 in Cal-51 and PP cells cultured in varying pH mediums with or without vitC for 2 days (2 mM vitC for PP, 0.5 mM vitC for Cal-51, n = 3). Data are represented as mean ± SEM. ***$p < 0.001$, ****$p < 0.0001$.

(P) Nuclear translocation of endogenous STAT1 in Cal-51 and PP cells cultured in vehicle- or vitC-containing medium for 2 days was assessed by immunofluorescence (0.5 mM vitC for Cal-51, 2 mM vitC for PP). Green represents anti-STAT1 and blue represents DAPI, with merged images allowing assessment of nuclear localization of STAT1, hereafter referred to as STAT1 immunofluorescence (scale bar, 20 μM).

(Q) Nuclear translocation of endogenous pSTAT1 in PP cells cultured in vehicle-, vitC-, or IFN-γ-containing medium was assessed by immunofluorescence (0.5 mM vitC for 2 days, 100 ng/mL IFN-γ for 15 min). Green represents anti-pSTAT1 and blue represents DAPI, with merged images showing the nuclear localization of pSTAT1 (scale bar, 15 μM).

(R) Nuclear translocation of endogenous STAT1 in STAT1-KO PP cells cultured in vehicle-, vitC-, or IFN-γ-containing medium was assessed by immunofluorescence (0.5 mM vitC for 2 days, 100 ng/mL IFN-γ for 15 min). Green represents anti-STAT1 and blue represents DAPI, with merged images showing the nuclear localization of STAT1 (scale bar, 15 μM).

(S) Measurement of human STAT1-WT and STAT1-Y701A vitcylation levels, as well as mouse STAT1-WT and STAT1-Y701A vitcylation levels in Cal-51 cells re-expressing human STAT1-WT-GFP, STAT1-Y701A-GFP, and PP cells re-expressing mouse STAT1-WT-GFP, STAT1-Y701A-GFP, respectively, were conducted. Cal-51 and PP cells were cultured in 2 mM vitC-containing or control medium for 12 h before harvesting.

(T) Measurement of human STAT1-WT and STAT1-Y701E vitcylation levels, as well as mouse STAT1-WT and STAT1-Y701E vitcylation levels in Cal-51 cells re-expressing human STAT1-WT-GFP, STAT1-Y701E-GFP, and PP cells re-expressing mouse STAT1-WT-GFP, STAT1-Y701E-GFP, respectively, were conducted. Cal-51 and PP cells were cultured in 2 mM vitC-containing or control medium for 12 h before harvesting.

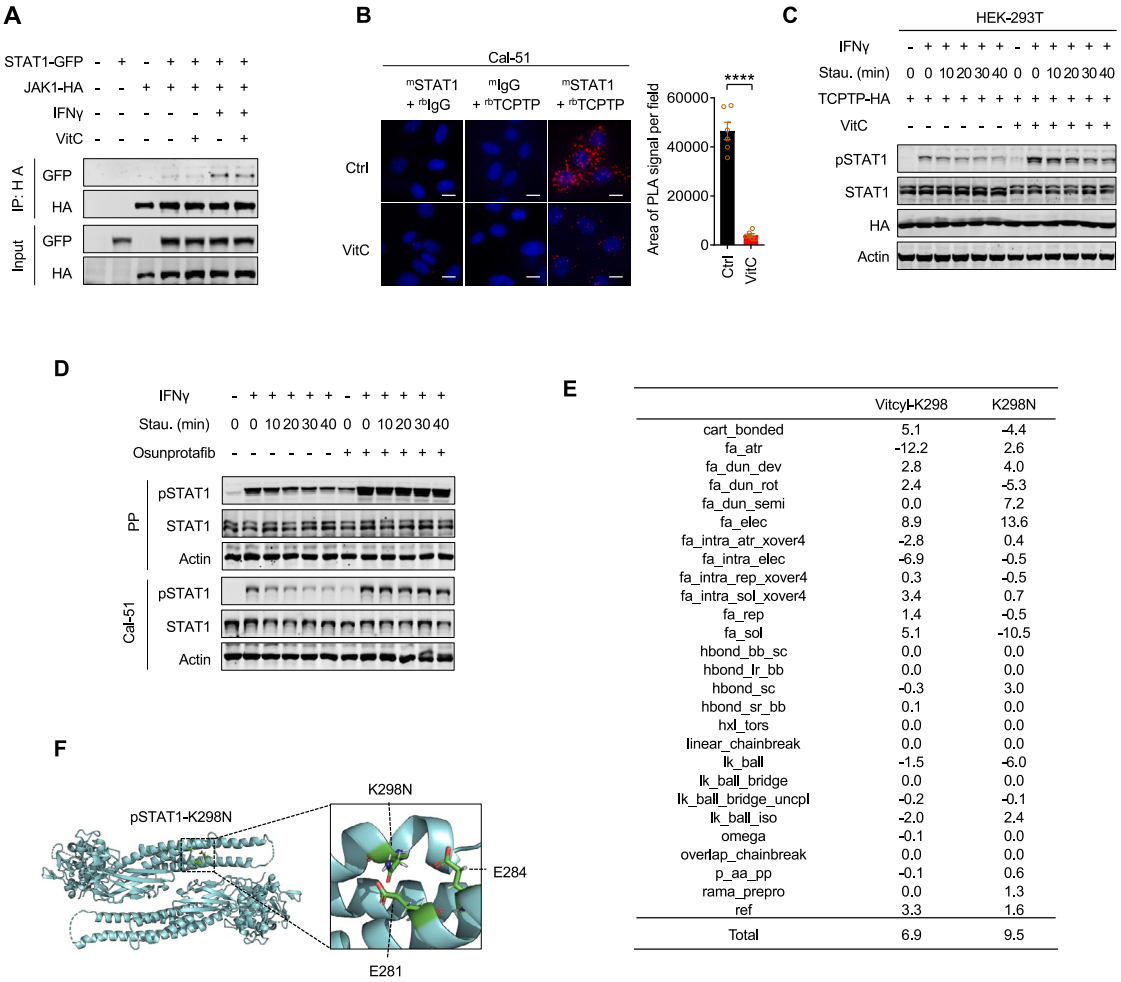
(U) HEK293T cells co-expressing STAT1-GFP and Ub-HA were treated with vehicle or 2 mM vitC for 2 days, followed by stimulation with 100 ng/mL IFN-γ for 1 h. 10 μM MG132 was added 3 h before harvesting cells. The ubiquitination levels of STAT1 were assayed by WB.

(V) STAT1 stability in Cal-51 and PP cells was measured by WB after culturing with 50 μg/mL cycloheximide for the indicated times, with or without vitC for 2 days (2 mM vitC for PP, 0.5 mM vitC for Cal-51).

(W) WB analysis for STAT1 in PP-sg_NC, PP-sgSTAT1_1, and PP-sgSTAT1_2 cells were performed.

(X) WB analysis for STAT1 in PP-sgNC, PP-sgSTAT1_1, and PP-sgSTAT1 cells re-expressing STAT1-WT-GFP, STAT1-K298R-GFP, or STAT1-Y701A-GFP was conducted.

(Y) WB analysis for pSTAT1 in PP-sgSTAT1 cells re-expressing STAT1-WT-GFP or STAT1-K298R-GFP cultured in indicated concentrations of vitC for 2 days. Cells were treated with 10 ng/mL IFN-γ for 1 h before harvesting.



	VitcyI-K298	K298N
cart_bonded	5.1	-4.4
fa_atr	-12.2	2.6
fa_dun_dev	2.8	4.0
fa_dun_rot	2.4	-5.3
fa_dun_semi	0.0	7.2
fa_elec	8.9	13.6
fa_intra_atr_xover4	-2.8	0.4
fa_intra_elec	-6.9	-0.5
fa_intra_rep_xover4	0.3	-0.5
fa_intra_sol_xover4	3.4	0.7
fa_rep	1.4	-0.5
fa_sol	5.1	-10.5
hbond_bb_sc	0.0	0.0
hbond_lr_bb	0.0	0.0
hbond_sc	-0.3	3.0
hbond_sr_bb	0.1	0.0
hxl_tors	0.0	0.0
linear_chainbreak	0.0	0.0
lk_ball	-1.5	-6.0
lk_ball_bridge	0.0	0.0
lk_ball_bridge_uncpl	-0.2	-0.1
lk_ball_iso	-2.0	2.4
omega	-0.1	0.0
overlap_chainbreak	0.0	0.0
p_aa_pp	-0.1	0.6
rama_prepro	0.0	1.3
ref	3.3	1.6
Total	6.9	9.5

Figure S5. STAT1 K298 vitcylation impairs STAT1 dephosphorylation, related to Figure 4

(A) HeLa cells co-expressing STAT-GFP and JAK1-HA were treated with a vehicle or 300 μM vitC for 24 h, followed by stimulation with 100 ng/mL IFN-γ for 15 min. The interaction between STAT1 and JAK1 was assayed by co-immunoprecipitation.

(B) STAT1-TCPTP PLA analysis (left) and quantification (right) of Cal-51 cells treated with a vehicle or 0.5 mM vitC for 2 days (scale bar, 15 μM). Data are represented as mean ± SEM. ****$p < 0.0001$.

(C) HEK293T Cells were transfected with TCPTP-HA and treated with a vehicle or 2 mM vitC for 2 days, then stimulated with 100 ng/mL IFN-γ for 15 min followed by incubation with 1 μM staurosporine for the indicated times. The pSTAT1 levels were measured by WB immediately.

(D) Cells were pretreated with a vehicle or 1 μM osunprotafib for 24 h, then stimulated with 100 ng/mL IFN-γ for 15 min followed by incubation with 1 μM staurosporine for the indicated times. The pSTAT1 levels were measured by WB immediately.

(E) Energy contribution difference of STAT1 K298N and K298 vitcylation. Numbers are reported in REU.

(F) Structures of pSTAT1 with the K298N mutation in the antiparallel dimer conformation from the last snapshot of molecular dynamics simulation. The K298N mutation results in the loss of the salt bridges between K298/E281 and K298/E284.



(legend on next page)

Figure S6. STAT1 K298 vitcylation facilitates MHC/HLA class I expression, related to Figure 5

(A) Quantitative PCR analysis of antigen processing and presentation gene expression in Cal-51 cells treated with either a vehicle or 0.5 mM vitC for 2 days ($n = 4$). Data are represented as mean ± SEM. $^{****}p < 0.0001$.

(B) Representative flow cytometry plots (left) and quantifications (right) of HLA class I expression on Cal-51 cells cultured with different concentrations of vitC for 2 days ($n = 3$). Data are represented as mean ± SEM. $^{**}p < 0.01$, $^{***}p < 0.001$.

(C) HLA (Cal-51)/H-2Kb (E0771)/H-2Kq (PP) and B2M flow cytometric analysis of indicated cells cultured with 2 mM (PP and E0771 cells) or 0.5 mM (Cal-51 cells) vitC or 100 ng/mL IFN-γ for 2 days. Blank and isotype antibody staining was added as a control.

(D) MHC/HLA class I flow cytometric analysis of indicated cells cultured with or without 2 mM vitC for 2 days. Data are represented as mean ± SEM. $^{**}p < 0.01$, $^{***}p < 0.001$, $^{****}p < 0.0001$.

(E) Flow cytometric analysis of HLA class I expression on Cal-51 cells cultured in different concentrations of IFN-γ (100 ng/mL, 24 h) with or without 0.5 mM vitC for 2 days ($n = 3$). Data are represented as mean ± SEM. $^{**}p < 0.01$, $^{****}p < 0.0001$.

(F) Flow cytometric analysis of HLA class I expression on Cal-51 cells cultured in different pH mediums with or without 0.5 mM vitC for 2 days ($n = 3$). Data are represented as mean ± SEM. $^{*}p < 0.05$, $^{***}p < 0.001$, $^{****}p < 0.0001$.

(G) Flow cytometry analysis of MHC I expression in PP-sgControl, PP-sgSTAT1_1, and PP-sgSTAT1_2 cells cultured in different concentrations of vitC for 2 days ($n = 3$). Data are represented as mean ± SEM. $^{**}p < 0.01$, $^{***}p < 0.001$, $^{****}p < 0.0001$.

(H) ROS levels and MHC/HLA class I expression levels were measured in Cal-51, E0771, and PP cells treated with various concentrations of vitC for 2 days ($n = 3$). Data are represented as mean ± SEM. $^{*}p < 0.05$, $^{**}p < 0.01$, $^{***}p < 0.001$, $^{****}p < 0.0001$.

(I) TET activity was measured in Cal-51, E0771, and PP cells treated with vehicle or 10 μM Bobcat 339 for 6 h ($n = 3$). Data are represented as mean ± SEM. $^{**}p < 0.01$, $^{***}p < 0.001$, $^{****}p < 0.0001$.

(J) HIF1α level was measured in Cal-51, E0771, and PP cells treated with vehicle or 0.2 μM IOX2 for 6 h.

(K) Flow cytometric analysis of pSTAT1 and MHC/HLA class I expression in Cal-51, E0771, and PP cells cultured in medium supplemented with the vehicle, vitC (2 days), 10 μM Bobcat 339 (3 days), vitC + 10 μM Bobcat 339, 0.2 μM IOX2 (3 days), or vitC + 0.2 μM IOX2 ($n = 3$). Data are represented as mean ± SEM. $^{*}p < 0.05$, $^{**}p < 0.01$, $^{***}p < 0.001$, $^{****}p < 0.0001$.

(L) Flow cytometry gating strategy for the DCs population is illustrated. Representative plots are shown. Hereafter for DCs gating.

(M) Flow cytometric analysis of H-2Kb and pSTAT1 expression on EL4-OVA cells treated with varying doses of vitC for 3 days ($n = 3$). Data are represented as mean ± SEM. $^{*}p < 0.05$, $^{**}p < 0.01$, $^{***}p < 0.001$, $^{****}p < 0.0001$.

(N) Flow cytometry gating strategy for the T cell population is illustrated. Representative plots are shown. Hereafter for T cells gating.

(O) WB analysis of pSTAT1 in B16-OVA cells cultured in varying concentrations of vitC for 2 days. Cells were treated with 10 ng/mL IFN-γ for 1 h before harvesting.

(P) Flow cytometric analysis of $CD8^+$ T (OT-I) cells co-cultured with EL4-OVA cells pretreated with 2 mM vitC. T cells ($CD45^+$ $CD3^+$ $CD8^+$) proliferation and activity were quantified as $CFSE^-$ and IFN-γ^+, TNF-α^+ cells, respectively ($n = 3$). Data are represented as mean ± SEM. $^{*}p < 0.05$, $^{**}p < 0.01$, $^{***}p < 0.001$, $^{****}p < 0.0001$.

(Q) WB analysis of STAT1 in B16-OVA-sgNC, B16-OVA-sgSTAT1, and B16-OVA-sgSTAT1 cells re-expressing STAT1-WT-GFP or STAT1-K298R-GFP was conducted.

(R) WB analysis of TET2 (left) in B16-OVA-sg_NC, B16-OVA-sg_TET2, and HIF1α (right) in B16-OVA-sg_NC, B16-OVA-sg_HIF1α, respectively.

(S–U) Flow cytometry analysis of pSTAT1 (S), OVA peptide presentation (T), and MHC I expression (U) in B16-OVA-sg_NC, B16-OVA-sg_TET2, and B16-OVA-sg_HIF1α cells cultured in 2 mM vitC for 2 days or 100 ng/mL IFN-γ for 24 h ($n = 3$). Data are represented as mean ± SEM. $^{**}p < 0.01$, $^{***}p < 0.001$, $^{****}p < 0.0001$.

(V) Quantitative PCR analysis of *Tap2* and *B2m* transcription in B16-OVA-sg_NC, B16-OVA-sg_TET2, and B16-OVA-sg_HIF1α cells cultured in 2 mM vitC for 2 days or 100 ng/mL IFN-γ for 24 h ($n = 3$). Data are represented as mean ± SEM. $^{*}p < 0.05$, $^{****}p < 0.0001$.

(W) Flow cytometric analysis of OT-I $CD8^+$ T cells co-cultured with B16-OVA-sg_NC, B16-OVA-sg_TET2, or B16-OVA-sg_HIF1α cells pretreated with 2 mM vitC. T cell ($CD45^+$ $CD3^+$ $CD8^+$) activation was quantified as IFN-γ^+, TNF-α^+ cells ($n = 3$). Data are represented as mean ± SEM. $^{**}p < 0.01$, $^{****}p < 0.0001$.

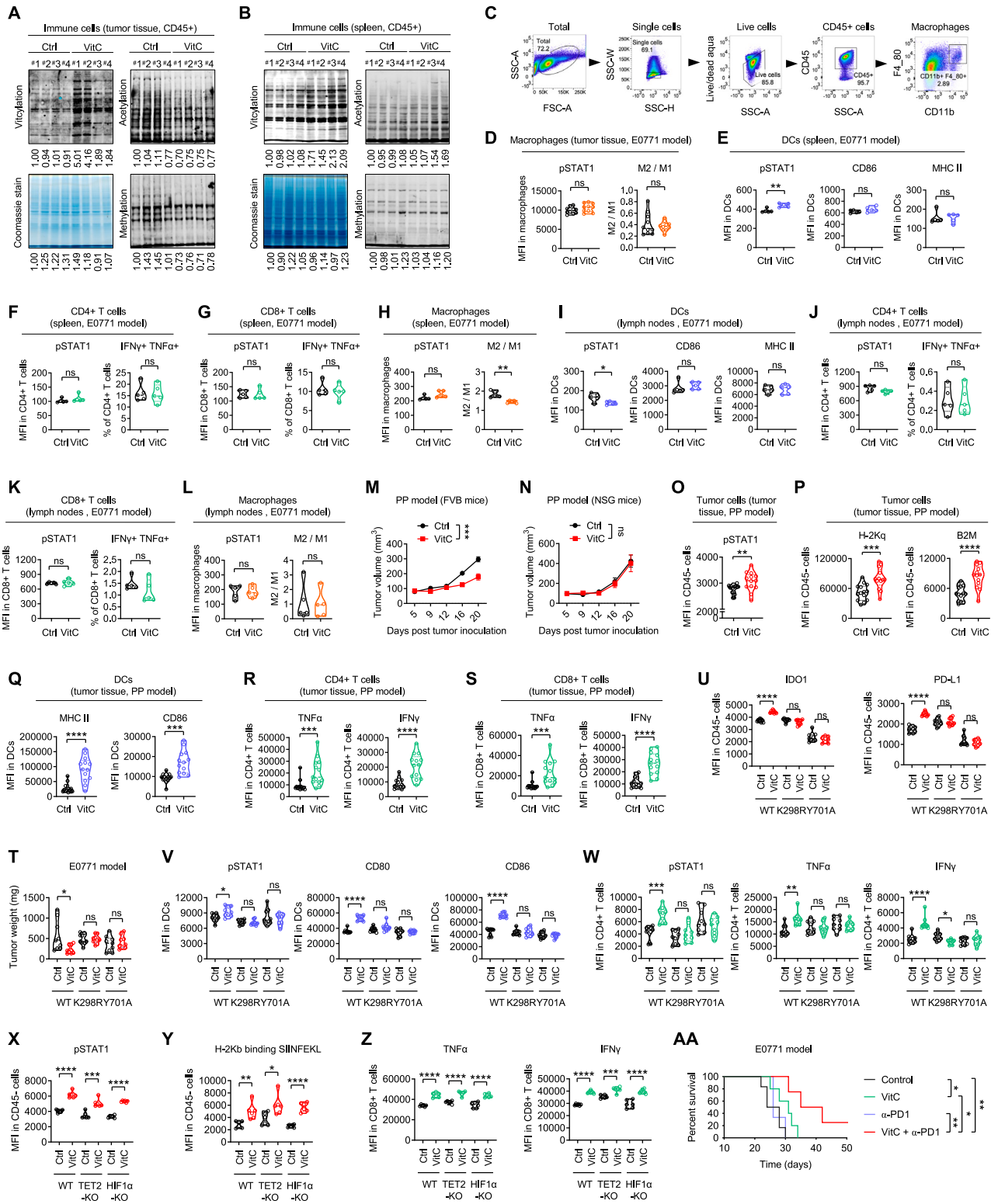


Figure S7. STAT1 K298 vitcylation boosts anti-tumor immunity *in vivo*, related to Figures 6 and 7

(A) Lysine vitcylation, acetylation, and methylation levels of immune cells (CD45$^+$) in E0771 tumors were measured by WB (n = 4 for each group). Protein levels were normalized by Coomassie staining.

(legend continued on next page)

(B) Lysine vitcylation, acetylation, and methylation levels of immune cells ($CD45^+$) in the spleen of E0771 tumor-bearing C57BL/6 mice were measured by WB ($n = 5$ for each group). Protein levels were normalized by Coomassie staining.
(C) Flow cytometry gating strategy for the macrophage population is illustrated. Representative plots are shown. Hereafter for macrophage gating.
(D) Flow cytometry analysis of the pSTAT1 level and M2/M1 polarization in macrophages in E0771 tumor tissue from vehicle- or vitC-treated mice (vehicle, $n = 9$; vitC treated, $n = 9$). Data are represented as mean ± SEM.
(E) Flow cytometry analysis of the pSTAT1 level, CD86, and MHC II expression in DCs in the spleens of vehicle- or vitC-treated E0771 tumor-bearing C57BL/6 mice (vehicle, $n = 5$; vitC treated, $n = 5$). Data are represented as mean ± SEM. $^{**}p < 0.01$.
(F and G) Flow cytometry analysis of the pSTAT1 level, TNF-α, and IFN-γ expression in $CD4^+$ T cells (F) and $CD8^+$ T cells (G) in the spleens of vehicle- or vitC-treated E0771 tumor-bearing C57BL/6 mice (vehicle, $n = 5$; vitC treated, $n = 5$). Data are represented as mean ± SEM.
(H) Flow cytometry analysis of the pSTAT1 level and M2/M1 polarization in macrophages in the spleens of vehicle- or vitC-treated E0771 tumor-bearing C57BL/6 mice (vehicle, $n = 5$; vitC treated, $n = 5$). Data are represented as mean ± SEM.
(I) Flow cytometry analysis of the pSTAT1 level, MHC II, and CD86 expression in DCs in the lymph nodes of vehicle- or vitC-treated E0771 tumor-bearing C57BL/6 mice (vehicle, $n = 5$; vitC treated, $n = 5$). Data are represented as mean ± SEM. $^{*}p < 0.05$.
(J and K) Flow cytometry analysis of pSTAT1 level, TNF-α, and IFN-γ expression in $CD4^+$ T cells (J) and $CD8^+$ T cells (K) in the lymph nodes of vehicle- or vitC-treated E0771 tumor-bearing C57BL/6 mice (vehicle, $n = 5$; vitC treated, $n = 5$). Data are represented as mean ± SEM.
(L) Flow cytometry analysis of the pSTAT1 level, M2/M1 polarization in macrophages in the lymph nodes of vehicle- or vitC-treated E0771 tumor-bearing C57BL/6 mice (vehicle, $n = 5$; vitC treated, $n = 5$). Data are represented as mean ± SEM.
(M and N) Tumor growth of PP allografts in FVB mice (M) and NSG mice (N) treated with vitC was analyzed (vehicle, $n = 5$; vitC treated, $n = 5$). Data are represented as mean ± SEM. $^{**}p < 0.0001$.
(O and P) Flow cytometry analysis of pSTAT1 (O), MHC I expression (P) on PP tumor cells ($CD45^-$) from vehicle- or vitC-treated mice (vehicle, $n = 14$; vitC treated, $n = 13$). Data are represented as mean ± SEM. $^{**}p < 0.01$, $^{***}p < 0.001$, $^{****}p < 0.0001$.
(Q) Flow cytometry analysis of MHC II and CD86 expression in DCs in PP tumor tissue from vehicle- or vitC-treated mice (vehicle, $n = 14$; vitC treated, $n = 13$). Data are represented as mean ± SEM. $^{***}p < 0.001$, $^{****}p < 0.0001$.
(R) Flow cytometry analysis of $CD4^+$ TNF-α^+ and $CD4^+$ IFN-γ^+ T cells ($CD45^+$ $CD3^+$) isolated from PP tumor tissue from vehicle- or vitC-treated mice (vehicle, $n = 14$; vitC treated, $n = 13$). Data are represented as mean ± SEM. $^{***}p < 0.001$, $^{****}p < 0.0001$.
(S) Flow cytometry analysis of $CD8^+$ TNF-α^+ and $CD8^+$ IFN-γ^+ T cells ($CD45^+$ $CD3^+$) isolated from PP tumor tissue from vehicle- or vitC-treated mice (vehicle, $n = 14$; vitC treated, $n = 13$). Data are represented as mean ± SEM. $^{***}p < 0.001$, $^{****}p < 0.0001$.
(T) Tumor weight of the xenografts of E0771-sgSTAT1_1 tumor cells re-expressing STAT1-WT-GFP, STAT1-K298R-GFP, or STAT1-Y701A-GFP treated with vehicle or vitC (vehicle, $n = 9$; vitC treated, $n = 9$).
(U) Flow cytometry analysis of IDO1 and PD-L1 expression on the xenografts of E0771-sgSTAT1_1 tumor cells re-expressing STAT1-WT-GFP, STAT1-K298R-GFP, or STAT1-Y701A-GFP treated with vehicle or vitC (vehicle, $n = 9$; vitC treated, $n = 9$). Data are represented as mean ± SEM. $^{****}p < 0.0001$.
(V) Flow cytometry analysis of pSTAT1 level, CD80, and CD86 expression in DCs on the xenografts of E0771-sgSTAT1_1 tumor cells re-expressing STAT1-WT-GFP, STAT1-K298R-GFP, or STAT1-Y701A-GFP treated with vehicle or vitC (vehicle, $n = 9$; vitC treated, $n = 9$). Data are represented as mean ± SEM. $^{*}p < 0.05$, $^{****}p < 0.0001$.
(W) Flow cytometry analysis of pSTAT1 level, TNF-α, and IFN-γ expression in $CD4^+$ T cells on the xenografts of E0771-sgSTAT1_1 tumor cells re-expressing STAT1-WT-GFP, STAT1-K298R-GFP, or STAT1-Y701A-GFP treated with vehicle or vitC (vehicle, $n = 9$; vitC treated, $n = 9$). Data are represented as mean ± SEM. $^{**}p < 0.01$, $^{***}p < 0.001$, $^{****}p < 0.0001$.
(X and Y) Flow cytometry analysis of pSTAT1 (X) and OVA peptide presentation (Y) on the xenografts of B16-OVA, B16-OVA (TET2-KO), and B16-OVA (HIF1α-KO) tumor cells treated with vehicle or vitC (vehicle, $n = 6$; vitC treated, $n = 6$). Data are represented as mean ± SEM. $^{*}p < 0.05$, $^{**}p < 0.01$, $^{***}p < 0.001$, $^{****}p < 0.0001$.
(Z) Flow cytometry analysis of TNF-α and IFN-γ expression in OT-1 $CD8^+$ T cells in the xenografts of B16-OVA, B16-OVA (TET2-KO), and B16-OVA (HIF1α-KO) tumor cells treated with vehicle or vitC (vehicle, $n = 6$; vitC treated, $n = 6$). Data are represented as mean ± SEM. $^{***}p < 0.001$, $^{****}p < 0.0001$.
(AA) Survival of E0771 allografts in C57BL/6 mice treated with vitC as a single agent or in combination with anti-PD1 antibody ($n = 4$). Data are represented as mean ± SEM. $^{*}p < 0.05$, $^{**}p < 0.01$.